Deformation of Host Rocks and Flow of Magma during Growth of Minette Dikes and Breccia-bearing Intrusions near Ship Rock, New Mexico

GEOLOGICAL SURVEY PROFESSIONAL PAPER 1202

Deformation of Host Rocks and Flow of Magma during Growth of Minette Dikes and Breccia-bearing Intrusions near Ship Rock, New Mexico

By PAUL T. DELANEY *and* DAVID D. POLLARD

GEOLOGICAL SURVEY PROFESSIONAL PAPER 1202

A description of the northeastern dike based on mechanical analyses of fracturing of host rock, flow of magma, and transport of heat

UNITED STATES GOVERNMENT PRINTING OFFICE, WASHINGTON : 1981

UNITED STATES DEPARTMENT OF THE INTERIOR

JAMES G. WATT, ***Secretary***

GEOLOGICAL SURVEY

Dallas L. Peck, *Director*

Library of Congress Cataloging in Publication Data

Delaney, Paul T.
Deformation of host rocks and flow of magma during growth of minette dikes and breccia-bearing intrusions near Ship Rock, New Mexico.

(Geological Survey professional paper ; 1202)
Bibliography: p. 59-61
Supt. of Docs. no.: I 19.16:1202
1. Dikes (Geology)--New Mexico--Ship Rock. 2. Intrusions (Geology)--New Mexico--Ship Rock. I. Pollard, David D. II. Title. III. Series: United States. Geological Survey. Professional Paper 1202.
QE611.5.U6D44 551.8'8 81-6769
AACR2

For sale by the Superintendent of Documents, U.S. Government Printing Office
Washington, D.C. 20402

CONTENTS

ILLUSTRATIONS

TABLES

DEFORMATION OF HOST ROCKS AND FLOW OF MAGMA DURING GROWTH OF MINETTE DIKES AND BRECCIA-BEARING INTRUSIONS NEAR SHIP ROCK, NEW MEXICO

By PAUL T. DELANEY and DAVID D. POLLARD

ABSTRACT

We have studied a small group of minette dikes and plugs that crop out within a flat-lying sequence of siltstone and shale near Ship Rock, a prominent volcanic throat of tuff breccia in northwestern New Mexico. Seven dikes form a radial pattern about Ship Rock; we describe in detail the northeastern dike, which has an outcrop length of about 2,900 m, an average thickness of 2.3 m, and a maximum thickness of 7.2 m. The dike is composed of 35 discrete segments arranged in echelon; orientation of dike segments ranges systematically from N. 52° E. to N. 66° E. A prominent joint set strikes parallel to the segments and is localized within several tens of meters of the dike. Regional joint patterns display no obvious relation to dike orientation. Small offsets of segment contacts, as well as wedge-shaped bodies of crumpled host rock within segments, mark the sites of coalescence of smaller segments during dike growth. Bulges in the dike contact, which represent a nondilational component of growth, indicate that wallrocks were brecciated and eroded during the flow of magma. Breccias make up about 9 percent of the 7,176-m^2 area of the dike, are concentrated in its southwest half, and are commonly associated with its thickest parts. We also describe three subcircular plugs; each plug is smaller than 30 m in diameter, is laterally associated with a dike, and contains abundant breccias. Field evidence indicates that these plugs grew from the dikes by brecciation and erosion of wallrocks and that the bulges in the contact of the northeastern dike represent an initial stage of this process.

From continuum-mechanical models of host-rock deformation, we conclude that dike propagation was the dominant mechanism for creating conduits for magma ascent where the host rock was brittle and elastic. At a given driving pressure, dikes dilate to accept greater volumes of magma than plugs, and for a given dilation, less work is done on the host rocks. In addition, the pressure required for dike growth decreases with dike length. From numerical solutions for dilation of cracks oriented like segments of the northeastern dike, we find that we can best model the form of the dike by treating it as composed of 10 cracks rather than 35. We attribute this result to coalescence of adjacent segments below the present outcrop and to inelastic deformation at segment ends. Using a driving pressure of 2 MPa (20 bars), we estimate a shear modulus of about 10^3 MPa for the host rocks, in agreement with laboratory tests on soft shale. A propagation criterion based on stress intensity at the segment ends indicates a fracture toughness of the host rocks of about 100 MPa·$m^{1/2}$, a hundredfold greater than values reported from laboratory tests. Segmentation of fractures is common in many materials and has been observed during fissure eruptions at Kilauea Volcano in Hawaii. At the northeastern dike, we attribute segmentation to local rotation of the direction of least principal compressive stress.

From continuum-mechanical models of magma and heat flow in idealized conduits, we conclude that magma flows far more rapidly and with less relative heat loss in plugs than in dikes. Although dikes are the preferred form for emplacement, plugs are the preferred form for the flow of magma. We present a numerical solution for volumetric flow rate and wall heat flux for the northeastern dike and find that although the flow rate is extremely sensitive to conduit geometry, the rate of heat loss to wallrocks is not. During emplacement of the northeastern dike, local flow rate increased where wallrocks were eroded and reached a maximum of about 45 times the mean initial rate, whereas the maximum rate of heat loss to wallrocks increased to only 1.6 times the mean initial rate. An inferred progression from continuous magma flow along a dike to flow from a plug agrees well with observations of volcanic eruptions that begin from fissures and later are localized at discrete vents. We find that the driving-pressure gradient for magma flow in the northweastern dike may have been about 25 Pa/m (0.25 bars/km), or 0.1 percent of the weight per unit volume of magma, and that less than 1 percent of the heat convected upward from the source region was lost to wallrocks.

INTRODUCTION

In this report we discuss the physical development of a small group of minette- and breccia-bearing intrusions, using field and theoretical methods. These intrusions were emplaced approximately 30 m.y. ago during the ascent of magma, from an unknown source region, through a crystalline basement complex and overlying sequence of flat-lying sedimentary rocks. The intrusions crop out on the east side of Ship Rock (fig. 1), a spectacular volcanic throat of tuff breccia in northwestern New Mexico. The northeastern dike (foreground, fig. 1), which is arranged in echelon and has an outcrop length of nearly 3 km, is the primary source of the data presented here. In front of Ship Rock are three small plugs with diameters of about 30 m; these plugs are laterally associated with the two other dikes that crop out on the east side of Ship Rock. In addition to minette, which is the igneous rock of the intrusions, the plugs contain breccias of minette mixed with fractured and comminuted material derived from the host rocks. Similar breccias are present locally in all the dikes. One purpose of our report is to document the structural details of these field relations.

Intimate spatial association of these dikes and

FIGURE 1.—Aerial view of Ship Rock from the northeast. Ship Rock, known to the Navaho as Tse Bitai (the Winged Rock), stands about 600 m above surrounding plain. Northeastern dike (foreground) is about 3 km in outcrop length. Three small plugs and two other dikes are visible in front of Ship Rock. Two large radial dikes are partly visible in background. Photograph by D. L. Baars.

plugs is not coincidental but reflects particular events during their formation. On the basis of our observations at Ship Rock, we reconstruct a temporal sequence that progresses from dike emplacement, through brecciation and removal of host rocks along part of the dike, to complete channeling of magma flow in circular pluglike conduits that continue to grow by erosion of host rocks until the intrusion process terminates. Another purpose of our report is to elaborate and substantiate this proposed temporal sequence of events for dikes and plugs.

We analyze two physical aspects of the emplacement process, using continuum-mechanical theories: (1) development of the cross-sectional form by fracture of host rocks and elastic dilation of the dikes, and (2) flow of magma through and loss of heat from dikes and pluglike conduits. We separate that part of the form of the northeastern dike due to elastic dilation from that due to erosion of host rocks and compare it with the theoretical form of a set of mechanically interacting pressurized magma-filled cracks. We then calculate the velocity field of the magma flowing through the conduits as well as the rate of heat loss from them. The final purpose of our report is to present the results of these theoretical studies of the important processes that take place during intrusion of basic magma at high levels in the Earth's crust.

GEOMETRIC FEATURES OF DIKES AND PLUGS

Viewed on a large scale (fig. 2), the intrusions on the east side of Ship Rock appear quite simple: dikes are long straight lines of uniform thickness, and plugs are circular. A map of one minette intrusion 25 km north-northeast of Ship Rock (fig. 3), however, suggests that this apparent simplicity is misleading. Viewed on a smaller scale, the minette intrusion is seen to consist of 30 distinct dike segments and a pluglike body; in addition, two small bulges are visible in the dike contact south of the plug. Field inspection of these bulges and the plug reveals that they are partly occupied by breccia. At still larger scales, more features could certainly be distinguished. In our experience, dike and plugs are more complex than is suggested by their usual representation on geologic maps as simple lines and circles.

We now define several terms to clarify our description of the intrusions near Ship Rock (fig. 4). *Outcrop length* is the total distance along the exposed part of a particular dike. Many sheet intrusions, particularly near their peripheries, are composed of discrete fingers of igneous rock pointing in the direction of propagation (Pollard and others, 1975); we refer to these fingers as *dike segments* and measure *segment length* along the propagation direction. In a cross section perpendicular to segment length, we measure *width* along the greater dimension and *thickness* along the lesser dimension. Between segments, we measure *offset* perpendicular to segment strike and *separation* (or *overlap*) parallel to strike. *Bridges* of host rocks separate closely spaced segments. *Horns* from sharp asymmetric ends on segments that are slightly offset. Dike segments coalesce in a plane at *cusps* and, where slightly out of plane, at *offsets*; the trend and plunge of cusps or offsets indicate propagation direction. *Buds* are anomalously thick parts of segments (Wentworth and Jones, 1940) where removal of the dilational component of the overall form would not bring adjacent walls back into contact. Where the intrusive contact forms a cylindrical body rather than a sheet, the term *plug* is used. Plugs may lead upward to *volcanic necks*. Both buds and plugs are commonly marked by the pressure of breccias. *Length* also refers to distance along the direction of magma flow in buds, plugs, and necks. We define two types of breccia: *monobreccia*, composed solely of highly fractured host-rock material; and *heterobreccia*, composed of minette as well as host rock. Examples of all these features are described in later sections of this report.

ACKNOWLEDGMENTS

We thank Otto Muller of Colgate University, Hamilton, N.Y., for his help during the initial investigation of the northeastern dike and for conducting a magnetic survey that aided in determining its lateral extent. We benefited from discussions with Herbert Shaw, Donald Swanson, and Eugene Shoemaker of the U.S. Geological Survey, Bruce Marsh of the Johns Hopkins University, Baltimore, Md., and Richard Jahns of Stanford University, Stanford, Calif. Arvid Johnson of the University of Cincinnati, Ohio, provided a constant source of advice throughout this research. Paul Segall of the U.S. Geological Survey assisted in development of the computer program for determining the dilation of mechanically interacting cracks. Milton Van Dyke of the Department of Applied Mechanics at Stanford suggested the perturbation method used to determine the flow of magma through the northeastern dike.

We thank the Navaho people for permission to work at Ship Rock.

GEOLOGICAL AND PHYSICAL SETTING

Ship Rock is situated on the Four Corners platform (Kelley and Clinton, 1960; Woodward and Callender, 1977), a tectonic element of the Colorado Plateaus

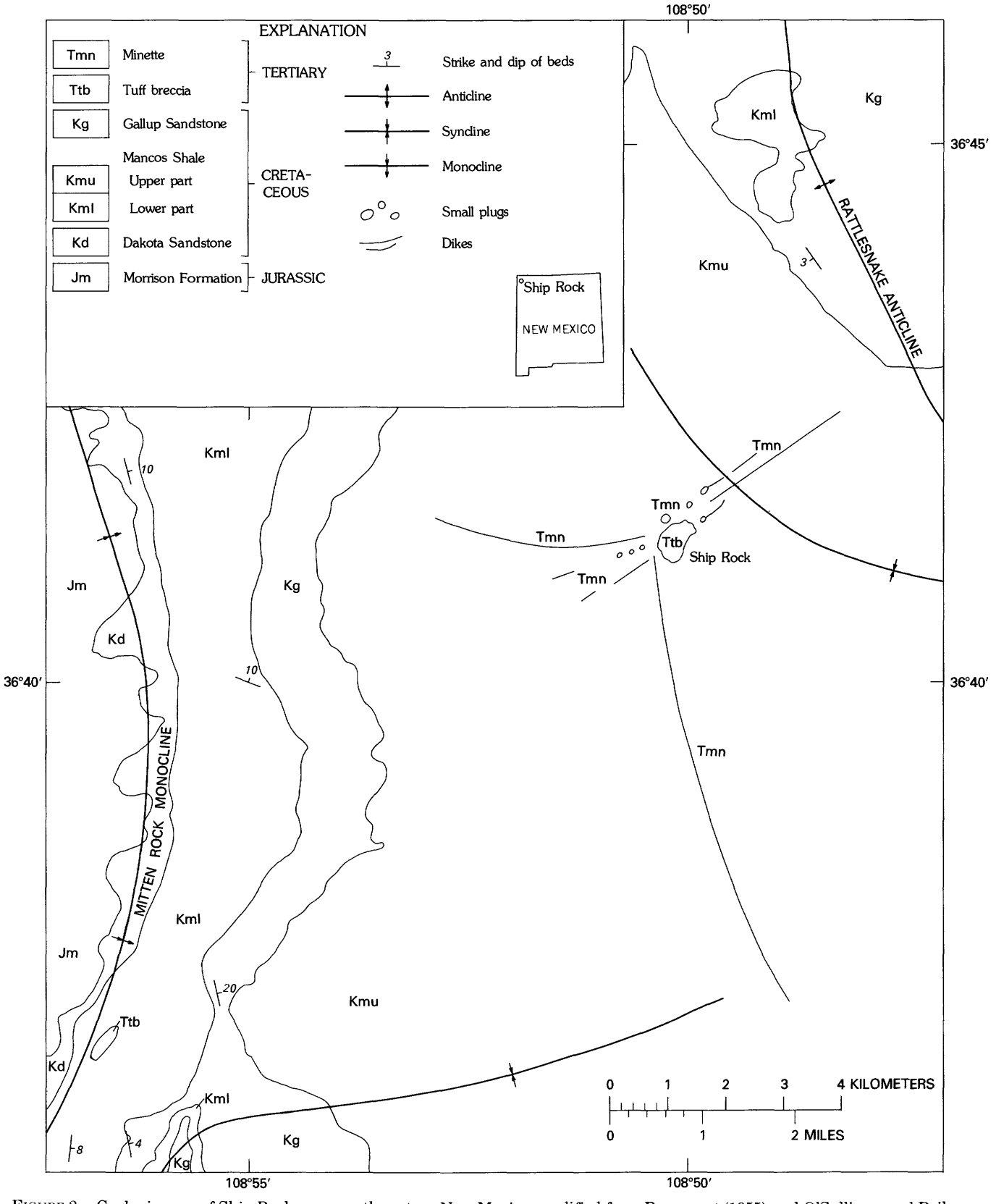

FIGURE 2.—Geologic map of Ship Rock area, northwestern New Mexico, modified from Beaumont (1955) and O'Sullivan and Beikman (1963).

province intermediate in structural height between the San Juan basin to the east and the Defiance uplift to the west. The map of the Ship Rock area compiled by O'Sullivan and Beikman (1963) reveals the following structural details. The northeast-trending Hogback monocline, with about 1,000 m of structural relief, bounds the Four Corners platform 25 km east of Ship Rock. To the west the boundary is less distinct; the north-south-trending Mitten Rock monocline (fig. 2), with about 500 m of structural relief, lies 30 km west of Ship Rock. Beyond the Red Rock monocline 25 km farther west, the total structural relief is about 1,000 m. Sedimentary rocks of the platform are 1,000 m thick near Ship Rock and are underlain by crystalline Precambrian basement rocks. The sedimentary strata are gently folded, and the limbs dip generally less than 5°. The Rattlesnake anticline 5 km northeast of Ship Rock (fig. 2) trends northwest, perpendicular to the northeastern dike. The axis of an adjacent syncline crosses the dike near its southwest end. Eight kilometers south of Ship Rock, a syncline trends east-west, locally perpendicular to the southern dike. The maximum dip of strata near the intrusions is about 3° (Beaumont, 1955).

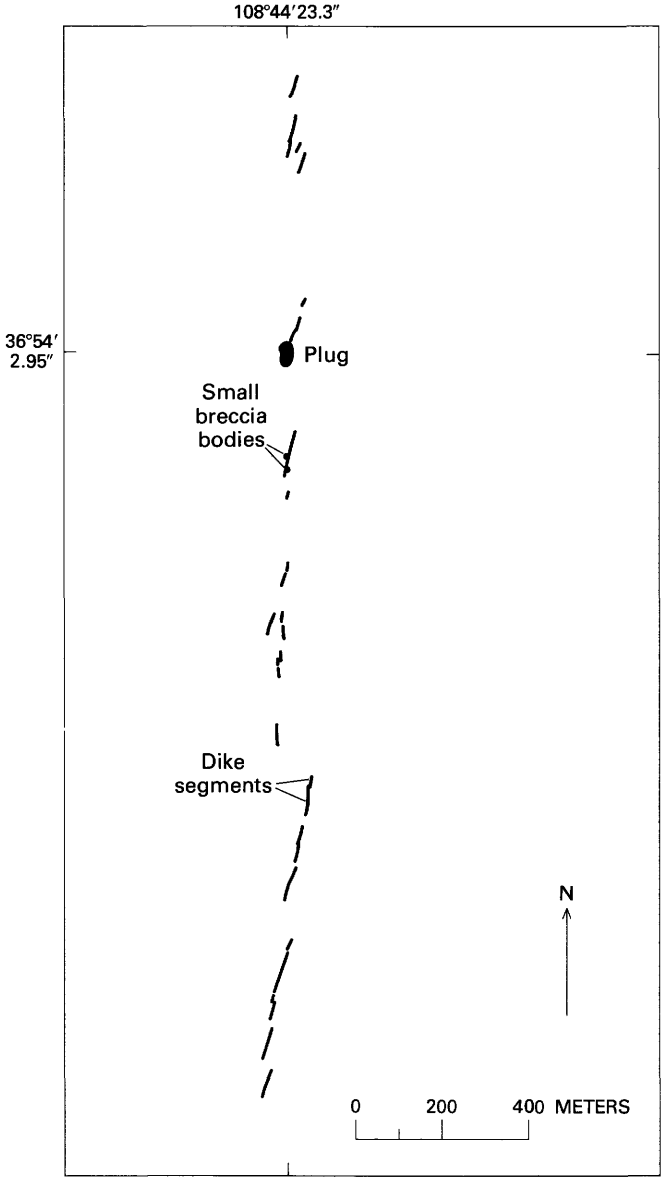

FIGURE 3.—Geologic map of minette intrusion 25 km north-northeast of Ship Rock. Host rock is the Mancos Shale. Intrusive forms include 30 dike segments, a plug, and two small breccia bodies or buds.

The monoclines that bound the Four Corners platform probably were formed during Late Cretaceous and (or) early Tertiary (Laramide) time (Woodward, 1973; Woodward and Callender, 1977), and the gentle folds near Ship Rock are presumably of the same age. Apatite from two samples of the southern dike at Ship Rock yielded fission-track ages of 27±3 and 32±3 m.y. (Naeser, 1971). Using K-Ar methods, Armstrong (1969) determined an age of 30.6 m.y. for rock in the same dike. Thus, we associate a middle Oligocene age with intrusive activity and infer that this activity postdates folding.

Ship Rock itself is about 500 m wide in its greatest horizontal dimension and stands about 600 m above the surrounding plain. Visible for many miles in all directions, it is one of the largest necks among a diffuse group of intrusions and associated extrusions that Appledorn and Wright (1957) referred to as the "Chuska volcanic field." This field occupies an area no wider than 60 km along the northernmost 150 km of the Arizona-New Mexico border. Petrographically, the intrusive rocks of the area include minette, vogesite, basaltic tuff, and tuff breccia (Williams, 1936; Appledorn and Wright, 1957), as well as kimberlite tuff of the Buell Park diatreme (Allen and Balk, 1954). The tuff breccia of Ship Rock is locally cut by irregular sheetlike stringers of minette. Sedimentary bedding near the margin of Ship Rock is flat lying and apparently undisturbed, except in places where wallrocks have slumped into the throat and are now intermingled with the tuff breccia. In those places, some breccias are composed almost entirely of sedimentary material; only the texture of the rock, and rare fragments of minette or flakes of biotite, reveal that a sandstone was comminuted to grain-size fragments as it was displaced during the volcanic event. Along the margins of Ship Rock, some sandstone beds have slumped more than 125 m. Williams (1936) noted an inward-dipping stratification of the tuff breccia near the top and along the margins of Ship Rock and concluded that the top could not be far below the original eruptive crater. By comparison with the

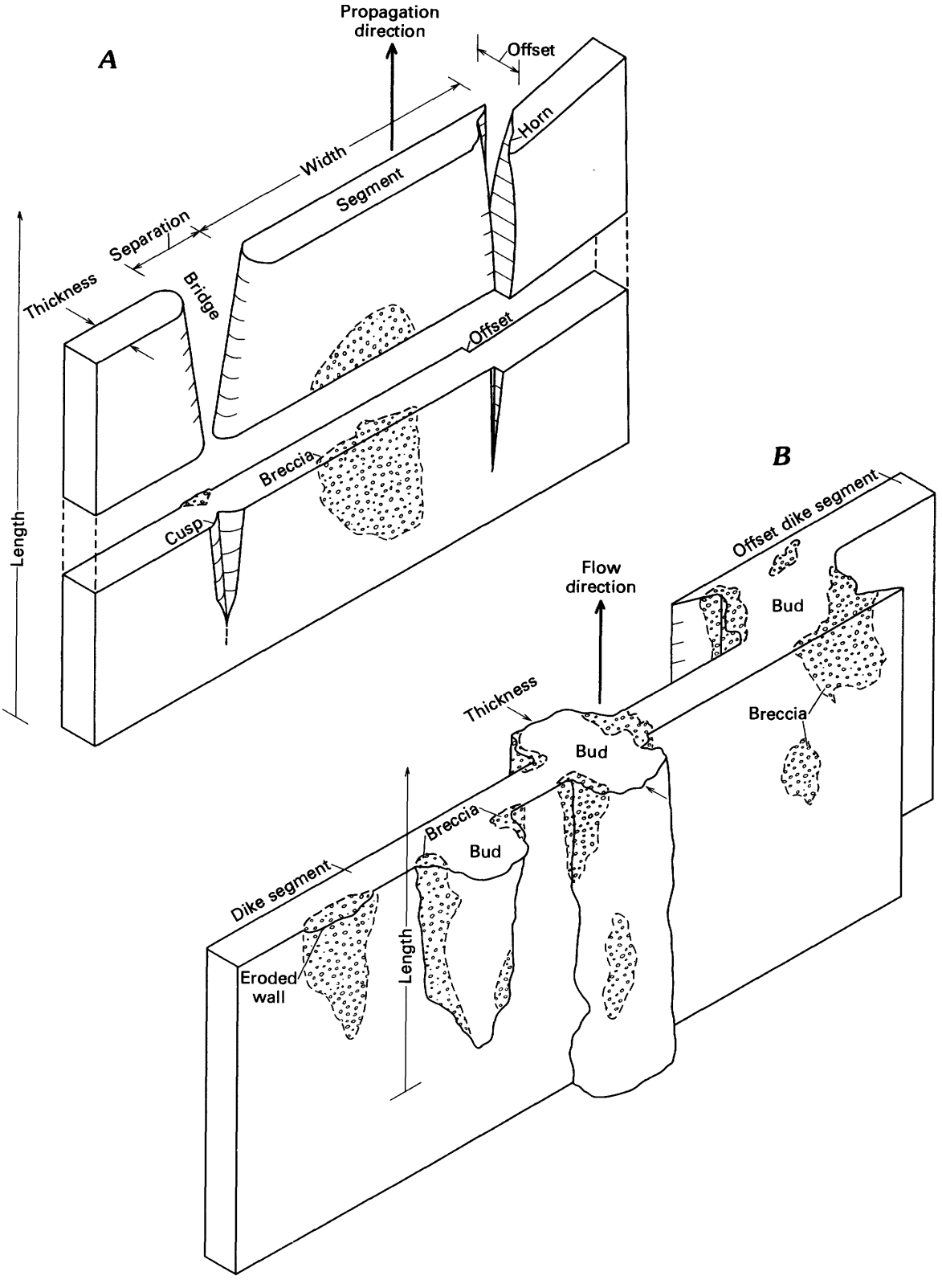

FIGURE 4.—Idealized forms of a dike (*A*) and a dike with buds (*B*). See text for definition of terms.

petrographically similar Washington Pass crater (Appledorn and Wright, 1957; Ehrenberg, 1978) about 70 km to the south, we infer that Ship Rock was emplaced during a maar-type eruption and that this eruption formed a crater as a negative topographic feature, with a floor perhaps 200 m below the surroundings. These estimates of the relief of the crater and the present relief of Ship Rock above the northeastern dike suggest a minimum value of about 750 m for the depth of dike emplacement.

Six conspicuous dikes near Ship Rock form a radial pattern. The largest of these dikes are 9, 4, and 3 km long and trend approximately S. 12° E., N. 80° W. and N. 55° E., respectively. The remaining dikes trend approximately N. 55° E., parallel to the northeastern dike, and are shorter than 1 km in outcrop length. Inspection of the geologic map (fig. 2) reveals that projections of the dikes intersect at a point on the west side of Ship Rock. Alinement of several dikes cropping out on opposite sides of Ship Rock suggests that they may merge at depth. The long dike striking east-west from Ship Rock contains some large buds near its east end. Seven small plugs and irregular breccia bodies are situated on trend with the dikes. Ages of these surroundings intrusions relative to Ship Rock are unknown.

Breccias are present in virtually all the intrusions around Ship Rock. The major components of these breccias are minette and fragments of shale and sandstone; fragments of minette that solidified before incorporation into the breccias are also present. Rounded cobbles of crystalline basement rock are present in some breccias but not in those of the northeastern dike. Typically, the breccias consist of subangular to angular lithic fragments and small irregular bodies of comminuted grains and fragments in a groundmass of minette; these fragments are rarely longer than 100 mm. Some breccias consist solely of crumpled host rocks and contain no minette. For instance, one breccia body, approximately 100 m wide and 50 m thick, on the west side of Ship Rock contains only fractured and comminuted shale. Other breccias are best described as poorly sorted multilithologic sandstone that includes small angular fragments of minette in the matrix. In some places the breccias have a layered appearance suggestive of flow banding. Calcite is present in virtually all the breccias; veins of calcite in host rocks adjacent to some intrusions contain fragments of minette and shale.

The sedimentary sequence in the San Juan basin contains rocks of from Cambrian to Eocene age. The Paleozoic rocks are predominantly calcareous, and the Mesozoic and Cenozoic rocks predominantly clastic. The intrusions crop out in the upper part of the Mancos Shale, which in this area intertongues with the Point Lookout Sandstone of the Mesaverde Group, all of Late Cretaceous age and marine origin. These sedimentary units range from tan argillaceous shale through siltstone to fine-grained sandstone. Although some beds are as thick as 1.5 m, most are thinner than 50 mm and laterally discontinuous. Reeside (1924) measured a total thickness of 2,500 m for the stratigraphic section above the Mancos Shale in the western part of the San Juan basin from a north-south section line 80 km east of Ship Rock. This measurement provides a maximum estimate for the depth of emplacement because all units thicken eastward from Ship Rock. For example, the Mancos Shale is about 200 m thick at Ship Rock (Stroebell, 1956) and about 600 m thick 80 km to the east (Reeside, 1924). A major regional angular unconformity occurs at the base of the Chuska Sandstone, the youngest Tertiary unit in the area, which crops out 25 km southwest of Ship Rock. Because the Chuska Sandstone is older than the minette and the top of the unit is approximately 1,000 m above the northeastern dike, the maximum estimate of 2,500 m is probably far greater than its actual depth. Between the extremes of 750 and 2,500 m, we accept 1,000 m as a good estimate for the depth of emplacement of the dike (table 1).

Densities of saturated sandstone and shale range from about 2.1 to 2.7 g/cm^3 (Daly and others, 1966). We take 2.4 g/cm^3 as an average density for the stratigraphic sequence above the present outcrop, at the time of emplacement (table 1). Using this value and assuming lithostatic loading, we calculate that

TABLE 1.—*Physical parameters for host rocks and minette magma*

[Values of properties of emplacement environment estimated primarily from geologic data; values of properties of shale and minette magma estimated from laboratory or analytical data]

Parameter	Symbol	Units	Value used	Estimated range
Properties of emplacement environment				
Depth	L	m	1,000	750–2,000
Mean density of host host rocks	ρ_r	g/cm^3	2.4	2.1–2.7
Lithostatic pressure	σ	[1]MPa	24	15–60
Properties of shale				
Shear modulus	μ	[1]MPa	[2]---	10^2–10^4
Poisson's ratio	ν	---	0	0.04–0.29
Fracture toughness	K_c	MPa·m$^{1/2}$	[2]---	0.5–5.0
Properties of minette magma				
Temperature	θ	°C	1,000	925–1,050
Viscosity	η	[3]Pa·s	100	50–500
Density	ρ_m	g/cm^3	2.60	2.6–2.7
Heat capacity	$\hat{C}_v$	J/g·°C	1.4	1.3–1.5
Thermal conductivity	k	W/m·°C	1.8	0.5–6.0
Thermal diffusivity	$k/\rho_m \hat{C}_v$	m^2/s	5×10^{-7}	10^{-7}–10^{-6}

[1] 1 MPa=10^6 N/m^2=10 bars.
[2] To be estimated.
[3] 1 Pa·s=10 poises.

the pressure at the depth of the present outcrop was about 24 MPa; the actual pressure may have been as low as 15 or as high as 60 MPa, depending primarily on the error in our estimate of emplacement depth.

Elastic moduli of clastic sedimentary rocks vary rather widely and depend on such factors as water content, confining pressure, and degree of cementation. We cannot easily estimate the effects of these factors. Birch (1966) reported a range of 0.04 to 0.29 for Poisson's ratio ν. Because Poisson's ratio enters our equations for dike dilation as $(1-\nu)$ and most reported values for friable sandstone and soft shale are small compared to unity, we are justified in setting $(1-\nu)$ equal to 1 (table 1). Thus we obtain values for the shear modulus μ by dividing reported values of Young's modulus in half. For several clastic sedimentary rock types, Birch (1966) reported a shear modulus of 3,200 to 47,000 MPa. These rock types include hard, indurated rock; but we are interested in soft, friable rock. For example, Hendron, Mesri, Gamble, and Way (1970) reported values as low as 5 to 115 MPa for undrained samples of soft gray and fissile black shale of Pennsylvanian age. Blair (1955, 1956) reported 6,300 to 9,100 MPa for the fine-grained Morrison Formation of Colorado, 2,800 MPa for the Dakota(?) Sandstone of New Mexico, and 3,500 to 4,200 MPa for a friable sandstone of Tennessee. Dixon (1970), using in-place methods, measured a range of about 400 to 1,700 MPa for sandstone and shale of the so-called Castiac Formation, and of 20 to 60 MPa for some clayey siltstones. Field tests commonly give smaller shear moduli than do laboratory tests, a discrepancy that is probably due to the presence of bedding planes, fractures, and variations in rock properties. We are interested in shear moduli that would be effective over lengths of hundred or thousands of meters. We estimate a likely range of 10^2 to 10^4 MPa for the shear modulus of the host rocks at Ship rock (table 1).

In a later analysis, we estimate a property of the host rock known as fracture toughness, K_c, a measure of the resistance to crack propagation (Broek, 1974). In our case, the crack is a dike or dike segment. Although relatively few experimental data are available for rocks, Clifton, Simonson, Jones, and Green (1976) reported a range in K_c of 0.75 to 1.46 MPa·m$^{1/2}$ for sandstones, siltstones, and shales at room temperature and pressure. Tests on the Indiana Limestone at confining pressures as high as 62 MPa show an increase in K_c from 0.93 to 4.2 MPa·m$^{1/2}$ (Schmidt and Huddle, 1977). Probably, higher temperatures would also increase fracture toughness, although no data on appropriate rocks are available; all these data are for dry rocks with cracks no wider than several centimeters. Thus, the estimated range of K_c (table 1) merely reflects the available data.

The minette, which occurs both in stringers within the tuff breccia of Ship Rock and in the dikes, plugs, and irregular breccia bodies, was originally described by Williams (1936). In hand samples, the minette is dark except for the shiny faces of mica flakes; the rock, commonly fine grained, is medium grained in some larger intrusions. Minette is distinguished by the presence of alkali feldspar (either orthoclase or sanidine), biotite or phlogopite, and diopside. Diopside, phlogopitic biotite, and alkali feldspar make up the commonest phenocryst assemblage at Ship Rock. Vugs are locally present and commonly filled with calcite. Thin-section examination reveals that this mineral is ubiquitous, especially along the margins of the intrusions, where it commonly occupies pseudomorphs of olivine and pyroxene. Vugs are distinguished from vesicles by their irregularity. No vesicles were found during examination of hand samples, although they were present in one of the six thin sections of minette examined. In general, phenocrysts in the minette constitute less than 20 percent of the thin sections. Olivine, though absent in the groundmass of all rocks of the Navajo petrographic province (Nicholls, 1969), is the dominant phenocryst mineral in some hand samples. Olivine phenocrysts are typically corroded or replaced by calcite and epidote. Local disturbance of the euhedral form of olivine where biotite is present implies a reactive relation between the two phases. The centers of diopside phenocrysts have a characteristic spongy texture (Ehrenberg, 1978). Microlites of feldspar and biotite, as well as those of apatite and iron, are visible in the groundmass. One minettic fragment in a thin section of a breccia sample contained plagioclase feldspar and abundant calcite-filled pseudomorphs of olivine; biotite constituted a smaller part of the sample than is common.

The temperature of the minette magma during emplacement is an important parameter in some of the analyses that follow. To estimate the magma temperature, we use reactions that are relatively insensitive to pressure and occur at the expense of olivine in the system $KAlSiO_4$-Mg_2SiO_4-SiO_2-H_2O (Luth, 1967). This system neglects the effects of iron and calcium, as well as of minor components, on mineral stability. Addition of iron to the system would lower the temperature estimate, and calcium should have only a minor effect. Phase equilibrium in the system, however, is extremely sensitive to both water and fluorine. Assuming that olivine, liquid, and a vapor phase were reacting to form pyroxene and phlogopite phenocrysts, the temperature of the

magma would have to have been below 1,000°C, even at pressures as high as 250 MPa. For pressures as low as 25 MPa, the temperature may have been as low as 900°C. Some minette plugs that are presently exposed at near-zero emplacement depth in the Washington Pass, Ariz., area (Ehrenberg, 1978) are nonvesicular in hand sample and were possibly undersaturated with respect to water during emplacement. If the minette at Ship Rock was similarly undersaturated, this temperature estimate is too low. Taking 950 °C as a good estimate of the magma temperature on the basis of phase-equilibrium data at saturation, and accepting the possibility that the minette was undersaturated with respect to water, we estimate the emplacement temperature to have been about 1,000°C (table 1). This estimate may differ from the actual magma temperature by 75°C.

Given a temperature and the chemistry of a magma, we can estimate its viscosity. Five bulk chemical analyses from the southern dike at Ship Rock are available (Williams, 1936; Kay and Gast, 1973; Ehrenberg, 1978). Viscosity, which is calculated empirically (Shaw, 1972), is assumed to be independent of pressure. We use the average of these five analyses and note that variations in chemistry between the samples are no greater than a few weight percent for any element. In addition, we assume that the water driven from samples on heating to 200°C is not juvenile and that it contaminated the samples after solidification. Measurements of the remaining water content range from 0.88 to 1.9 weight percent. At 1,000°C, calculated viscosities are 67 and 164 Pa·s for samples with high and low water content, respectively. For a variation in magma temperature of ±50°C, the viscosities would range from 37 to 129 Pa·s for samples with high water content and from 86 to 329 Pa·s for a sample with low water content. If the magma was indeed undersaturated, the samples containing greater than about 1 weight percent water were probably contaminated after solidification. We take 100 Pa·s as a reasonable estimate of the viscosity of the minette magma (table 1). This value could be in error by as much as a factor of 5, owing to inaccuracies in the data and method of calculation.

We estimate values for the heat capacity, thermal conductivity, and density of minette magma (table 1); all these parameters are relatively insensitive to variations in temperature and pressure. Magma density ρ_m is taken as 2.6 g/cm^3 (table 1), a value we consider accurate to within 5 percent (Bottinga and Weill, 1970). The heat capacity $\hat{C}_v$ and thermal conductivity k of magma differ little from those of rocks and are typically about 1.4 J/g·°C and 1.8 W/m·°C (Clark, 1966; Hanley and others, 1978), respectively. These values imply a thermal diffusivity of about 5×10^{-7} m^2/s.

MAPPING METHODS AND PRECISION OF DATA

We describe our mapping methods in detail because they are unconventional and because we wish to estimate our precision in locating contacts and determining dike thickness. We selected the northeastern dike for detailed mapping because it displays an intriguing variety of forms and is more accessible than nearby dikes, which stand as sheer walls rising as high as 30 m above steep talus slopes. The northeastern dike has been eroded at nearly the same rate as the Mancos Shale, so that it can be walked upon along its entire outcrop length. Elevation of the dike is 1,675 m and 1,620 m at its southwest and northeast ends, respectively, and so the total relief is 55 m; local relief rarely exceeds several meters. The minette and baked shale are sufficiently resistant to erosion to preserve good exposures of intrusive contacts, except where the dike is partly obscured by soil along the 150 m of outcrop near its northeast end. Variation in dike thickness is a critical parameter in the analyses in later sections of this report. A preliminary survey of the dike revealed an average thickness of about 2 m, a maximum thickness of about 7 m, and substantial sections thinner than 1 m along its 2,900-m width. We considered that a precision of about 10 percent in dike-thickness measurements was necessary to compare theoretical results with the observed form of the dike. The procedure employed to achieve this precision is described below.

Vertical aerial photographs, taken along the northeastern dike at about 610 m above ground with a 305-mm lens and 60-percent overlap, yielded 17 contact prints at about 1:2,000 scale. A narrow strip from the center of each photograph was enlarged eight times and used as a base map. Altogether, the enlarged photographs form a strip map 0.2 by 13 m. We used a planetable and alidade to construct a straight line along N. 56° E., nearly parallel to the dike, across all photographs. Repeated measurements of points on the photographs suggest that this line does not diverge more than 0.1 m from straightness over distances of 1 km. Each photograph was scaled by measuring the distance between two identified points on the ground and in the photograph. The mean of 17 scales is 1:228.5±5.8, with somewhat less variation on any one photograph. We made no attempt to correct for these small differences in scale between or within photographs.

Intrusive contacts were drawn on the photographs with a pen line about 0.25 mm wide, equivalent to

about a 5-cm width on the ground. Where the contact is clearly exposed and could be located within several centimeters on the ground, the principal error was introduced in locating and drawing lines on the photographs. This could be done generally within one pen-line width on the photographs or within 5 cm on the ground. Where not exposed, the contact was located in small trenches at intervals of less than 3 m; between these points, we used straight-line interpolation to locate the contact. In general, a conservative estimate of the precision in locating the contacts would be within 0.1 m. With this precision for each of two contacts and an average dike thickness of 2.3 m, we believe our measurements of thickness to be within 0.2 m, or 10 percent, for most of the dike; our largest errors were at the northeast end. The principal error in measurements of dike width is introduced by the varying scales of the photographs, and measurements across several photographs are probably accurate to within 5 percent.

Locations of contacts were digitized to facilitate calculations and comparison with theoretical results. The coordinates of points along contacts relative to the N. 56° E. line were determined at increments of 5.08 mm on the map or of 1.16 m on the ground. Additional points were inserted to improve resolution where necessary. Errors introduced in transferring map measurements to digital data are considerably smaller than those introduced when locating points on the photographs. The resulting data set for all contacts contained 7,660 coordinates. Theoretical analysis requiring dike-form or dike-thickness profiles were performed using a data subset of 5,452 coordinates that excluded internal contacts and coordinates where there were no adjacent points on both sides of the dike.

Our map of the northeastern dike is reproduced from the digitized data in several strips (pl. 1). Because the dike is best viewed as a continuous feature, we suggest that the reader paste the strips end to end. Specific sites along the dike are referred to by their distance from the southwest end along a line trending N. 56° E. In addition, each segment is identified by number, beginning from the southwest end.

NORTHEASTERN DIKE AND ASSOCIATED STRUCTURES

Division of the northeastern dike into 35 segments, with intervening areas of the Mancos Shale, is readily apparent on the map. Variations in dike thickness, in segment width, thickness, and orientation, and in distribution of breccia are also evident. Dike segments range from 8 to 395 m in width, from 0.6 to 4.6 m in average thickness, and from 3 to 979 m^2 in cross-sectional area (table 2). Cross-sectional areas of breccias range from 0 to 201 m^2, and the strike of segments from N. 52° E. to N. 66° E. Bar graphs of segment length, average thickness, and area (fig. 5) reveal no apparent systematic variation in these parameters along the outcrop. However, the strikes of segments do vary systematically along the dike, and the breccias are concentrated in its west half. In this section we describe the orientation of the dike segments and joints as well as structures related to dike propagation and brecciation of the host rock.

ORIENTATION OF THE DIKE

The average strike of the northeastern dike, measured from one end of the outcrop to the other, is N. 56.4° E. The strike of each segment was determined from the orientation of a straight line drawn between segment ends (table 2) and plotted as a function of distance along the dike (fig. 6*A*). Strictly speaking, the segments are not arranged in echelon, where all members are parallel and offset from one another in the same sense. Rather, each segment has a somewhat different strike and may be offset in either direction from a neighboring segment. Strikes of segments systematically vary within a range of 14° along the outcrop length of the dike. Segments striking the most easterly (segments 4, 6–11) crop out at 550 m and at 800–1,400 m from the southwest end of the dike. Segments striking the most northerly (segments 1, 23, 24, 31, 32) crop out at 25 m, at 1,800–2,200 m, and at 2,600–2,700 m. A more continuous measure of strike was calculated from our digitized data set. The local strike at every point along the dike wall (fig. 6*B*) was determined from the orientation of a line connecting adjacent points; this strike was then averaged with that for the corresponding point on the opposite side of the dike. Local strike of the dike may diverge significantly from the strike of any given segment, owing to numerous small structures, such as buds and offsets, along the outcrop. Although orientation of dike segments does vary along their widths, relations between strike and width of segments, as well as sense and amount of offset between segments, are such that along 2,900 m of outcrop, the northeastern dike deviates less than 40 m from a straight line connecting its ends.

We measured the attitude of the contact of the northeastern dike in 20 localities; the orientations of poles to the contact were plotted on the lower hemisphere of an equal-area projection (fig. 7*A*). The average of all dips reveals that the dike is, in general, a vertical structure. The contact dips outward by an average of 81°±11° on the northwest side and 82°±9° on the southeast side; however, a sampling error has

likely been introduced, because overhanging contacts between the dike rock and the Mancos Shale tend to be obscured by rubble. The apparent outward dip of the contact is probably due to this error.

ORIENTATION OF JOINTS

We also measured the orientations of 49 systematic joints adjacent to the northeastern dike (fig. 7*B*). We define a "systematic joint" as one that is vertically continuous through at least a few beds or is longer than 1 m and is part of a set of similarly oriented joints. Such joints can be found in most well-exposed outcrops of silty beds within the Mancos Shale and in virtually all outcrops along the dike. Isolated fractures that are not straight along their length or width were not included in our measurements. Joints near the dike (fig. 8*A*) are highly planar over distances of as much as tens of meters, cut through all the exposed beds, and are spaced as closely as a few centimeters. Such joints are abundant within a few meters of the dike and easily identified where the shale is resistant to weathering. The most distant joint that we found in this set was 15 m from the end of one segment. Comparison of plots of poles (figs. 7*A*, 7*B*) reveals a strong correlation between the orientation of the dike contact and that of the joints. This relation is readily observable in the field, where strikes and dips of systematic joints are commonly within a few degrees of the local dike contact.

To test whether systematic joints adjacent to the northeastern dike are part of a regional pattern, we measured the strike of 194 systematic joints on the

TABLE 2.—*Geometric data for the northeastern dike*

Segment number	Strike (N.°E.)	Width (m)	Maximum thickness (m)	Average thickness (m)	Total area (m^2)	Area of heterobreccia (m^2)	Area of monobreccia (m^2)	Number of stations
1	52	53	1.4	1.1	59	---	---	48
2	60	395	6.5	2.5	968	181	20	341
3	61	88	5.6	3.8	363	21	104	77
4	66	14	1.6	1.0	15	1	2	14
5	60	54	4.5	2.6	141	8	---	48
6	57	142	3.7	2.6	361	14	---	124
7	62	71	2.8	2.0	139	1	---	63
8	63	53	3.1	1.6	86	6	---	47
9	63	104	7.2	4.6	485	63	40	91
10	60	33	3.0	1.6	58	1	14	30
11	65	14	1.0	.6	8	---	---	14
12	64	41	5.3	1.4	58	18	---	37
13	55	9	.6	.4	3	---	---	9
14	60	35	2.1	1.4	49	2	---	31
15	61	81	5.4	2.8	222	14	20	71
16	63	136	3.4	2.6	345	23	---	118
17	64	64	3.3	2.5	157	9	---	58
18	60	8	1.5	1.2	8	---	---	8
19	63	136	5.5	3.1	412	60	2	118
20	62	78	2.9	2.1	166	10	---	69
21	59	197	3.3	2.4	469	13	---	172
22	58	138	3.8	2.1	286	24	4	121
23	54	328	3.3	2.5	829	1	---	285
24	53	69	2.4	1.7	115	---	---	61
25	60	49	2.6	2.2	105	---	---	44
26	58	156	2.7	2.2	254	---	---	101
27	59	220	2.5	2.0	430	1	---	190
28	60	33	2.2	1.9	60	---	---	30
29	57	12	1.4	1.1	14	---	---	13
30	61	38	.9	.7	26	---	---	35
31	55	15	.7	.6	8	---	---	14
32	54	93	2.1	1.6	147	---	---	82
33	61	31	2.3	1.9	56	---	---	28
34	61	91	2.4	1.8	161	---	---	80
35	63	61	3.0	2.0	118	---	---	54
Entire dike	56	2901	7.2	2.3	7181	470	206	2726

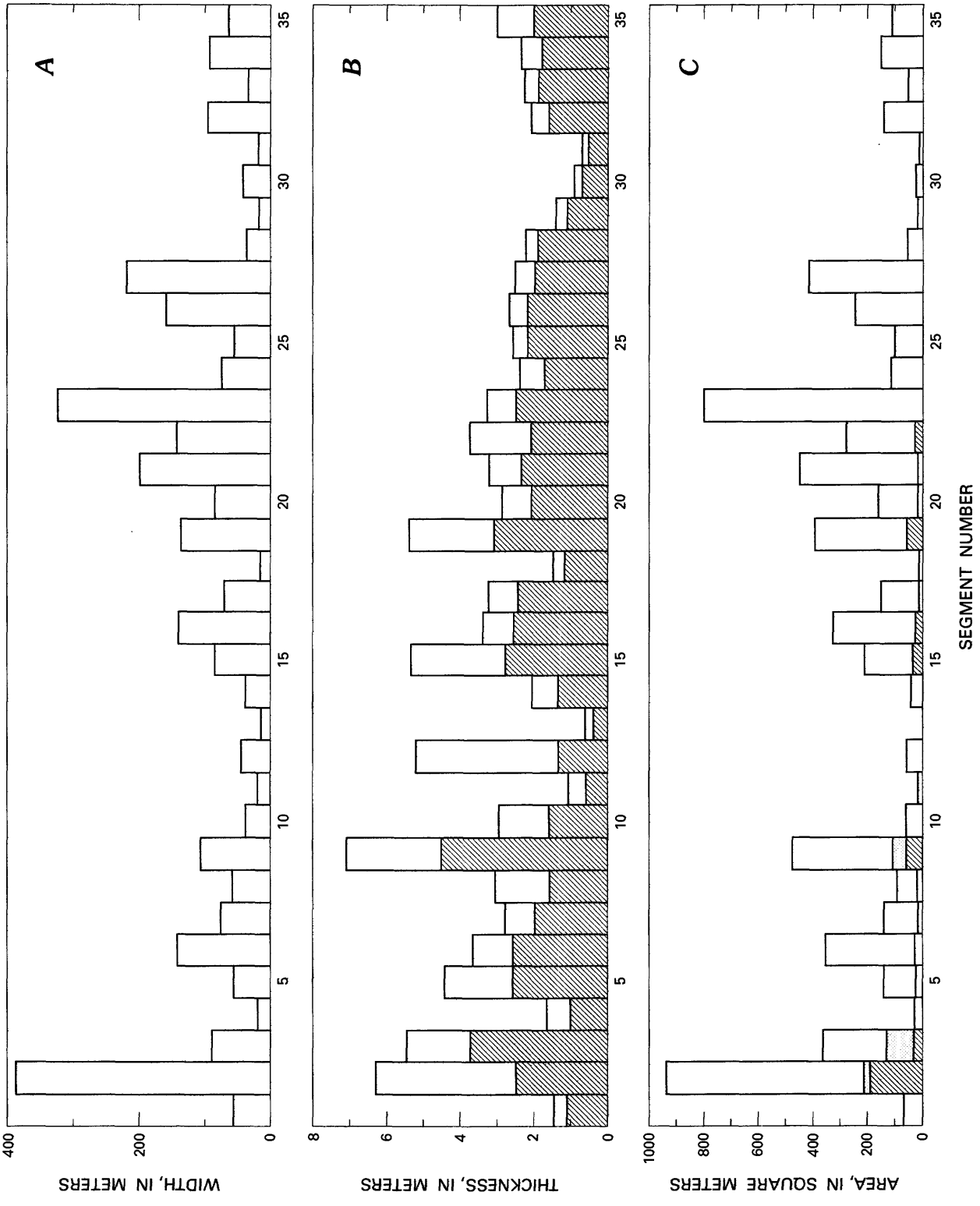

FIGURE 5.—Selected geometric data for segments of northeastern dike. *A*, Width (outcrop length). *B*, Average (crosshatching) and maximum thickness. *C*, Area of entire segment, area of heterobreccia (crosshatching), and area of monobreccia (stippling). See text for description of breccia units.

east side of Ship Rock (fig. 9). Relief is modest in this area, and only a few beds are sufficiently resistant to erosion to form low outcrops that preserve joints. Commonly, a bed of siltstone overlays finely bedded shale that is thus protected from erosion. These beds (marked by dotted lines in fig. 9) span about 60 m of the local stratigraphic sequence around the west end of the dike. Many regional systematic joints within siltstone beds fail to pass into adjacent shales. The regional systematic joints are commonly shorter, not so straight, fail to cut all beds in a given outcrop (fig. 8*B*), and thus are not so apparent a feature as those adjacent to the dike. No variation in preferred orientation was observed among seven traverses (A-G, fig. 9) along outcrops, and so all data were grouped together and plotted on a single rose diagram. A maximum in the frequency of strike of regional systematic joints occurs between N. 70° E. and N. 90° E. In contrast, strikes of segments of the northeastern dike fall between N. 52° E. and N. 66° E., a local minimum on the frequency diagram. These data clearly indicate that minette magma did not fill joints of the regional set. If the regional joints are older than the dike (a relation we could not establish with certainty), they exerted no structural control on the dike as it propagated. These results strongly suggest that the origin of the dike-parallel joints is closely related to the emplacement of the dike.

STRUCTURES RELATED TO DIKE PROPAGATION

Although bedding is nearly horizontal in the areas away from the northeastern dike, we recorded dips of as much as 36°on beds immediately adjacent to the dike. Dips are consistently directed toward the dike and commonly are about 25°. Because the host rocks are poorly exposed along the entire outcrop length, it is difficult to estimate how much of the dike contact is against those tilted beds. Nevertheless, the tilted beds appear to be confined to that part of the dike between 1,300 and 2,300 m. Bedding dips of 20°-30° SE. were recorded between segments 22-23 and 26-27.

The offset and separation of the 35 dike segments are the most apparent measures of deviation of the northeastern dike from an idealized tabular form. "Separation" (fig. 4) is defined as the horizontal distance between the projections of tips of adjacent segments onto a reference line *parallel* to the strike of the segments; separation is negative if tips overlap. "Offset" (fig. 4) is defined as the distance between the projections of tips of adjacent segments onto a reference line *perpendicular* to the strike of the segments.

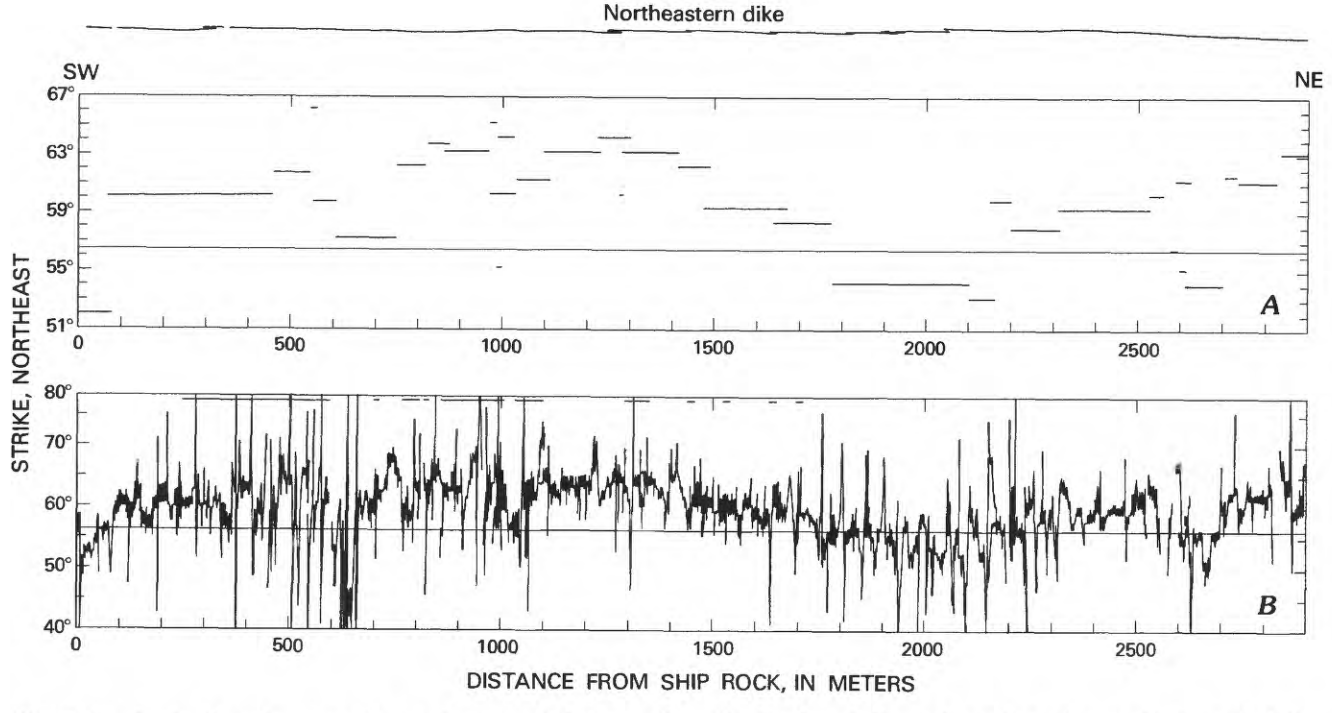

FIGURE 6.—Strike of northeastern dike as a function of distance along dike. Outline of dike is shown for reference. *A*, Average strike of dike segments, measured from relative positions of segment ends; strike of entire outcrop length is also shown (horizontal line). *B*, Continuous variation in local strike, measured from orientation of contacts between digitized points; broken line at top denotes brecciated parts of dike wall.

If adjacent segments are not parallel, these two parameters vary according to the choice of reference line. Plotting offset and separation between segments (fig. 10*A*), using the strikes of both segments as reference lines, we note that overlap tends to increase with offset. The amount of offset and overlap correlates with the form of segment ends (fig. 10*B*): pairs

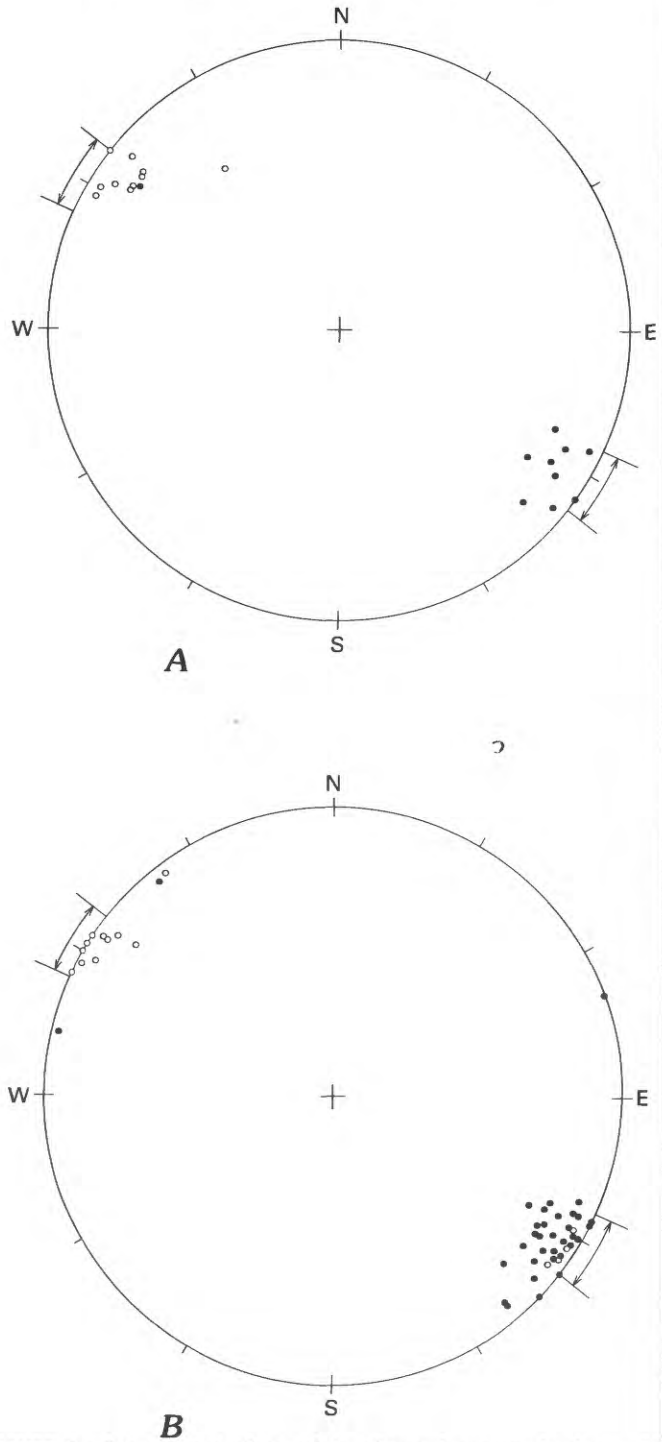

FIGURE 7.—Lower-hemisphere plots of equal-area projections of poles to northeastern dike and adjacent systematic joints. Dots denote measurements from northwest side of dike, and circles from southeast side. Arrows show range in orientation of poles to all dike segments. *A*, Poles to dike contacts; 10 measurements from each side of dike. *B*, Poles to systematic joints; 34 measurements from northwest side and 15 from southeast side.

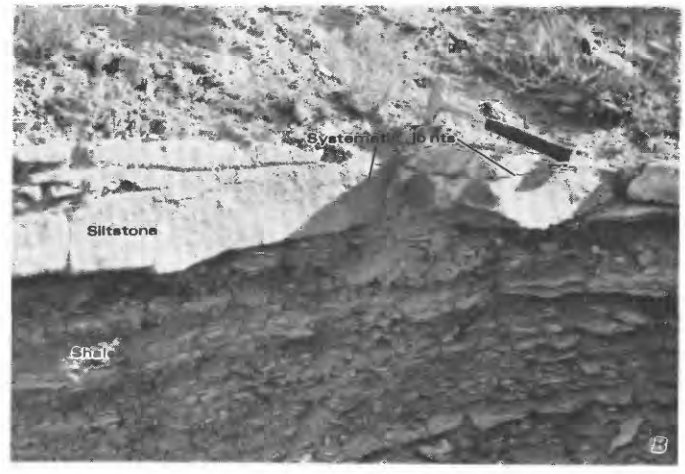

FIGURE 8.—Typical systematic joints. A, Adjacent to northeastern dike. Systematic joints are longer than 5 m and cut all exposed siltstone and shale beds of the Mancos Shale. *B*, About 1 km northwest of dike. One systematic joint cuts a siltstone bed but fails to penetrate underlying shale beds on the Mancos Shale.

of segments with large overlaps tend to have tapered tips (for example, segment pairs 20-21 and 21-22), whereas those with small overlaps (for example, segment pairs 27-28 and 32-33) tend to have blunt tips. In addition, pairs of segments that are only slightly offset tend to have asymmetric tips (for example, segment pairs 16-17, 21-22, and 26-27).

We have described offsets between adjacent segments, but in many places intrusive contacts are offset as much as 0.5 m within a single segment. These offsets (fig. 11*A*) are conspicuous at 1,635, 1,860, 2,010, 2,215, and 2,235 m, where offsets of both contacts of the segments match. These matching offsets mark places where two segments, which propagated with a slightly offset configuration, coalesced into a single wider segment. At 1,805 and 2,470 m, horns mark the coalescence of dike segments; horns are found where segment ends are markedly asymmetric and do not coalesce in the same plane. The geometry of segment pair 16-17 (fig. 10*B*) is a probable configuration for the growth of horns during coalescence.

Some segments have coalesced during propagation even where they are not offset. In those places, small cuspate bodies of fractured host rock commonly remain along the dike wall to mark the sites of coalescence (Pollard and others, 1975). The cusps (fig. 11*B*) are composed of breccias that range from crumpled shale to fragments of shale partly intruded by minette. In general, cusps are found in opposing positions on both walls of a segment. However, some cusps apparently were obliterated by erosion due to flowing magma that left only a single cusp—(for example, at 225-240 m and at 1,550-1,600 m). Our ability to find cusps depended strongly on the degree of exposure. Because breccia commonly weathers more easily than either minette or shale, we believe that many more cusps exist than are shown on our map (pl. 1), particularly near the northeast end of the dike. The local direction of dike propagation is given by the trend and plunge of cusps and offsets, but we were unable to make such measurements owing to the absence of relief along the walls of the dike. Because cusps and offsets mark places where two

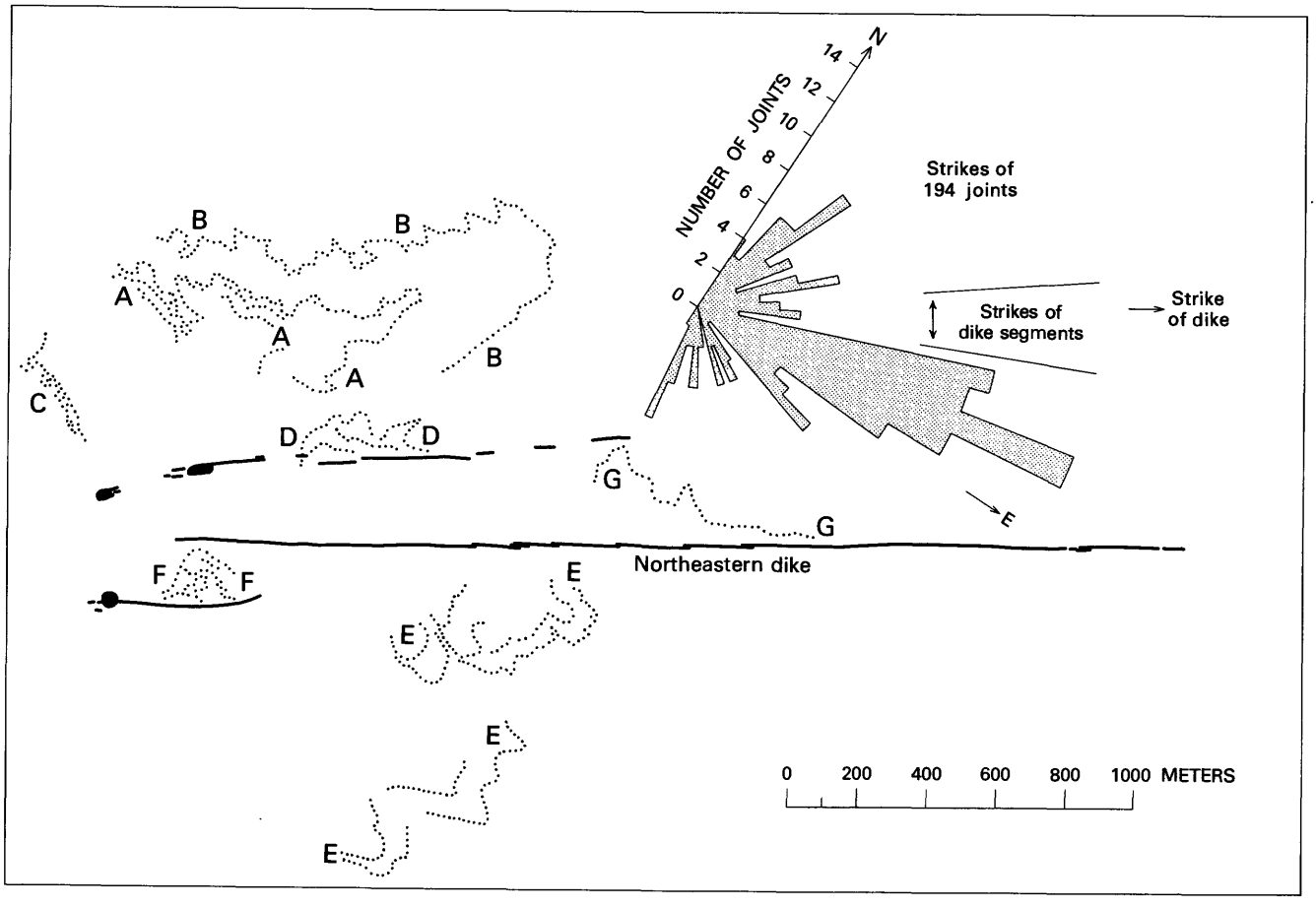

FIGURE 9.—Map of northeastern dike and rose diagram of systematic joints. Strikes of systematic joints were recorded from resistant beds of the Mancos Shale (dotted contours); letters denote traverses described in text. Orientation of 194 systematic joints displays no apparent relation to that of northeastern or nearby dikes.

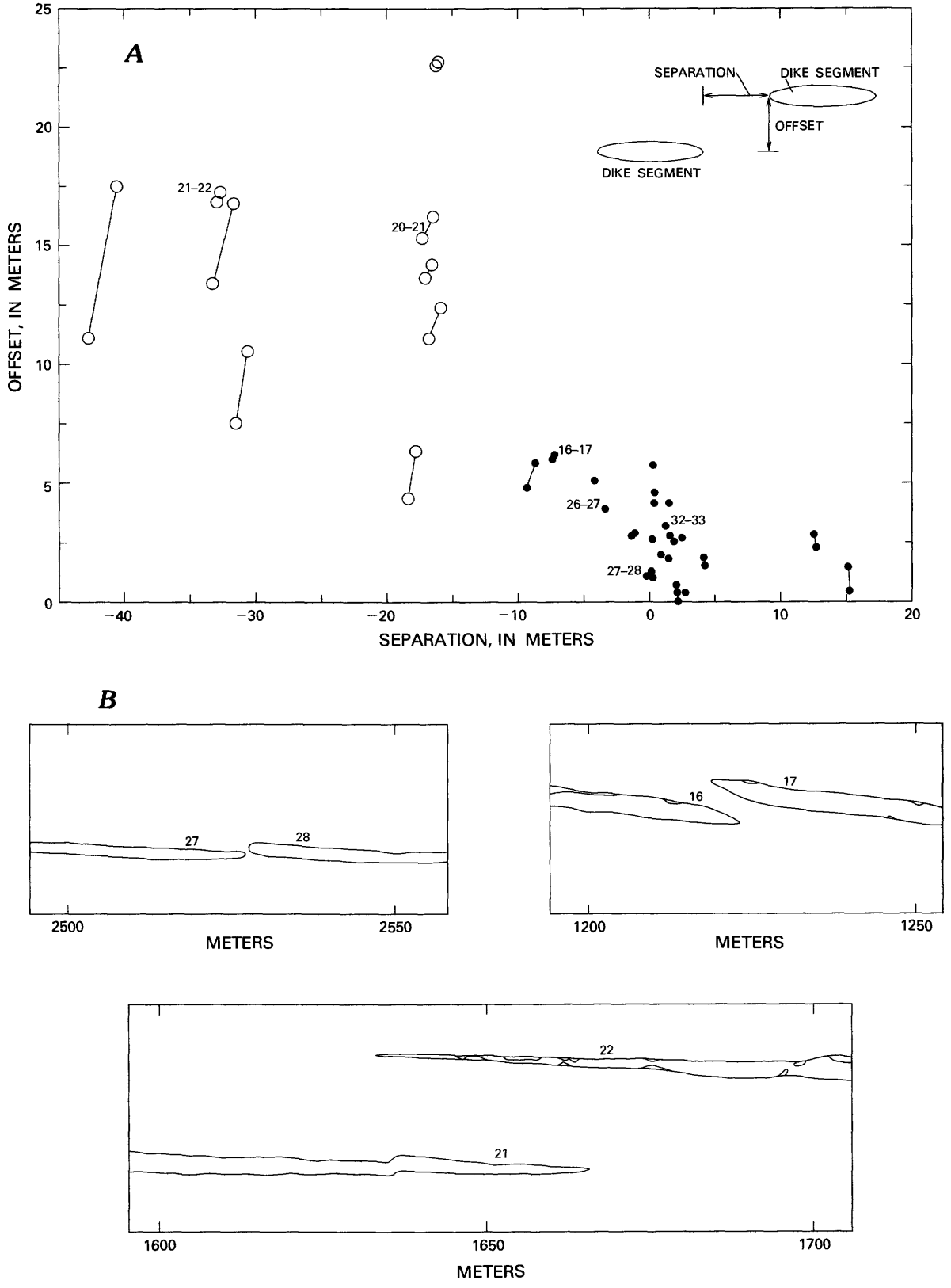

FIGURE 10.—Offset and separation relations for segments of northeastern dike. *A*, Offset as a function of separation (or overlap) for adjacent segments. Offset and separations are measured using strikes of adjacent segments as reference lines, and the two data points are connected by lines. Closed circles denote adjacent segments with less than 10 m of offset or separations; open circles, more than 10 m of offset or separation. Those segment pairs referred to in text are labeled. *B*, Typical forms of segment ends with different offset and separation. Numbers refer to dike segments in plate 1.

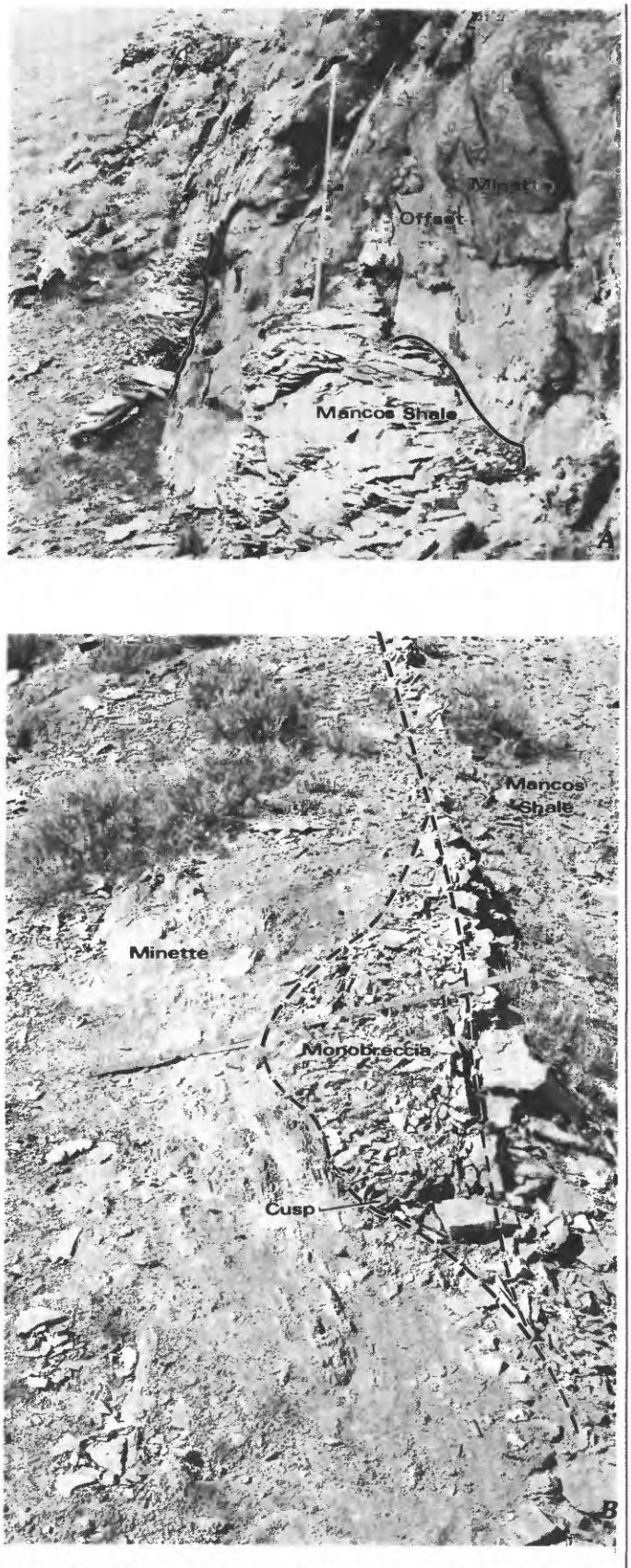

FIGURE 11.—Examples of dike offsets and cusps. *A*, Offset marking site where two segments coalesced at 2,010 m. *B*, Cusp marking coalescence at 1,750 m. Ruler is 1 m long.

dike segments coalesced, there is evidence that many segments narrower than 10 m coalesced to form the 35 segments of the northeastern dike.

STRUCTURES RELATED TO BRECCIATION OF HOST ROCKS

We distinguish two breccia units on our map of the northeastern dike (pl. 1). The first unit, called "heterobreccia," may contain minette in addition to material derived from the host rocks and is less commonly composed almost wholly of host rocks comminuted to a gravelly texture. The second breccia unit, called "monobreccia," consists of fractured, but poorly comminuted, host rock that appears to have been displaced only slightly during dike emplacement. Clasts in the monobreccia are subangular to angular and locally form an interlocking pattern. When referring to rocks of both breccia units, we use the term "breccias" to emphasize their duality.

Examination of the distribution of breccias (fig. 5*C*) yields several interesting relations. Significant amounts of breccias occur only in the west two-thirds of the northeastern dike and occupy 656 m^2, or about 9 percent of the total cross-sectional area of the intrusion (table 2). Dike segment 2 contains the most breccias, 38 percent of the total; and segment 3 contains the most monobreccia, 56 percent of the total. Segments 2 and 3 together contain 49 percent of the breccias. The four segments containing the most breccias are also those that have the highest average thicknesses. Those segments whose form is the most irregular also contain significant amounts of breccias.

Some small cuspate breccia bodies occur where dike segments coalesced, as described above. Other long tabular breccia bodies occur along the dike contact. Some of these longer bodies (for example, at 250–270 m and at 1,530–1,540 m) occupy areas where the contact protrudes slightly; we suggest that these breccia bodies were derived from the adjacent host rocks. Other breccia bodies (for example, at 1,100–1,130 m and at 1,370–1,385 m) lie along parts of the dike contact that do not protrude. Because the walls of the dike would fit back together if the minette and breccias were removed, we suggest that these breccia bodies were formed elsewhere and transported to the present exposure by flowing magma.

Among the most notable features along the northeastern dike are the large bulges at 415, 1,000, and 1,310 m. Each of these buds is at least twice as thick as the average for the remainder of the associated segment. Two buds are confined to one side of the dike, and the bud at 1,000 m enlarges the segment along both contacts. Dike segment 9, the thickest of the 35 segments, contains a substantial amount of breccia: 103 m^2. We suggest that this segment has

been enlarged by erosion of host rocks along its entire width. Segments may also have coalesced by enlargement due to brecciation at segment ends. For example, straight parts of segment 3 are offset at about 510 m, but connected by breccias. In all these places, dike walls would not fit neatly back together, and so these buds represent a nondilational component of the intrusive form.

The importance of alteration of dike form by erosion of host rocks is illustrated by a thickness profile of the northeastern dike (fig. 12*A*). The average thickness of the dike is 2.3 m, and its thickness varies appreciably in its southwest half. By removing those data from our digitized set that correspond to parts of the dike where, by inspection of the map (pl. 1), wallrocks have been eroded, we see that the dike thickness is more uniform and that its average thickness is 0.3 m less (fig. 12*B*). Thus, the thickest parts of the dike coincide with sites of brecciation.

We constructed a geologic map (fig. 13) of the bud at 1,310 m (segment 19, pl. 1). Large parts of this bud are devoid of breccias, which presumably were carried away by flowing magma. The minette is medium grained in the central part of the bud and finer grained elsewhere. Joints within the minette tend to follow the outline of the contact with the wallrocks. The heterobreccia unit, the more common of the breccias, consists of mixtures of wallrock material and minette; relative proportions range from dominantly minette containing a few shale "xenoliths" (fig. 14*A*) to abundant angular clasts of shale, as long as 5 cm, containing minor amounts of minette and finer grained shaly material in the interstices. The monobreccia unit consists of fractured and comminuted Mancos Shale and is devoid of minette; clasts locally are larger than 10 cm in their greatest dimension. We also distinguish outcrops of the Mancos Shale that have been thoroughly fractured but apparently not displaced; these rocks commonly have a gradational contact with the Mancos Shale. The fractured Mancos Shale is distributed along much of the contact with the northeastern dike, and better exposures would undoubtedly reveal still more of the unit. Commonly, outcrops of the fractured Mancos Shale contain a single set of parallel fractures, spaced at intervals of less than a few centimeters, that curve to maintain parallelism with the dike wall (fig. 14*B*). Locally, continued fracturing of wallrocks permitted internal rotation and displacement, and thus created more breccia (fig. 14*C*). The similar orientations of the dike contacts, the fractures in the fractured Mancos Shale, and the adjacent systematic joints are all compelling evidence for the key role of these fractures in the brecciation process.

OTHER DIKES AND PLUGS NEAR SHIP ROCK

In addition to our detailed mapping of the northeastern dike, we studied other dikes and plugs on the east side of Ship Rock. Two smaller dikes are subparallel to and on either side of the northeastern dike (fig. 9); both these dikes intersect plugs.

The northern dike is composed of about 14 segments arranged discontinuously along its 800-m total width. Two plugs intersect the dike at its southwest end (fig. 9). The northeastern plug is about 10 m thick and 20 m wide; the western plug is about 25 m in diameter (fig. 15). Segments of the northern dike near the northeastern plug are buried beneath alluvium but are alined through the center of the plug. The elongate form of this plug indicates that it may be thought of as a large bud. The small dike segment extending northeastward from the northwestern plug (fig. 15) parallels the northern dike. Relations between heterobreccia and minette are irregular and difficult to observe in this plug because of its vertical sides. The heterobreccia (fig. 16) is composed of minette, rounded granitic clasts, and clasts of sedimentary rock (mostly siltstone and shale) that lithologically resembles the local host rocks. The minette occurs as both angular and elongate sinuous fragments. The breccias are interlayered with minette to form a nearly vertical banding in the plug.

The southern plug (fig. 17) is about 30 m in diameter and composed primarily of minette, with some breccias around its perimeter. Systematic joints are visible in the wallrocks adjacent to the plug; one set parallels the southern dike in five of the seven localities where we made measurements (fig. 17). From the northeast side of the plug, the southern dike extends 442 m before being buried beneath sand. The dike trends N. 60° E. near the plug but follows a path that curves gently toward N. 70° E. and then back to N. 35 ° E. at its northeast end. This pronounced curvature distinguishes the southern dike from the nearly straight northern dike (fig. 9). The southern dike comprises three segments, each offset to the left. The orientation of a well-exposed cusp formed by two coalesced segments indicates that the dike propagated nearly vertically. The average thickness of the southern dike is 1.3±0.5 m, on the basis of 42 measurements at intervals not exceeding 15 m. On the southwest side of the plug, this dike is 1.3 m thick and extends 2 m from the plug, where it is obscured by colluvium. Another dike segment, 10 m farther southwest and offset to the right, is partly visible through the colluvial deposits. Only minor amounts of breccias are present along the southern dike.

The contact zone between the southern plug and

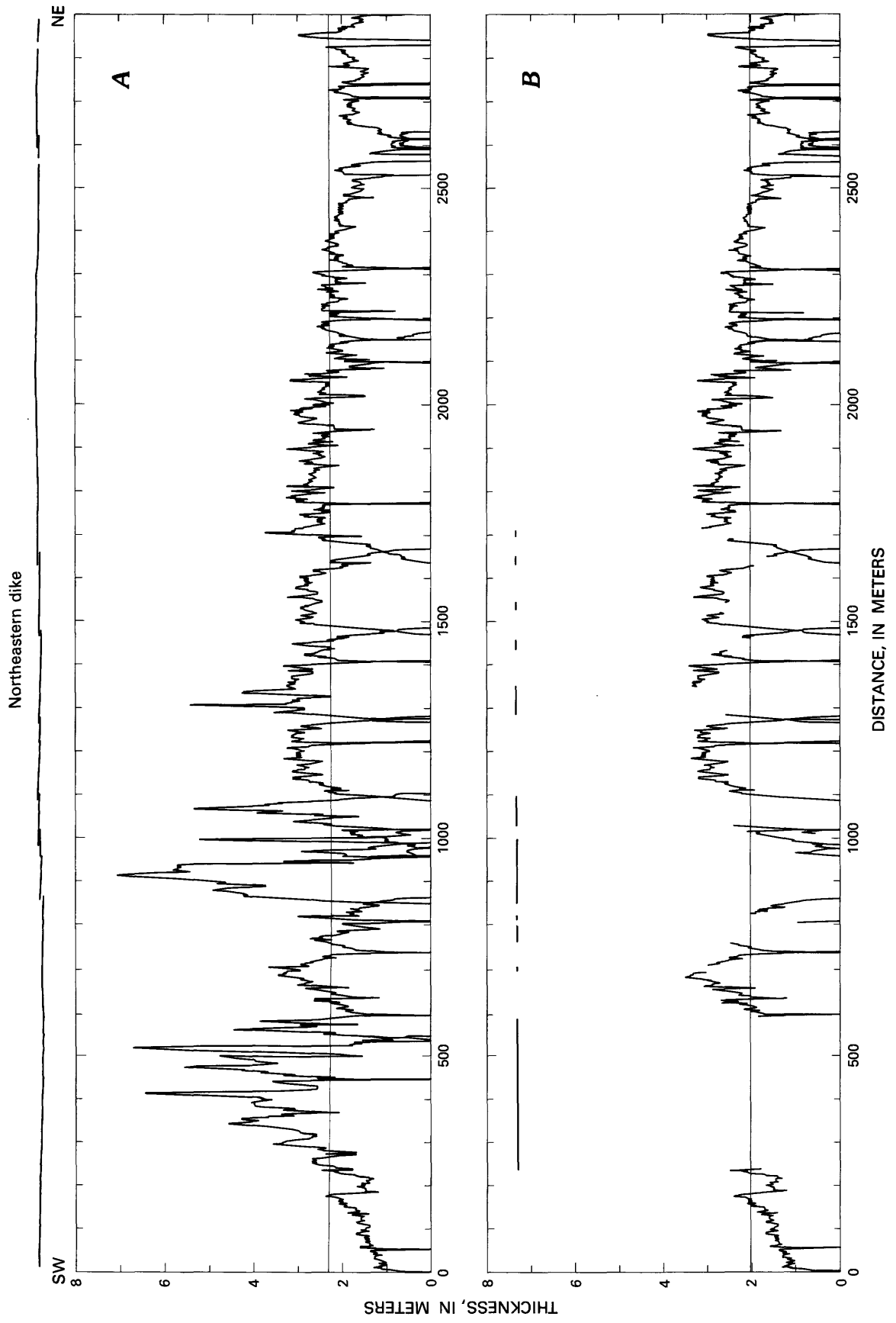

FIGURE 12.—Thickness of northeastern dike as a function of distance from Ship Rock. *A*, Measured dike thickness along outcrop length; average thickness is 2.3 m. *B*, Thickness after removal of data from all parts of dike enlarged by brecciation of host rocks (broken line at top); average thickness is 2.0 m.

dike, which is obscured on the northeast side, is more evident on the southwest side (fig. 17*B*). The minette in the dike is separated from that in the plug by a ring of breccia that cuts the minette of the dike and merges into a zone of fractured minette in the plug. The fractures in both the breccia and minette are filled with calcite and some fine-grained material derived form the wallrocks. A local vertical joint set strikes northeast, parallel to the dike. Joints, bedding planes, and abundant irregular fractures adjacent to the plug are filled with calcite, which also occurs as a secondary mineral in the siltstone host rock. Near the plug, the minette of the dike contains some fragments of siltstone (locally more than 20 volume percent), and both the siltstone fragments and biotite flakes are alined parallel to the dike walls. The minette of the plug, which is darker and denser in hand samples than that of the dike, contains fragments of rock similar to the siltstone in the host rock. The ring of breccia outside the minette of the plug is diverse in composition; the most common breccia is poorly sorted sandstone composed principally of quartz grains in a matrix of calcite, limonite, and clay (fig. 18). Minette is absent in the groundmass but forms discrete grains that solidified before incorporation into the breccia. The breccia and some nearby minette are fractured and coated with calcite in some places; the amount of calcite and the proportion of sedimentary material embedded in the calcite decrease with distance into the plug.

A plausible explanation for these observations is that the southern dike with its large plug (fig. 17) is further developed than the northeastern dike with its small buds. The southern plug is subcircular in plan view and has a diameter much greater than the thickness of the dike. The buds of the northeastern dike are no more than a few times thicker than the mean dike thickness. Although the minettes of the southern dike and plug are petrographically similar, the presence of breccia that grades into the minette of the plug but sharply contacts the dike suggests that the dike solidified while magma remained mobile in the plug. During that time, brecciation and erosion of both host rock and dike rock enlarged the plug to many times the thickness of the dike.

DIKE DILATION AND PROPAGATION

We use elasticity theory and fracture mechanics to investigate the dilation and propagation of dikes. A comparison of analytical expressions for host-rock

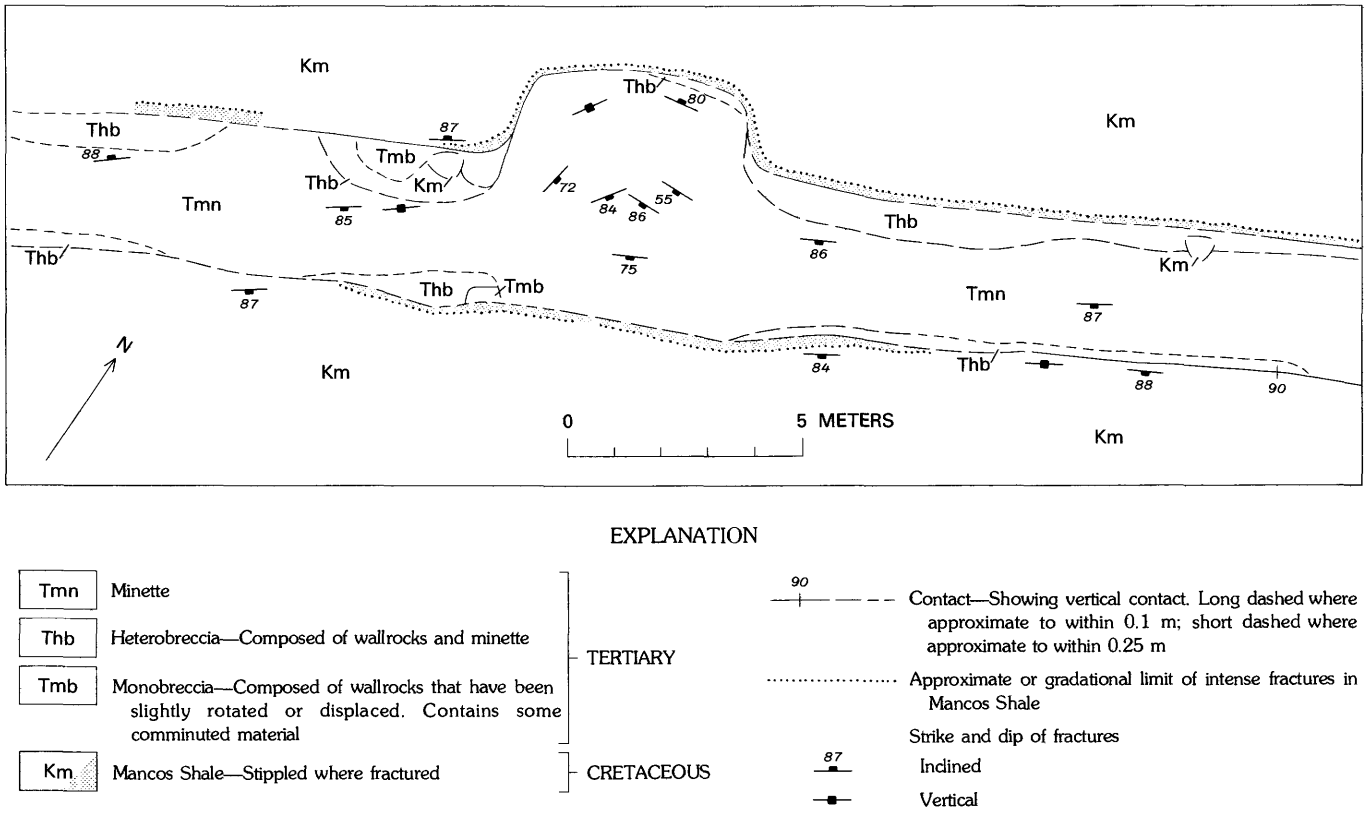

FIGURE 13.—Geologic map of bud from segment 19 of northeastern dike.

deformation around idealized tabular dikes and circular plugs reveals that emplacement of a dike should precede that of a plug if the host rocks behave as brittle elastic solids. An approximate solution for the mechanical interaction of multiple cracks provides a tool for analyzing the northeastern dike, which is

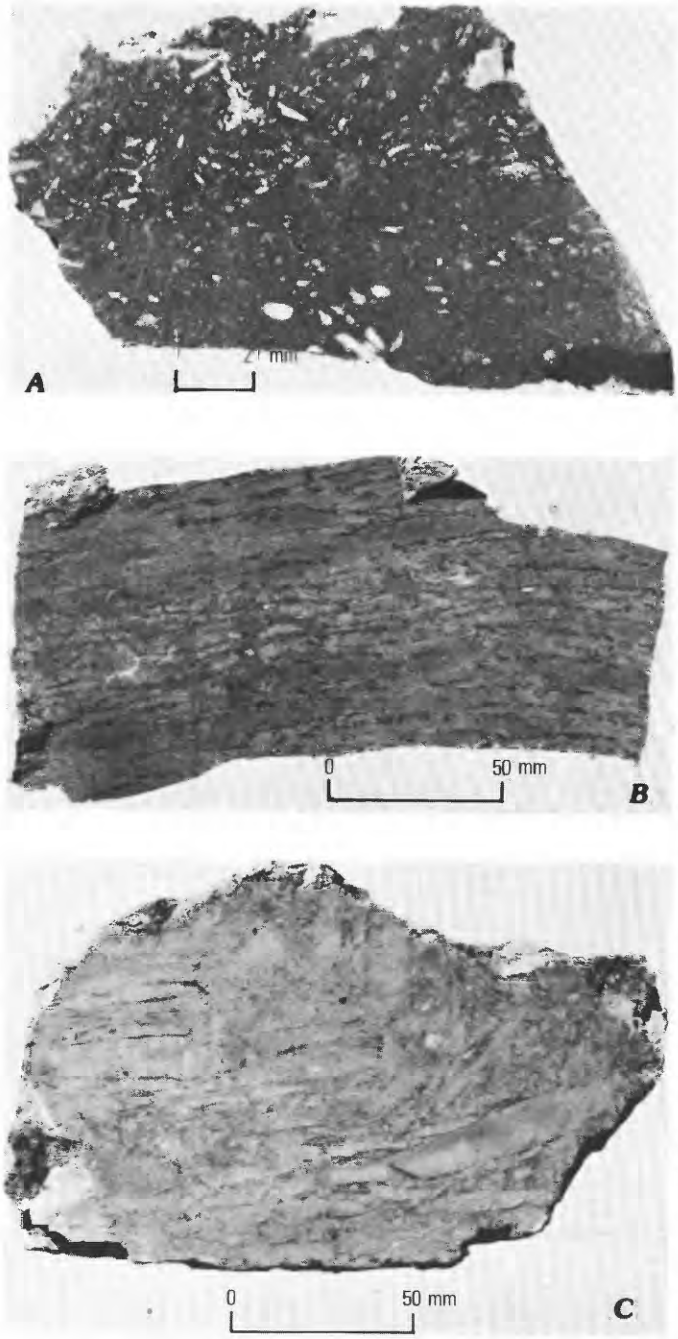

FIGURE 14.—Specimens of rocks from bud on dike segment 19. *A*, Heterobreccia. *B*, Fractured Mancos Shale from northernmost part of bud; fractures parallel contact with minette. *C*, Monobreccia from northernmost part of bud. Note brecciation and internal rotation and displacement of shale fragments.

FIGURE 15.—Northwestern plug. Two small dike segments are visible in front, and Ship Rock stands behind. Plug is about 25 m in diamter. Host rock is Mancos Shale.

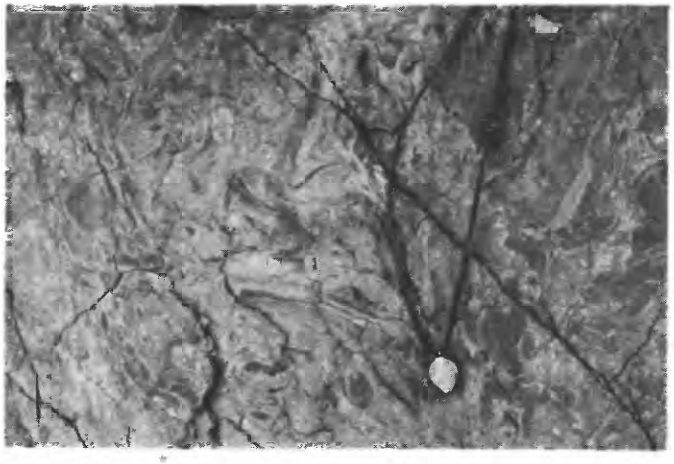

FIGURE 16.—Heterobreccia from northwestern plug, composed of fragments of siltstone, shale, and minette in a groundmass of finely comminuted sedimentary and igneous material. Streaky layering between dark stringers, and clasts of minette and intermixed light sandy material, suggest irregular flow banding.

characterized by 35 discrete segments, and for estimating the ratio of magma driving pressure to elastic shear modulus. We compare the cross-sectional forms of segments dilated by a uniform pressure with the measured forms of dike segments and find them to agree remarkably well. We then use a theory for the propagation of dikes based on the stress intensity at crack ends to study the relation observed between offset and overlap of segments, and to explain the curved form of the southern dike. We suggest that the northeastern dike propagated upward into a region in which the least principal stress was differently oriented, where it responded by forming an echelon pattern of segments. The absence of any regional joint set parallel to the dike and the large stress intensity calculated for segment ends indicate that magma was not simply filling joints but was being forcibly emplaced along newly created fractures.

HOST-ROCK DEFORMATION AROUND TABULAR AND CIRCULAR INTRUSIONS

We believe that the host rocks were deformed in a brittle elastic manner at Ship Rock because of the shallow depth of emplacement and the short duration typical of this kind of igneous activity. To compare several intrusive forms quantitatively, we study the deformation around elliptical cylindrical conduits subjected to uniform internal pressure (Timoshenko

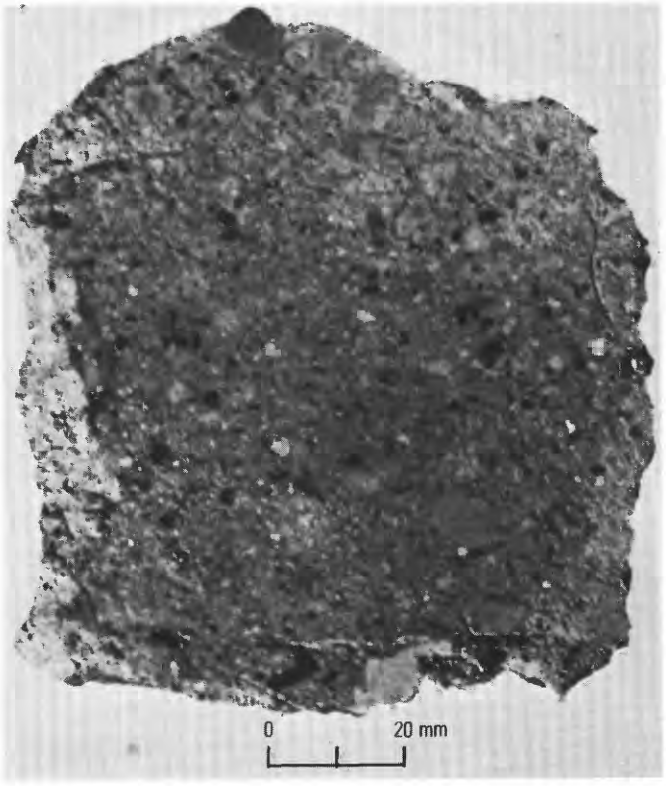

FIGURE 18.—Specimen of heterobreccia from between plug and dike on southwest side of southern plug, composed of coarse-grained sandy material, mostly of sedimentary origin. Dark grains are minette.

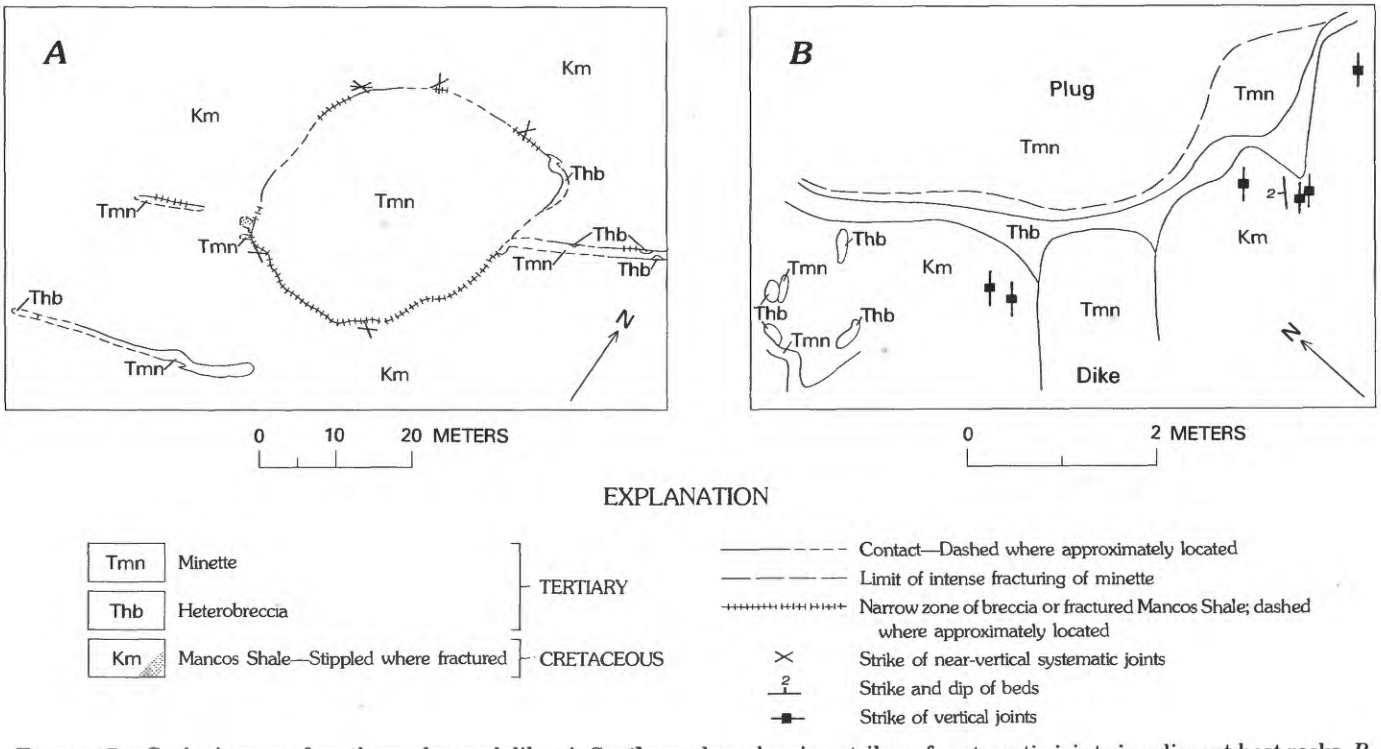

FIGURE 17.—Geologic map of southern plug and dike. *A*, Southern plug, showing strikes of systematic joints in adjacent host rocks. *B*, Relations between southern dike and plug.

and Goodier, 1951, p. 179-204; Muskhelishvili, 1975, p. 347-360). To demonstrate the mechanical advantages of a tabular form, we conduct the following thought experiment. We imagine a large source region for basaltic magma at depth; extending upward from this region are many magma-filled conduits that differ only in the axial ratios of their elliptical cross sections. The entire system is in static equilibrium, and the conduits are so far apart that they do not interact mechanically. We assume that the densities of magma and host rock are identical, and so the driving pressure (the difference between magmatic and lithostatic pressure) does not change with depth. Now, we increase the pressure in the source region so that magma is intruded upward, and ask: (1) which conduit accepts the greatest volume of magma for a given increase in pressure?, (2) around which conduit is the work done on the host rock the least for emplacement of a given volume of magma?, and (3) which conduit is most likely to grow by tensile fracturing of the host rock? We answer each of these questions during the following theroretical analysis.

The conduit boundary C (fig. 19) is an ellipse centered at the origin, with half-axes a and b, and the semimajor axis a is along the real coordinate of the complex z-plane, where $z=x+iy$. The elliptical form permits study of conduits ranging in cross section from tabular ($a>>b$) to circular ($a=b$). It is convenient to introduce the geometric parameters $S=(a+b)/2$ that controls the *size* of the ellipse and $A=(a-b)/(a+b)$ that controls its *axial ratio*. For tabular conduits $A=1$, and for circular $A=0$. The conduits have length L perpendicular to the z-plane, and all features of geometry and deformation vary only in the z-plane; thus the problem is two dimensional, and we specify a plane-strain deformation. The host rock is approximated by elastic material outside the conduit, and regional stresses are ignored. The mechanical effects of magma are approximated by the internal pressure, and we neglect all effects of heat transport and magma flow. We postulate that zero body forces act in the (horizontal) z-plane and that the material is homogeneous, isotropic, and linearly elastic.

The fundamental equations of static equilibrium, and the compatibility of strains and displacements, reduce to the single biharmonic equation $\nabla^4 U=0$, where $U(x, y)$ is the Airy stress function. This stress function may be represented by two functions of the complex variable z in the form $U=\text{Real}\,[\bar{z}\varphi_1(z)+\chi_1(z)]$ (Muskhelishvili, 1975, p. 105-115), where the bar denotes the complex conjugate. A third stress function, $\psi_1(z)$, is related to $\chi_1(z)$ by $\psi_1(z)=d\chi_1/dz$. Determination of the two complex stress functions $\varphi_1(z)$ and $\psi_1(z)$ constitutes a solution to a plane problem of elasticity when those functions result in stresses or displacements that satisfy the prescribed boundary conditions. Stress and displacement anywhere is the elastic solid are determined from these stress functions.

A general solution for an elliptical conduit subjected to arbitrary loading was obtained by Muskhelishvili (1919). Here, a particular solution for internal pressure P is given in terms of the complex stress functions $\varphi(\zeta)$ and $\psi(\zeta)$, where $\zeta=\rho e^{i\theta}$ are the polar coordinates related to z through the Joukowski transformation (Carrier and others, 1966, p. 157-158), which maps the region exterior to the elliptical contour C onto the region exterior to a unit circle γ:

$$z=\omega(\zeta)=S(\zeta+A\zeta^{-1}), \tag{1}$$

where $S>0$, $0\leqslant A\leqslant 1$, and $|\zeta|\geqslant 1$.

This transformation is employed in deriving the stress functions because integration around a circle is somewhat easier than around an ellipse. From Muskhelishvili (1975, p. 353), the appropriate complex functions are

$$\varphi(\zeta)=-PSA\zeta^{-1} \tag{2A}$$

and

$$\psi(\zeta)=-PS\left\{\zeta^{-1}+A\zeta^{-1}[(1+A\zeta^2)/(\zeta^2-A)]\right\}. \tag{2B}$$

To answer the first question posed in our thought experiment, we calculate the change in volume ΔV of the elliptical conduit for a given change in pressure. We first determine the displacements in terms of the complex stress functions. Muskhelishvili (1975, p. 113) gave the following equation, originally derived by G. V. Kolosov:

$$2\mu(u+iv)=(3-4\nu)\,\varphi(\zeta)-[\omega(\zeta)\overline{\varphi'(\zeta)}/\overline{\omega'(\zeta)}]-\overline{\psi(\zeta)}, \tag{3}$$

where the displacements u and v are positive in the x- and y-directions, μ is the elastic shear modulus, and ν is Poisson's ration; the prime denotes differentiation. On the conduit wall, $\zeta=\zeta_0=e^{i\theta}$, and from equations 2 and 3, the displacements u_0 and v_0 are given by

$$u_0+iv_0=PS[\zeta_0-A(3-4\nu)\zeta_0^{-1}]/2\mu. \tag{4}$$

The total volume change ΔV is calculated to first order in P/μ by integrating the local volume change $LDds$ around the conduit contour C (fig. 19), where D is the displacement component normal to the wall and ds is a differential of the arc parameter defining position along C:

$$\Delta V = L\int_C D\,ds$$
$$= L\int_C \left(u_0 \frac{dy}{ds} - v_0 \frac{dx}{ds}\right) ds$$
$$= L \cdot \mathrm{Imag} \int_C (u_0 - iv_0)\,dz_0. \quad (5)$$

After rewriting all terms as functions of ζ_0, the volume change is given by

$$\Delta V = (PS^2L/2\mu) \cdot \mathrm{Imag} \int_\gamma [\zeta_0^{-1} - A(3-4\nu)\zeta_0](1 - A\zeta_0^{-2})\,d\zeta_0. \quad (6)$$

We evaluate the integral, using Cauchy's residue theorem (Levinson and Redheffer, 1970, p. 186-196), and find that

$$\Delta V = PS^2L\pi[1 + A^2(3-4\nu)]/\mu. \quad (7)$$

Comparing conduits having different axial ratios, we see that tabular conduits ($A=1$) are preferred over all others for relieving excess pressure in the source region, in that they achieve the greatest volume change and thus can accept the most magma.

The mechanical work done on the host rock during emplacement of a given volume of magma is calculated as the final equilibrium pressure times the change in volume of the conduit. We only evaluate the work of dilation; we do not include any work done during fracture and inelastic deformation, nor that done either to overcome viscous resistance to the flow of magma or to raise the magma from depth. Eliminating the pressure term from equation 7, the work done is given by

$$\Delta E = \mu(\Delta V)^2 / \pi S^2 L[1 + A^2(3-4\nu)]. \quad (8)$$

For the same volume of magma emplaced, the least

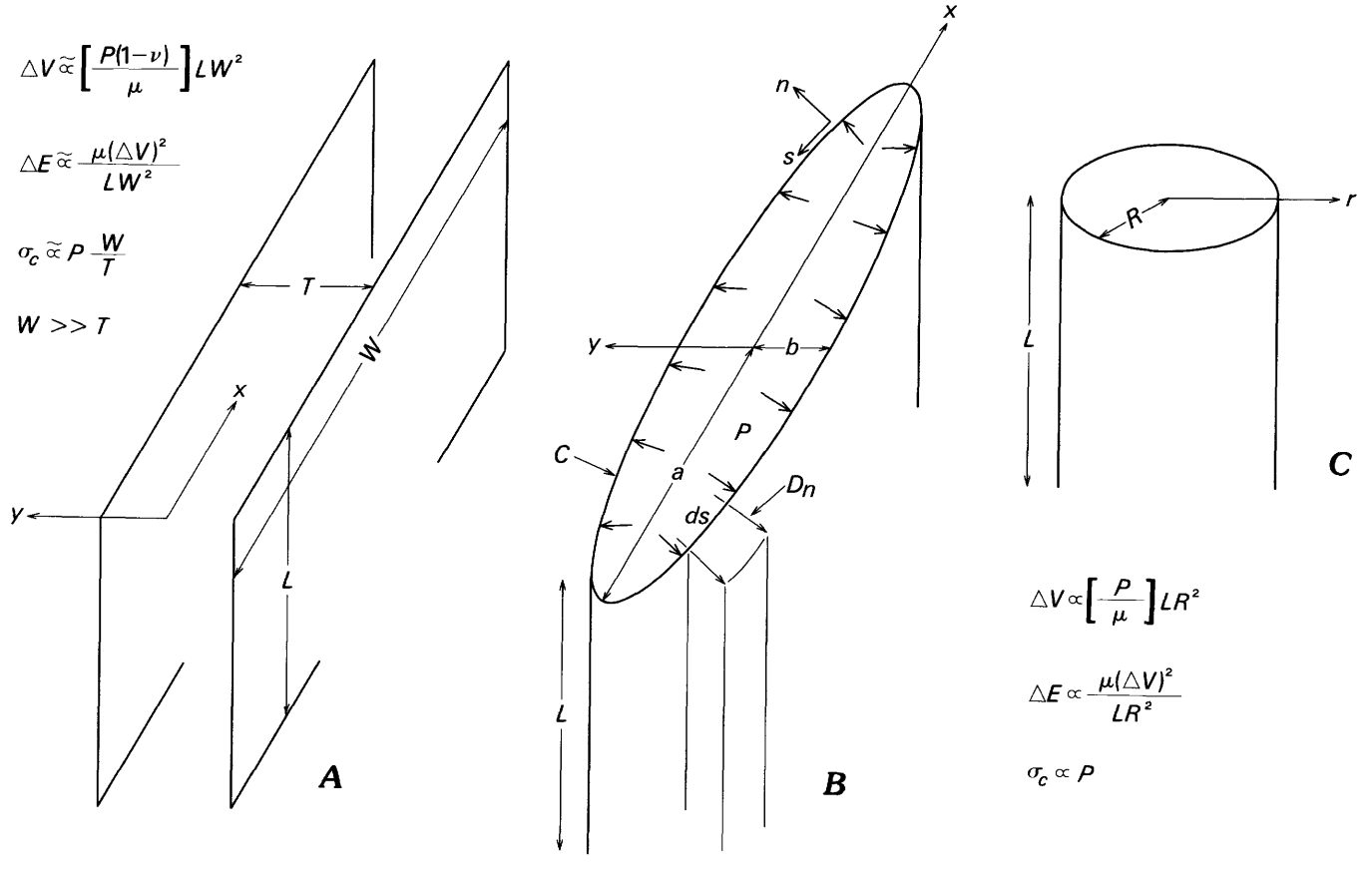

FIGURE 19.—Geometry and parameters of model used to calculate elastic deformation around idealized conduits, showing end members in spectrum of elliptical forms. *A*, Tabular conduit of thickness *T*, width *W*, and length *L*. *B*, Elliptical conduit with semimajor and semiminor axes *a* and *b*, respectively; *C*, contour of conduit wall; *s* and *n*, arc parameters defining position parallel and normal to *C*, respectively; *ds*, differential arc length along *C*; D_n, component of displacement normal to wall; *C*, Circular conduit of radius *R*; *r*, coordinate radial to conduit; ΔV, volume change; *P*, pressure; ν, Poisson's ratio; μ, elastic shear modulus; ΔE, work done on host rock; σ, component of normal stress acting parallel to wall. Coordinate directions are *x*, *y*, and *z* for tabular and elliptical conduits; *r* and *z*, for circular.

work is done around a tabular conduit (A=1), whose axial ratio provides the greatest mechanical advantage over the host rock, so that a given volume is emplaced at the lowest pressure. By comparing circular and elliptical conduits, using equation 8, we determine radii and axial ratios that result in equivalent work done when the conduits are subjected to the same change in volume (fig. 20). Geometries of two spatially associated plugs and dikes near Ship Rock indicate that the work done to emplace a given volume of magma is less for typical dikes than for typical plugs. Thus, in terms of the work done in elastic deformation during emplacement of magma, dikes are a more efficient conduit form than are plugs.

Magma may also be emplaced when an intrusion grows by fracturing of the host rock. To answer the third question posed in our thought experiment, we focus attention on fractures in the conduit wall that open to accept magma, and calculate the distribution of stress at an intrusive contact as induced by a uniform magmatic pressure. More complete analyses that include far-field stresses and comprehensive failure criteria were carried out by Roberts (1970) and Pollard (1973). We use an expression (Muskhelishvili, 1975, p. 115) for the sum of any two orthogonal stresses at a given point and consider those points on the conduit wall:

$$-P+\sigma=4\cdot\mathrm{Real}[\varphi'(\zeta_0)/\omega'(\zeta_0)]. \quad (9)$$

The normal stress perpendicular to the wall is the magmatic pressure P, and σ is the normal stress acting parallel to the wall. The shear stress acting on the wall is postulated to be zero. Motion of a viscous magma generates wall shear stress, but we show below that the magnitude of this stress is small relative to the host-rock strength. The sum of these stresses is

$$-P+\sigma=4PA(\cos 2\theta-A)/(1-2A\cos 2\theta+A^2). \quad (10)$$

Normal stresses are considered positive when tensile. The stress is greatest at the end of the semimajor axis a of an elliptical conduit, where θ=0° and

$$\sigma=P\{1-[4A/(A-1)]\}=P[2(a/b)-1]. \quad (11)$$

Stresses range from a tension of magnitude P for a circular conduit (A=0) to one of infinite magnitude for a thin tabular conduit (A=1). Fracture should occur when σ reaches a critical value, the tensile strength of the host rock.

If elastic dilation of the conduit is insufficient to relieve driving pressure, then a fracture opens and propagates from the wall of that conduit having the greatest axial ratio. During elastic dilation, magma is partitioned among all conduits, but a fracture propagates only from one conduit that then accepts all the magma necessary to relieve pressure in the source region. This fracture continues to propagate at successively lower pressures because its axial ratio is increasing. The stress analysis shows that, when growth of a conduit by fracturing creates space for magma emplacement, dikes are clearly the preferred intrusive form because fracturing occurs at lower magmatic pressures for a tubular conduit than for any other conduit form.

We conclude that the initial form for emplacement of basaltic magma in a particular locality should be that of a dike because it permits emplacement with the least work done in elastic dilation of the conduit and with the lowest driving pressure during propagation of magma-filled fractures. Plugs must grow by an entirely different mechanism. This interpretation is strongly supported by our field observations, which indicate that plugs grow by brecciation and erosion of the wallrocks of a dike. After a plug forms in this way and magma solidifies in the dike, a substantial

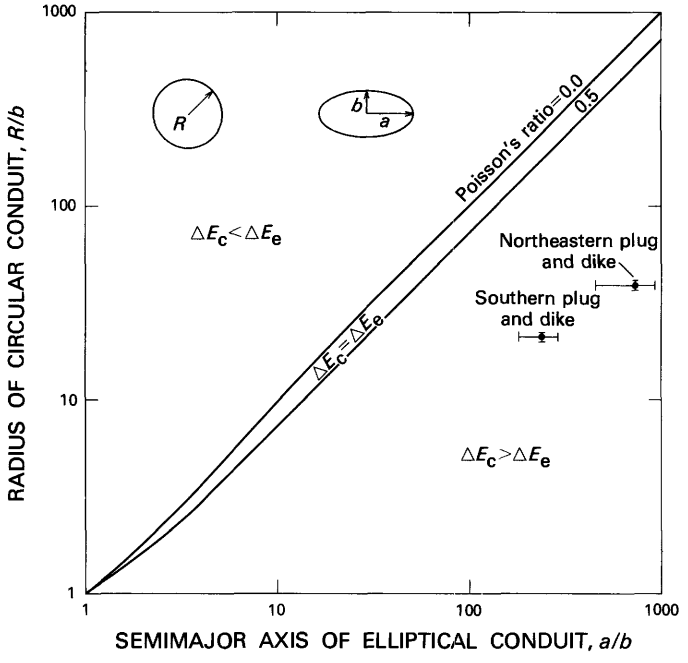

FIGURE 20.—Radius R of circular conduit as a function of semimajor axis a of elliptical conduit, both normalized by semimajor axis b of elliptical conduit. Two curves represent limits on possible range of Poisson's ratio and divide graph area into two fields in which work ΔE_c done on elastic host rock during emplacement of given volume of magma in a circular conduit is either greater or less than work ΔE_e done in elliptical conduit. Two data points with error bars are for spatially associated plugs and dikes near Ship Rock.

increase in magmatic pressure would lead to propagation of another dike away from the plug wall rather than to a significant increase in cross-sectional area of the plug. Laboratory experiments (Hubbert and Willis, 1957), as well as field tests of hydraulic fractures (Howard and Fast, 1970), demonstrate the fracturing of a cylindrical conduit by internal pressure.

SOLUTION TO DILATION AND PROPAGATION EQUATIONS

Individual segments of the northeastern dike display a wide variety of forms (pl. 1). Some observed variations in thickness are clearly due to removal of host rock from the intrusive contact. However, we suggest that the segment form, in places not subject to such removal of host rock, is due to elastic dilation of magma-filled cracks. Dilation and propagation of a crack are driven by magmatic pressure and are resisted by the regional stress and by the strength and elastic stiffness of the host rock. We model a continuous dike or isolated segment, using the solution expressed in equation 2 for a single elliptical conduit in an infinite elastic medium with the initial thickness of the conduit (or crack) set to zero (A=1). On the other hand, the northeastern dike is composed of many segments that were close enough to interact mechanically. Therefore, the local stress introduced by these interactions must be included in our analysis. Unfortunately, solutions for multiple interacting cracks are rare and rather complex (Sneddon and Lowengrub, 1969), and an analytic solution for the particular arrangement of interest does not exist. To study the forms of dike segments, we develop an approximate solution based on the principle of superposition for linear solutions in elasticity.

Each dike segment was loaded by internal magmatic pressure, far-field regional stress, and local stress induced by adjacent segments. Although we do not know the magnitude or distribution of any of these stresses, we may deduce several conditions on them. Pressure gradients and shear stress due to magma flow are neglected because we believe that the present segment forms were attained after cessation of flow. As flow ceased, the host deformed and the conduit changed shape until equilibrium was established under conditions of static pressure in the magma. Because static pressure gradients due to magma weight would be zero in the horizontal plane, we view pressure in that plane as uniform. We follow Anderson (1938) and propose that dike segments were perpendicular to the regional least principal compressive stress, such that no shear stress acted parallel to any segment. We postulate that the regional principal stress was uniform over typical segment widths of, say, several hundred meters. Thus the principal variations in loading along any segment were the local stresses induced by adjacent segments. An important tacit assumption here is that the northeastern dike represents one intrusive event during which magmatic pressure could equilibrate upon cessation of flow throughout the dike.

The relation between magmatic pressure and regional least principal compressive stress is best understood by considering the following characteristic of elastic-crack problems. A particular distribution of normal stress on the wall of a crack and the same distribution, but opposite in sign, of normal stress perpendicular to the crack in the far field result in identical distributions of the normal component of displacement on the crack wall. For example, a uniform driving pressure in the crack causes the same normal displacement as a uniform tension in the far field. Other examples for linear distributions of driving pressure and far-field stress were given by Secor and Pollard (1975) and Pollard (1976). Thus we can mimic the normal displacements of the dike wall (dilation) caused by magmatic pressure and regional least principal compressive stress by applying a uniform normal stress only to a crack wall. This normal stress is the driving pressure p of the magma and is equal to the difference between the magmatic pressure and the regional least principal stress; the regional greatest principal stress acts parallel to the dike and does not contribute to dilation.

Dilation of a single crack creates a nonuniform stress state in the region near that crack. As an example, we plot contours of the component of normal stress acting perpendicular to a single crack and induced by a unit driving pressure (fig. 21). A broad region ahead of the crack is under a tensile stress, but on either side of the crack, the stress induced by dilation is compressive. These stresses are greater than 10 percent of the driving pressure over a region extending about one crack length ahead of and several crack lengths to the side of the crack. Additional cracks outside this region can be studied without including the effects of their interaction. However, segments of the northeastern dike fall well within regions of mutual interaction. The method used to include these interactions is called the Schwarz-Neumann alternating technique or the method of successive approximations (Sokolnikoff, 1956, p. 318-326; Muskhelishvili, 1975, p. 389-390). This method is particularly useful for solving elasticity problems involving stress conditions specified along several different boundaries—here, along multiple cracks. Analytical solutions for the deformations around each crack taken separately are successively

superimposed; each new superposition gives the stresses that match the boundary conditions on one crack but causes mismatches on all others. Stresses on these other cracks are adjusted toward the desired boundary conditions by successive superpositions until the approximation is satisfactory.

This numerical procedure requires a method for superposition of the stress fields due to several cracks. Consider a global coordinate system $z_0=x_0+iy_0$ and a crack centered at z_{0n} of half-width a_n and oriented at angle α_n to $0x$ (fig. 22*A*). A coordinate system $z_n=x_n+iy_n$ is associated with the crack. Another crack is described by these parameters and coordinates with subscript m. A point in coordinate system n is related to one in system m according to

$$z_m=(z_{0n}-z_{0m})\exp(-i\alpha_{0m})+z_n\exp[i(\alpha_{0n}-\alpha_{0m})] \quad (12)$$

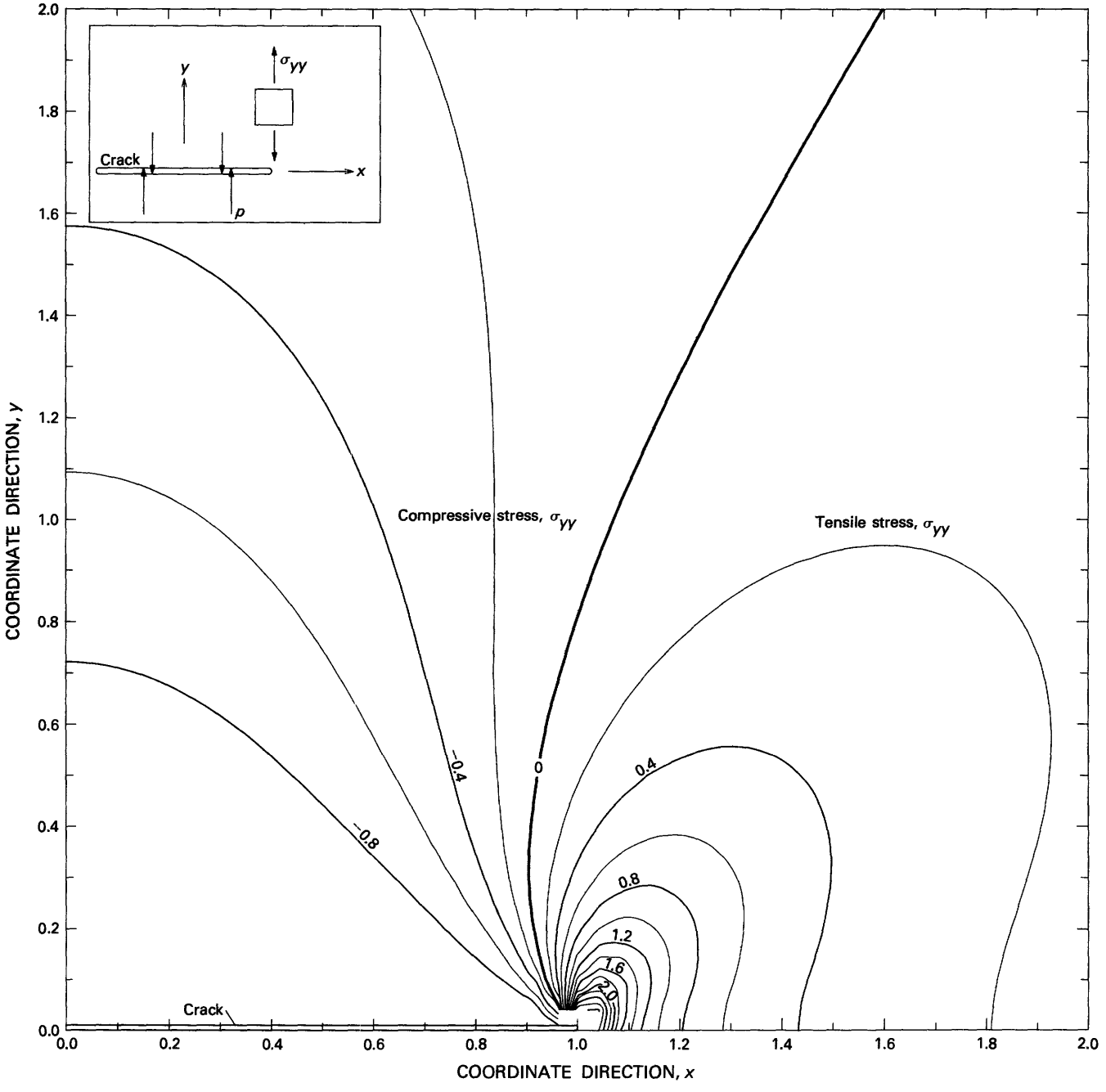

FIGURE 21.—Contours of stress component acting normal to pressurized crack, plotted in quadrant adjacent to crack; contours represent various ratios of stress σ_{yy} to driving pressure p. Contours are characterized by regions of compressive stress at side of crack and regions of tensile stress ahead of crack. Tensile stress increases to infinity at end of crack.

(Pučik, 1972). Stress components in the two systems are related by

$$\sigma^m_{xx}+\sigma^m_{yy}=\sigma^n_{xx}+\sigma^n_{yy} \qquad (13A)$$

and

$$-\sigma^m_{xx}+\sigma^m_{yy}+2i\sigma^m_{xy}=(-\sigma^n_{xx}+\sigma^n_{yy}+2i\sigma^n_{xy})\exp\,[2i(\alpha_{0m}-\alpha_{0n})], \qquad (13B)$$

and displacement components by

$$u^m+iv^m=(u^n+iv^n)\exp\,[i(\alpha_{0n}-\alpha_{0m})] \qquad (14)$$

(Muskhelishvili, 1975, p. 137-141).

The fundamental solution is for a crack in the z-plane subjected to a uniform normal stress N and uniform tangential stress T on opposing intervals of the crack wall (fig. 22*B*). The appropriate complex stress functions were given by Pollard and Holzhausen (1979, eq. 5). We use this analytical solution to approximate nonuniform distributions of normal and tangential stresses on a crack wall by making the intervals of uniform stress sufficiently small and by superimposing solutions for stresses applied on adjacent intervals. For example, we consider a stress state due to uniform pressure in a single crack (fig. 21); here, the interval extends from one crack tip to the other. Now, we imagine introducing a second crack of unit half-length a along the line $0.8\leqslant x\leqslant 2.8$, $y=0.2$. Pressure in the first crack induces a compressive stress across the left-hand part of the second crack and a tensile stress across the right-hand part. To remove this normal-stress distribution, we divide the second crack into numerous intervals and apply the appropriate tension and compression along the left-hand and right-hand parts, respectively; then, we apply a uniform pressure in the second crack. These two operations alter the stress acting on the first crack; this stress must be adjusted back toward a uniform pressure in successive steps. We adjust shear stresses in the same manner. Stresses and displacements anywhere in the region are calculated for each superimposed solution and accumulated during succeeding steps. We use the difference between normal components of displacement on opposing points of the crack wall to characterize the dilation. The component of displacement parallel to the crack is ignored, even though it is of the same magnitude. This procedure is justified because the normalized displacements u/a and v/a are of the same order of magnitude as p/u, and for materials as stiff and weak as rock we find that $p/u<<1$. Displacements before failure and propagation of a dike segment are very small relative to the segment width, and so displacements parallel to this width have little effect on the cross-sectional form.

Now, we consider propagation of dike segments, using the methods of linear elastic fracture mechanics (Tetelman and McEvilly, 1967, p. 38-85; Broek, 1974, p. 3-23, 67-90). This theory relies on the fact that the stress field near the tips of a crack may be approximated by equations of the form

$$\sigma_{ij}(r,\theta)\simeq K_I f_{ij}(\theta)/(2r)^{1/2} \qquad (r<<a), \qquad (15)$$

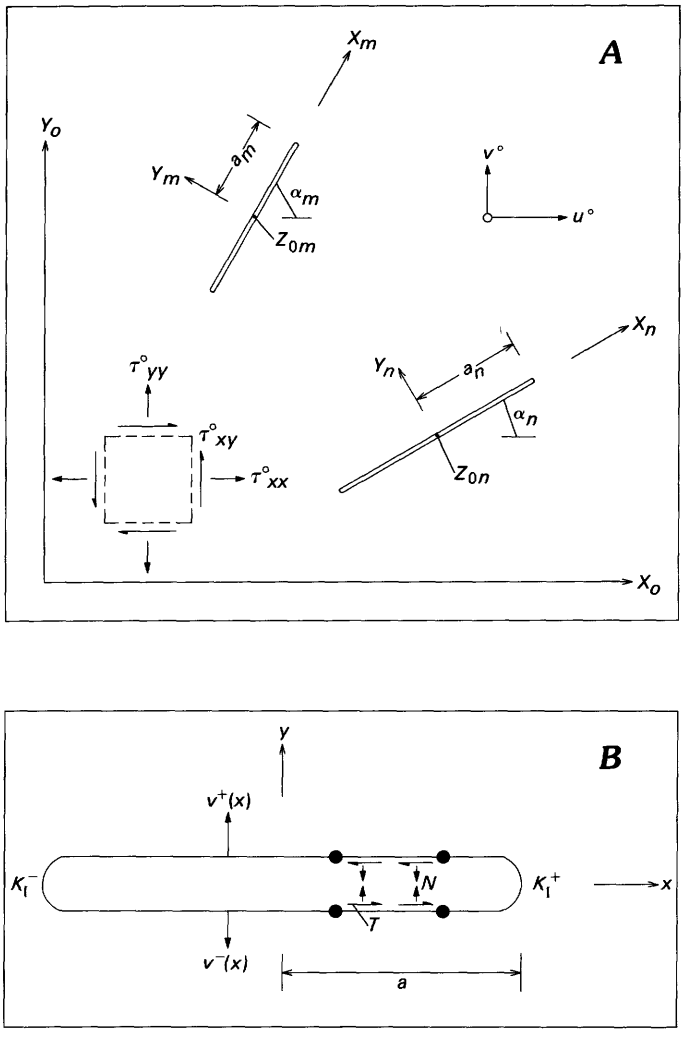

FIGURE 22.—Geometry and parameters of model used to calculate dilation and propagation of multiple interacting cracks by method of successive approximations. *A*, Parameters for cracks include center z_0 relative to global coordinates (x_0, y_0), half-width a, angle α, and local coordinates (x, y). Each parameter is identified with a particular crack by an appropriate subscript. Stresses denoted by σ, and displacement by (u, v); positive directions indicated by arrows. *B*, Normal and tangential stresses N and T, respectively, acting uniformly over two opposing intervals of crack wall (area between dots); dilation is given by difference $v^+(x)-v^-(x)$. K_I^+ and K_I^- are mode I stress-intensity factors at $x=\pm a$, where a is half-width of crack.

where the σ_{ij} are the stress components, (r, θ) are coordinates in a polar system centered at the crack tip, K_I is the stress-intensity factor, and the f_{ij} are functions only of the angle θ. Equation 15 is valid for any loading on the crack wall or in the far field that leads to dilation. The distribution of stress, controlled by the $f_{ij}(\theta)$ and $1/r^{1/2}$, is independent of the loading, whereas the magnitude of stress is directly proportional to the stress-intensity factor. The failure criterion is that the crack will propagate if K_I increases to K_c, the critical stress intensity or fracture toughness, presumed to be a material property. Magmatic pressure and regional stresses contribute only to dilation and the resulting mode I stress-intensity factor. Crack interaction, however, may introduce a shear stress parallel to the crack that leads to a mode II stress-intensity factor. The relation between this factor and propagation is obscure, although Erdogan and Aksogan (1974) and Sih (1974) suggested that shear stress should cause cracks to propagate out of their plane. A left-lateral shear creates a negative K_{II} and causes propagation into the first and third quadrants; a right-lateral shear creates a positive K_{II} and causes propagation into the second and fourth quadrants. The direction of propagation depends on the magnitude of the ratio K_{II}/K_I, such that deviations from in-plane propagation increase as the ratio increases. We calculate the stress-intensity factors from the first complex stress function (Sih and others, 1962):

$$K_I - iK_{II} = (2/a^{1/2})\varphi'(\zeta) \qquad (\zeta = \pm 1), \quad (16)$$

where the derivative is evaluated at $\zeta=+1$ for the positive end of the crack and at $\zeta=-1$ for the negative end. For each superposition, an increment to the stress-intensity factors is calculated for the ends of the crack on which the load is applied.

MECHANICAL INTERACTION OF DIKE SEGMENTS

To illustrate the possible effects of interaction on dike-segment form, we consider two examples. In the first example (fig. 23*A*), a pair of collinear cracks, with distal ends at $x=+1$ and $x=-1$, are dilated under uniform pressure, and the ratio $p(1-\nu)/\mu$ is arbitrarily set at 0.01. The form of several pairs with different widths are difficult to distinguish from the symmetrical elliptical forms of isolated cracks, although closely spaced adjacent ends are somewhat blunter than distal ends.

More striking interactions are apparent in the second example (fig. 23*B*), in which we consider a pair of parallel but offset cracks. Once again, the distal ends are held at $x=+1$ and $x=-1$, but now the cracks are offset by 0.1. For solutions in which the separation of adjacent ends is positive and greater than the offset, the crack form is nearly elliptical. As the separation decreases and becomes negative (cracks overlap), a pronounced change in form due to interaction occurs near adjacent ends: the sides of cracks closest to one another are warped inward, opposite sides straighten, and the adjacent ends become tapered. These theoretical forms should be compared with the forms of adjacent segment ends of the northeastern dike (pl. 1; fig. 10*B*). Although some inelastic deformation probably occurred near the ends of these segments, their forms are nearly identical to those of the elastic cracks.

Now we illustrate the effects of segment interaction on dike propagation, using the same pairs of pressurized cracks. The mode I stress-intensity factors increase at both ends of collinear cracks as the amount of separation decreases (fig. 24*A*). For separations less than 0.5, stress intensity at the distal ends of the cracks increases less rapidly than at adjacent ends. Thus we expect collinear dike segments to propagate preferentially toward one another and to coalesce, owing to greater stress intensities at adjacent ends. This expectation is corroborated by field observations of the northeastern dike; many collinear segments apparently coalesced to form wider segments and left cusps of breccias. A very few examples of collinear segments (pairs 18-19, 27-28) exhibit closely spaced but separated ends; for these segments, we suggest that the site of coalescence lies just below the outcrop.

Offset cracks have mode I stress-intensity factors at both ends that vary inversely with the amount of separation, similar to collinear cracks (fig. 24*B*). However, as separation decreases to zero and cracks overlap, the stress intensities at adjacent ends decrease abruptly and fall below values at distal ends for overlap greater than offset. Stress intensities at distal ends increase monotonically toward unity, the magnitude expected for a single crack of unit half-length. Thus, offset dike segments should propagate perferentially toward one another until adjacent ends overlap somewhat, and then these ends should cease propagating. Data on offset and separation (or overlap) presented earlier (fig. 10) corroborate this conclusion: most offset segments of the northeastern dike overlap adjacent segments by distances comparable to their offset.

To examine the propagation path of the offset cracks, we calculate the ratio K_{II}/K_I at distal and adjacent ends (fig. 24*C*). At distal ends, the near-zero ratio for all separations suggests a straight propagation path. At adjacent ends, the small positive ratio

for positive separations greater than the step indicates a weak tendency for paths to diverge. As the separation approaches zero, the sign of the ratio changes and the magnitude dramatically increases, a behavior indicating a greater tendency for paths to converge. The final configuration at adjacent ends should look something like two interlocking hooks. An example of this type of interaction is evident in the relation between the northeastern and southern dikes (fig. 9). Although these two dikes are nearly parallel along outcrops that are distant, as the outcrops are traced toward adjacent ends their paths first diverge and then converge. Swain and Hagan (1978) produced a similar configuration for two cracks in a small laboratory specimen of plastic. This configuration has been observed for dike segments (Pollard, 1973, p. 256) and for tensile cracks in granite (Johnson, 1970, p. 364), basalt, and mud. In contrast, the northern dike is nearly straight along its entire outcrop, although it overlaps the northeastern dike considerably. The apparent absence of mechanical interaction between the two dikes suggests that the northern dike was not contemporaneous with the two dikes to the south; that is, sufficient time passed between emplacement for stresses to return to ambient values.

Individual segments of the northeastern dike (pl. 1) are nearly planar. We suggest that the tendency for out-of-plane propagation due to mechanical interaction was overwhelmed by an anisotropy either in stress or in material properties that was oriented

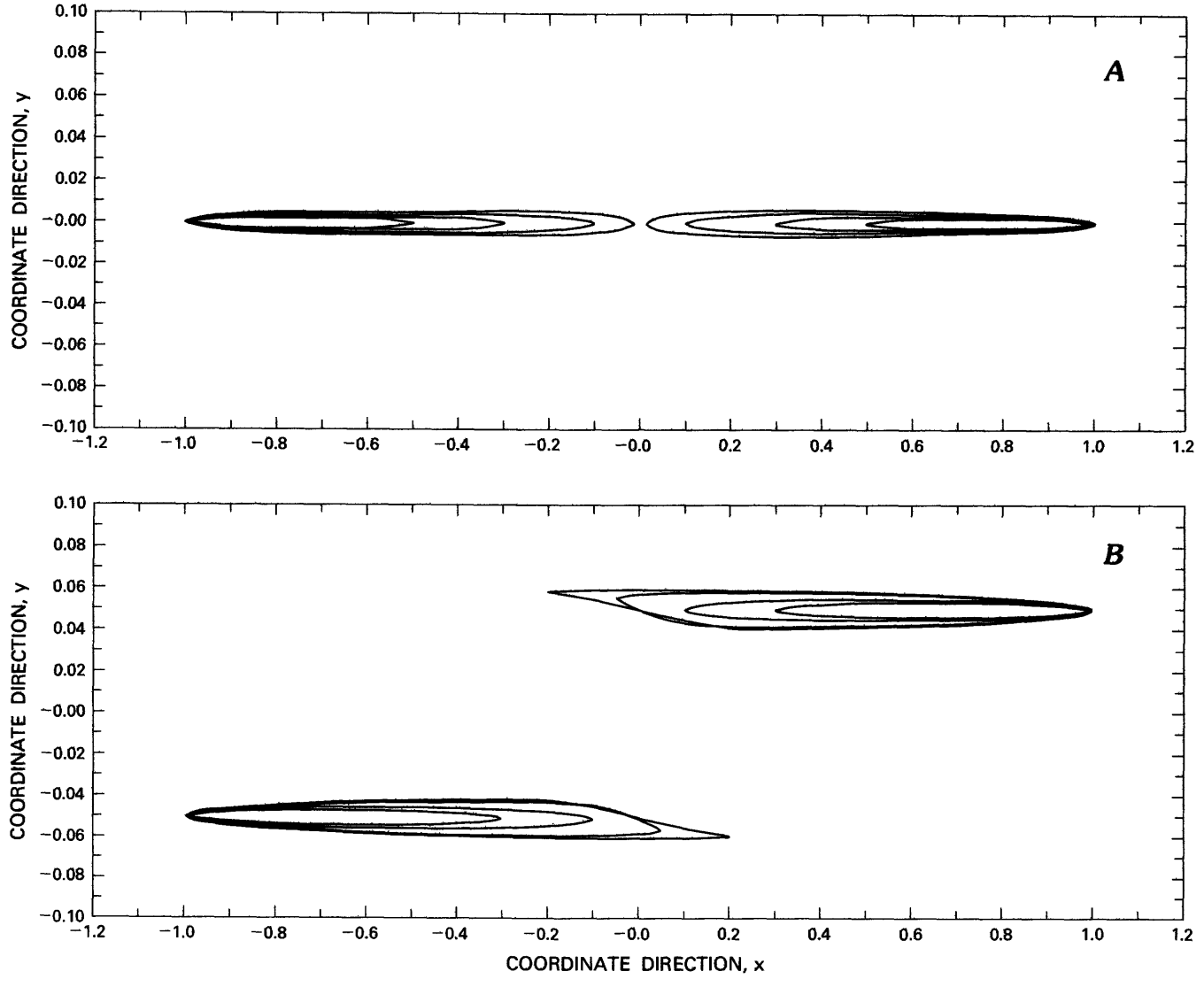

FIGURE 23.—Shapes of dilated pairs of collinear and offset cracks subjected to unit pressure. *A*, Distal ends of collinear cracks are fixed at $x=+1$. For small separations, slightly greater dilation of adjacent ends results in relative blunting of tips. *B*, Distal ends of offset cracks are fixed at $x=+1$ and offset by 0.1. Adjacent ends warp considerably owing to interaction at small separations. Overlap results in asymmetry of adjacent ends and relative sharpening of tips.

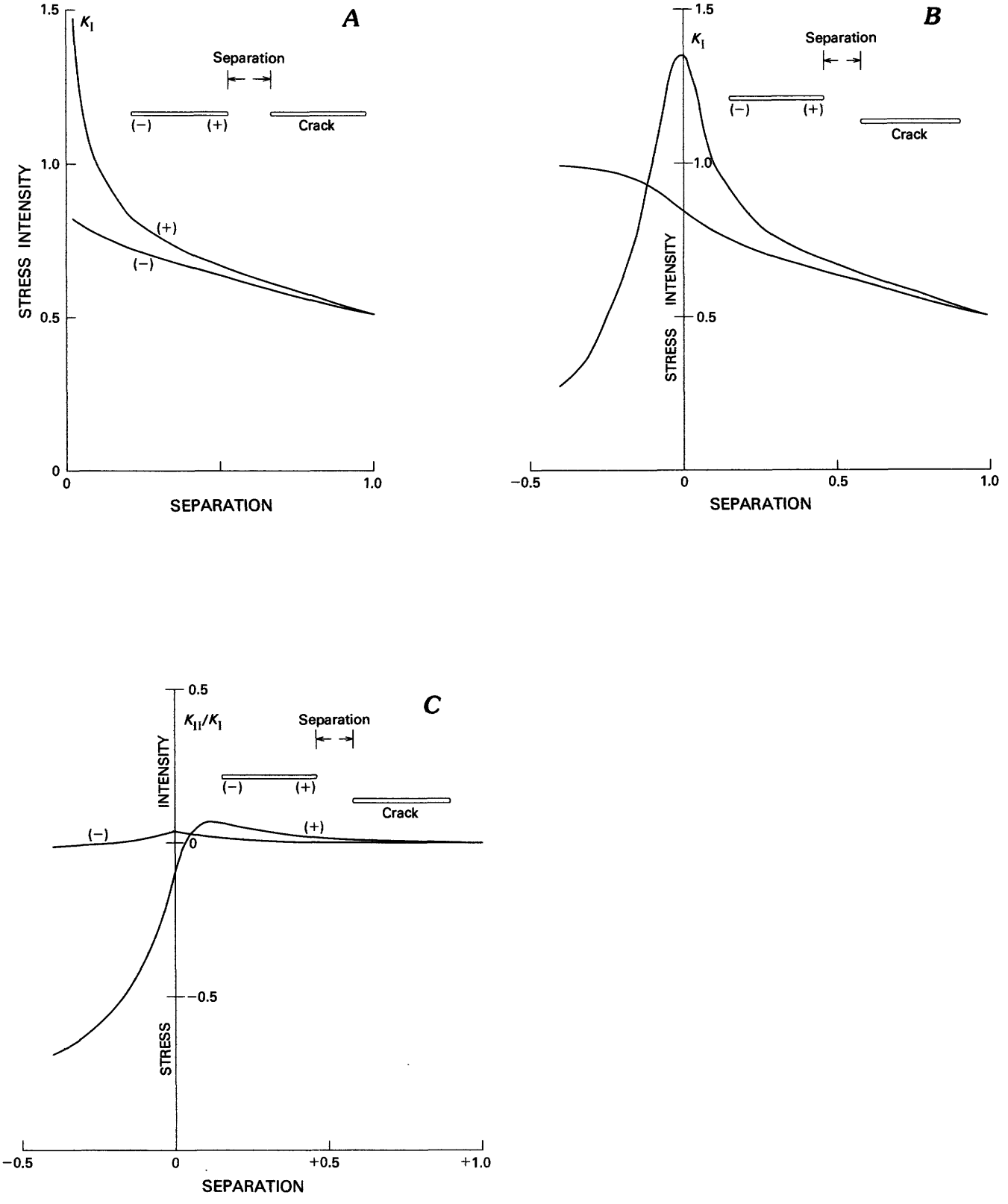

FIGURE 24.—Stress-intensity factors as a function of separation of pairs of collinear and offset cracks subjected to unit pressure (see fig. 23). Distal ends are fixed at x=+1, and offset is 0.1. *A*, Mode I stress-intensity factor K_I as a function of separation of adjacent ends of pairs of collinear cracks. *B*, Mode I stress-intensity factor K_I as a function of separation of adjacent ends of pairs of offset pressurized cracks. *C*, Ratio of mode II to mode I stress-intensity factors K_{II}/K_I as a function of separation of adjacent ends.

parallel to the segments. A difference in magnitude between the horizontal principal stresses induced by the continuous dike at depth could have produced the required anisotropy. A relatively great compressive stress acting parallel to the segments would tend to stabilize in-plane propagation. Anisotropy due to regional joints is ruled out because such joints do not strike parallel to the segments (fig. 9). Joints that crop out within 10 m of the dike are parallel to segments (fig. 7*B*); if these joints formed above the advancing dike, they would have hindered out-of-plane propagation. We have not been able to identify the particular cause of the anisotropy, but propagation paths inferred from the magnitude of the ratio K_{II}/K_I were not followed by these dike segments.

DILATION OF NORTHEASTERN DIKE

We have studied the dilation of 35 cracks arranged in a pattern similar to that of segments of the northeastern dike. The cracks were straight cuts connecting points at the measured ends of segments, and a uniform pressure was applied in these cracks. The ratio of applied pressure to elastic shear modulus was set arbitrarily at 10^{-5}, and Poisson's ratio at 0.25; these values were modified later by comparing the predicted-dilation and observed-thickness profiles. Crack interaction was treated by the method of successive approximations described above. The width of interval over which uniform stresses were applied to the crack wall, and the acceptable difference between calculated stress on the wall and applied pressure, were adjusted to smaller values until most calculated dilations differed by less than 10 percent from the previous solution. Thus we selected an interval width of 10 m and an acceptable difference in stress of 10 percent. Because this interval width was constant over a variety of cracks with differing degrees of interaction, the accuracy of solution varies somewhat from crack to crack. Typically, we believe our results to be within about 10 percent of the correct solution.

Dilations calculated by our method should have the proper relative form but may be disproportionate in magnitude if the arbitrary choices of applied pressure and elastic shear modulus do not match those of the dike and host rock. To determine the proper proportion, we use the method of multiple linear regression (Crow and others, 1960, p. 168—175). The equation for the linear model is

$$T_i(x)=C_1D_i(x)+d_i, \qquad (17)$$

where T_i is the measured dike thickness, D_i is the dilation calculated from displacements perpendicular to the strike of a segment, x is the distance along the N. 56° E. line, d_i is the deviation of the measured value from the calculated value, and $C_1=p(1-\nu)/\mu$ is an unknown constant that must be determined to proportion the dilation. We measure thickness perpendicular to a line approximately parallel to the strike of the dike. Because the maximum deviation in strike from this line is 10°, a maximum error of 2 percent in the thickness values is introduced. Effects of segment curvature and offset are not taken into account.

Rearranging equation 17 to solve for d_i and determining the sum of the sqaured deviations over n measurements, we calculate the minimum value of this sum with respect to C_1 and thus determine the unknown constant. Multiplying C_1 by D_i determines the predicted dilation T_i' that represents the best least-squares fit to the data, in the sense described above. We also calculate the estimated standard error, which measures the scatter in the observed-thickness data about the predicted-dilation curve. Where these deviations are normally distributed about the mean, approximately 68 percent of the thickness values should fall within one standard error of points on the dilation curve.

The plots of observed thickness and predicted dilation (fig. 25*A*) contain a large standard error of 1.22 m, greater than 50 percent of the average dike thickness (2.3 m). This result and the plot of residuals (fig. 26*A*) indicate a poor fit. In particular, large positive residuals are associated with the presence of substantial breccia in segments near the west end of the dike. This correlation is most pronounced in segments 2, 3, 5, 9, 12, and 15, and in the west end of segment 19, where an isolated peak in residuals corresponds to a bud. Inspection of the map (pl. 1) confirms that the segment walls would not fit neatly back together in those places. We conclude that dike thickness is anomalously great there owing to brecciation and erosion of wallrocks. Dilation of a crack would not mimic these segment forms very well, and so contributions to thickness due to brecciation should be removed from the analysis. Because erosion by flowing magma thickened the dike, our estimate of the pressure-to-modulus ratio (0.0062) is too great.

We do not know the forms of the dike segments before their enlargement due to erosion by flowing magma. Rather than attempt to estimate the extent of this enlargement, we have simply removed all thickness data for parts of the dike that contain substantial breccia or that have walls which clearly do not fit together (see fig. 12*B*). Carrying out the least-squares regression once more, we obtain a significantly improved standard error of 0.78 m, only 39 percent of the average thickness (2.0 m) in the reduced

data for the northeastern dike.

In our analysis, we consider all cracks as extending to great depth with no change in geometry and therefore no coalescence. A careful inspection of observed and predicted forms suggest that several dike segments may have behaved as a single segment. For example, the predicted dilation of the short segment 28 (pl. 1; fig. 25*A*) is much less than its observed thickness, and the observed thickness of segment 28 is almost the same as that of the much wider segment 27. These two segments are separated by a narrow bridge of shale and probably coalesce just below the outcrop. Considering the great stress in this region between pairs of closely spaced segment ends, the elastic limit of the host rock probably was exceeded. Where this rock weakened considerably, the adjacent dike segments could dilate as if connected.

To test the hypothesis that some segments behaved as if joined, we compare the predicted crack dilation and observed segment thickness for various combinations of linked segments. No offsets are observed along the dike when it is mapped at a small scale (fig.

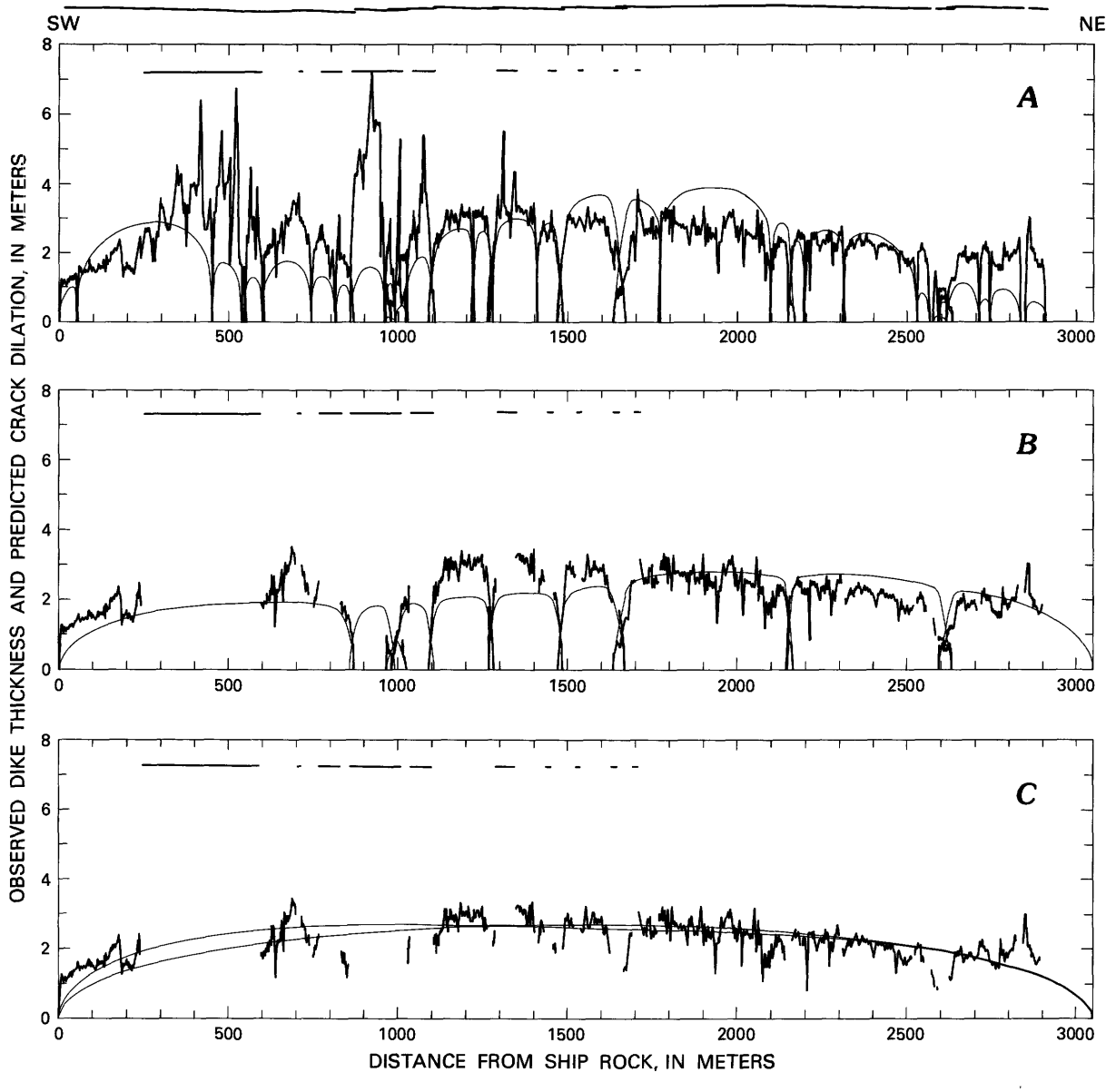

FIGURE 25.—Observed dike thickness (jagged curve) and predicted crack dilation (smooth curve) as a function of distance from Ship Rock. *A*, Thickness and dilation of 35 cracks; broken line at top denotes brecciated parts of dike wall. *B*, Thickness and dilation of 10 cracks, obtained after removing data for brecciated parts of dike wall, joining together closely spaced segments, and removing data near adjacent ends of jointed segments (see fig. 10*B*). *C*, Thickness and dilation of single crack under uniform driving pressure and linear pressure gradients; plot was obtained by joining all segments together and removing data near segment ends.

2), but as the scale is increased the most pronounced offsets become visible (fig. 9). Segmentation at this scale is equivalent to linking segments with less than 10 m of offset (fig. 10*B*). Large offsets imply that adjacent segments do not coalesce at shallow depths below the outcrop. We treat segments 1-8, 9-10, 11-12, 13-15, 16-17, 18-20, 21, 22-24, 25-30, and 31-35 as 10 cracks, and remove the thickness data near the joined ends of segments in the least-squares determination of the ratio of driving pressure to shear modulus. The width of the easternmost segment, 35, was extended because a magnetometer survey (O. H. Muller, written commun.,1977) indicated that the dike rock is obscured by fluvial gravel and that minette is present 150 m northeast of the mapped end.

The data on observed thickness and predicted dilation for a dike made up of 10 segments (figs. 25*B*, 26*B*) have a standard error of 0.56 m, or 25 percent of the average thickness of the dike. In addition, the observed-thickness and predicted-dilation profiles are similar. The walls of theoretical cracks and dike segments (fig. 25*B*) are nearly straight over much of their width; and where segments overlap, both the predicted and observed cross-sectional forms taper toward a sharp tip. Our estimate of the pressure-to-modulus ratio is 0.0018. We conclude that the dike did not behave as 35 separate cracks in an elastic solid but rather more like the 10 cracks that we have just proposed. The inelasticity of narrow bridges of the Mancos Shale and the coalescence of dike segments

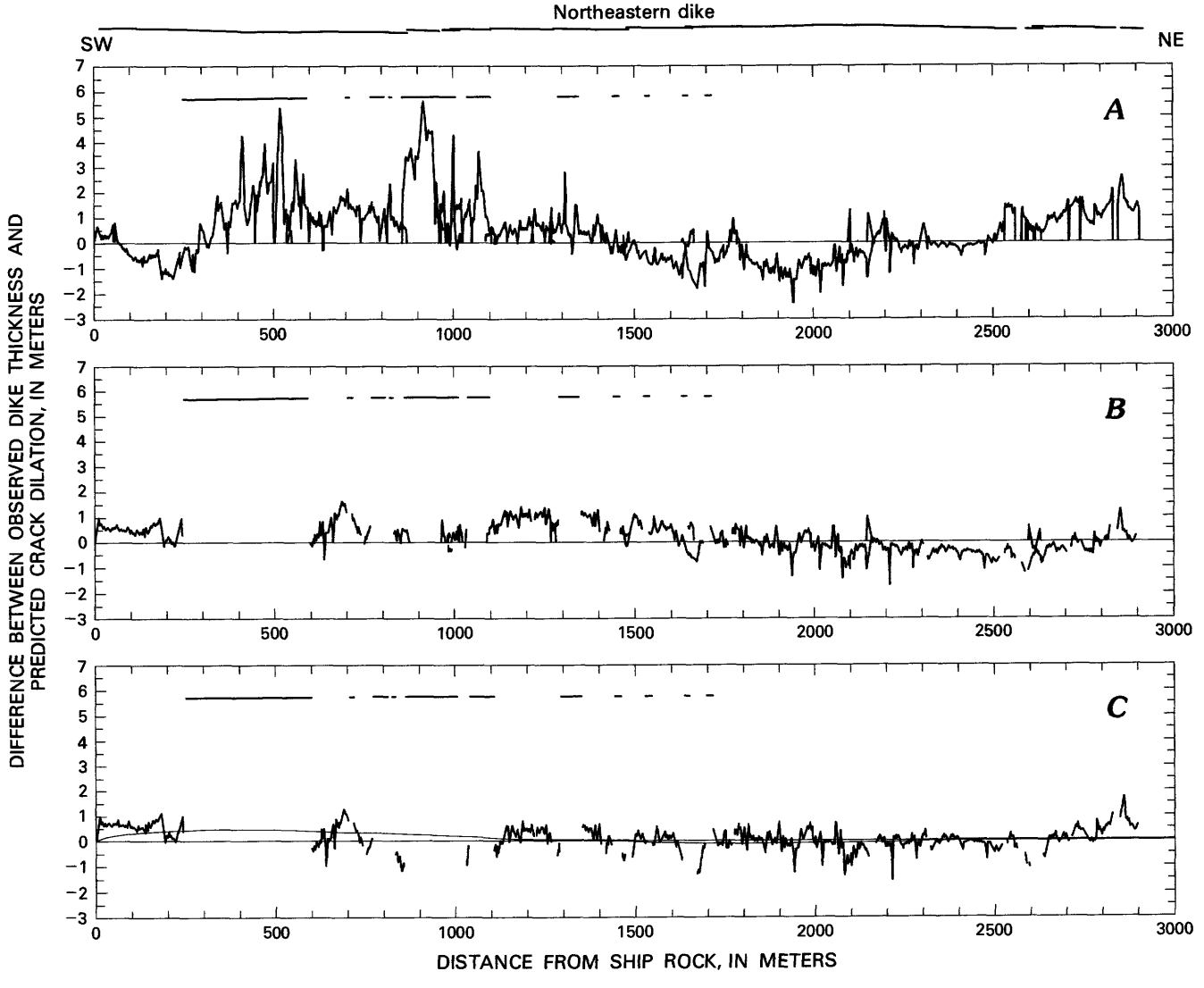

FIGURE 26.—Residuals between observed dike thickness and predicted crack dilation as a function of distance from Ship Rock; plots *A*, *B*, and *C* correspond to those in figure 25.

at shallow depth both contributed to this behavior.

ANALYTICAL SOLUTION FOR SINGLE DIKE SEGMENTS

A gradual systematic change in residuals, from positive near the west end of the northeastern dike to negative near its east end, suggests that the driving pressure was not constant over the entire dike but decreased from west to east. To examine this change over the 3-km outcrop length, we ignore the fine details of intrusive form and consider the dike as a single crack, for which analytical solutions are available for simple distributions of the driving pressure.

We obtain a solution for a uniform normal stress distributed over a single crack from equations 2*A* and 2*B*, where A=1. The stress functions for a linear normal-stress gradient that results in a symmetrical distribution of stress over the crack were derived by Lachenbruch (1961), and the dilation equation was given by Pollard (1976). The stress functions and dilation equation for a linear normal-stress gradient that results in an asymmetric distribution of stress over the crack were given by Pollard and Muller (1976). Superimposing the three solutions (fig. 27) gives the boundary conditions

$$-\sigma_{yy}=S(x)=S_0+S_s|x|+S_a x;$$

$$\sigma_{xy}=0,$$

for $|x|\leqslant a$, $y=0$. These driving-stress distributions for a single isolated crack result in a suitable range of cross-sectional forms and allow considerable insight into dike dilation and the subtle effects of stress gradients. The results, which we obtain as straightforward analytical expressions, make these simplifications attractive.

Defining the dimensionless variables $X=x/a$ and $D(X)=2v_0/a$, the important equations for our purposes are:

$$\tfrac{1}{2}D(X)=C_1(1-X^2)^{1/2}$$
$$+C_2\left\{(1-X^2)^{1/2}+X^2\ln|X/[1-(1-X^2)^{1/2}]|\right\}$$
$$+C_3X(1-X^2)^{1/2} \qquad (|X|\leqslant 1), \quad (19A)$$

where
$$C_1=S_0(1-\nu)/\mu,$$
$$C_2=S_s a(1-\nu)/\pi\mu,$$
and
$$C_3=S_a a(1-\nu)/2\mu; \qquad (19B)$$

$$S(X)=S_0+S_s a|X|+S_a aX; \qquad (19C)$$

and
$$K_I^{\pm}=[S_0+S_s(2a/\pi)+S_a(a/2)]a^{1/2}. \qquad (19D)$$

The three terms on the right-hand side of equation 19*A* represent the contributions to the thickness of the crack from each of the three boundary conditions. The relative importance of these terms depends on the relative magnitudes of the three constants, C_1, C_2, C_3, which may be either positive or negative but together must give a positive or zero thickness. Negative values of thickness indicate interpenetration of the crack walls and thus are physically inadmissible.

As before, we determine values of the constants C_1, C_2, and C_3 from field data on intrusive forms, using the method of multiple linear regression. The linear model is represented by

$$T_i(X)=C_1F_{1i}(X)+C_2F_{2i}(X)+C_3F_{3i}(X)+d_i, \qquad (20)$$

where T_i is the measured half-thickness normalized by the measured half-width, F_{1i}, F_{2i}, and F_{3i} are the postulated functions of X from equation 19*A*, X is the distance along the N. 56° E. line measured from the dike center and normalized by the half-width, d_i is the deviation of the measured from the postulated thickness, and C_1, C_2, and C_3 are the unknown constants. We rearrange equation 19 to solve for d_i, and determine the sum of the squared deviations over n measurements. The minimum value of this sum with respect to the three constants is calculated by solving three simultaneous equations, using Cramer's method (Gere

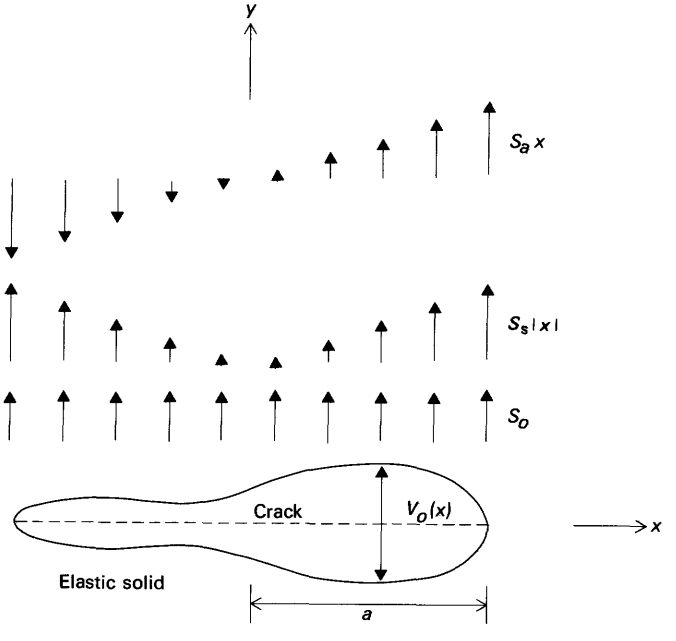

FIGURE 27.—Geometry and parameters of model used to calculate cross-sectional form of a crack in an elastic medium subjected to uniform normal stress (S_0), symmetrical linear stress gradient ($S_s|x|$), and asymmetric linear stress gradient ($S_a x$). Dilation is given by $2v_0(x)$; a is half-width of crack.

and Weaver, 1965, p. 81-83). We multiply each constant by the value of the respective function to determine the predicted dilations that represent the best least-squares fit to the data in the sense described above.

Returning to the data for the northeastern dike, we now treat the dike as a single crack of width 3,050 m (fig. 25*C*) and remove thickness data near the ends of all adjacent segments and from brecciated parts of the dike. The dilation described by equation 20 fits these data with a standard error of only 0.41 m (table 3). The uniform driving stress in this model is smaller than in the 10-crack model because we ignore all bridges of host rock between segments. We suggest that the single-crack result represents a lower bound for the constant C_1. The constants C_2 and C_3 are of the same order of magnitude as C_1 but represent changes in driving stress over the half-width of the crack—here, 1,525 m. Thus the stress gradients are small relative to the uniform driving stress. The negative sign of C_3 indicates a decrease in driving stress from west to east that was suggested by the plot of residuals (fig. 26*B*).

PROPAGATION OF NORTHEASTERN DIKE

Although many segment ends, cusps, and offsets are exposed along the northeastern dike, none displays sufficient relief to allow an unambiguous determination of the principal propagation direction of the dike. Because several structures suggest a steep plunge, we first consider a vertical propagation direction. Our conclusions are not altered qualitatively if this direction is inclined. Calculating values for the normalized mode I stress-intensity factors at the ends of the 10 cracks used to model the dike segments provides us with an estimate of the fracture toughness of the Mancos Shale. We consider and reject the possibility of the minette filling preexisting joints in the Mancos Shale. Then we propose an explanation for the segmentation based on a spatial change in orientation of the axis of least principal compressive stress.

The propagation criterion requires that the mode I stress intensity at segment ends equal the fracture toughness of the host rock. We calculate a normalized stress intensity for each crack tip in the set of cracks, using equation 16 and the method for solving multiple-crack problems introduced above. Magnitudes of normalized stress intensities for 35 cracks arranged like the 35 dike segments show little consistency and vary widely. However, for the 10-crack model, judged to be the best two-dimensional representation of the dike, the stress intensities cluster in a small range and are similar for the ends of adjacent cracks (table 4). The single-crack representation of the northeastern dike gives normalized stress-intensity factors (table 4) consistent with the results for 10 cracks. Segment ends, corresponding to the tips of the 10 overlapping cracks, presumably propagated until stress intensities fell just below the fracture toughness of local beds of the Mancos Shale, and then stopped propagating.

The question whether magma simply dilates preexisting fractures or creates its own fracture surface has been raised by many geologists. For example, Williams (1936, p. 131) stated that many volcanoes (or volcanic necks) in the Navaho-Hopi country are situated without regard to preexisting geologic structures. Shoemaker, Roach, and Byers (1962, p. 346) suggested that the trend of fractures (or dikes) propagated by intruding magma was governed primarily by regional tectonic stresses rather than preexisting local structures. On the other hand, some geologists (Johnson, 1961; Currie and Ferguson, 1970; Macdonald and Abbott, 1970) have inferred that magma simply dilates preexisting joints. However, these workers did not acknowledge that such an intrusive mechanism constrains the possible stress intensities and cross-sectional forms of dikes. The fracture toughness across a joint is essentially zero, and so the stress intensity at the leading edge of the magma body must also be negligible.

Now we consider stress distributions that result in a negligible stress intensity at the end of an isolated crack as a model for magma emplacement along a joint. We use the symmetrical part of the stress distribution defined by equation 19*C* and choose a negative gradient, so that the driving stress decreases toward the crack ends (fig. 28). From equation 19*D*

TABLE 3.—*Values of model parameters for the northeastern dike*

Number of segments	Number of data points	C_1	C_2	C_3	Standard error (m)
35	2,654	6.23×10^{-3}	—	—	1.22
10	1,875	1.79×10^{-3}	—	—	.56
1	1,609	$.64\times10^{-3}$	$.22\times10^{-3}$	$-.14\times10^{-3}$	.41

TABLE 4.—*Normalized mode I stress-intensity factors and fracture toughness of host rocks*

Segments	Half-width (m)	$K_I^-/p\cdot a^{1/2}$	$K_I^+/p\cdot a^{1/2}$	K_c^- (MPa·m$^{1/2}$)	K_c^+ (MPa·m$^{1/2}$)
1-8	433.7	1.1	2.4	45	98
9-10	68.6	5.8	2.9	97	48
11-12	29.0	3.3	2.7	35	29
13-15	61.9	2.3	6.1	36	96
16-17	96.5	6.2	6.4	97	101
18-20	109.7	4.9	5.1	103	107
21	98.6	5.6	3.6	111	72
22-24	265.0	2.4	2.5	78	82
25-30	242.4	3.6	2.0	112	61
31-35	326.3	2.0	1.8	61	53
1-35	1525.0	1.2	1.0	97	74

for $K_I 0$, we find that a particular crack with a_0 is associated with each stress distribution:

$$a_0 = S_0\pi/2S_s, \quad (21)$$

where a_0 is an equilibrium width, in that a crack under this stress distribution would be neither propagating nor closing. However, the pressure gradient would tend to drive a fluid farther along the crack until it cooled to the point where its strength balanced the pressure gradient. The form of the partly filled crack (fig. 28) is given by

$$\tfrac{1}{2}D(X) = C_2\left\{(1-X^2)^{1/2} - X^2 \ln\left|X/[1-(1-X^2)^{1/2}]\right|\right\}. \quad (22)$$

Comparing this crack form, which has a thick middle and tapering ends, with that of all segments of the northeastern dike, we conclude that none are approximated by it. In addition, we find that the normalized stress-intensity factors (table 4) are significantly greater than zero. We conclude that the minette magma did not partly fill joints.

Possibly, magma propagated to the ends of relatively short joints as dike segments with forms described by equation 22, and then continued propagating, in the form observed today, by fracturing the Mancos Shale. These short joints could not have been members of the regional set because regional joints do not parallel the dike segments (fig. 9). Many local joints crop out within 10 m of the dike and strike nearly parallel to it; some of these joints may have formed just above the propagating dike, owing to the great tensile stresses caused by dike dilation. We illustrated above (fig. 21) the distribution of tensile stress that might produce such joints; the magma may have entered and flowed along some of these joints before propagating through the Mancos Shale

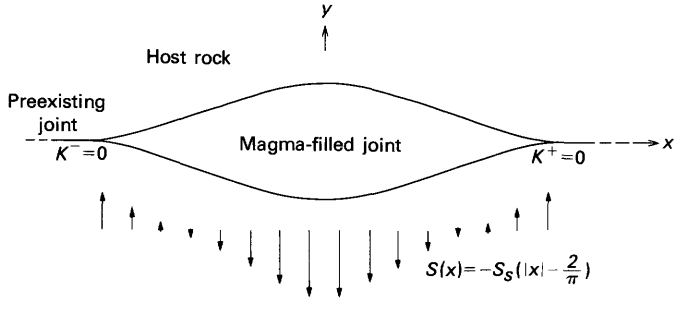

FIGURE 28.—Cross-sectional form of a crack subjected to a uniform linearly varying symmetrical stress distribution. Dilation is shown greatly exaggerated relative to width. This condition on driving pressure results in zero stress intensity (K_I) at crack ends and therefore is appropriate for magma pressurizing a preexisting joint.

by creating new fractures.

The echelon pattern of dike segments (pl. 1) is commonly observed in cross sections of mode I (or opening) fractures. For example, in metals a single cleavage fracture intersecting a twist boundary between two crystals commonly changes into a set of partial fractures (analogous to the dike segments) about 1 μm wide, arranged in echelon (Tetelman and McEvilly, 1967, p. 102-107; Broek, 1974, p. 33). In glass, single tension fractures propagating into a region where the principal tensile stress has a different orientation also change into partial fractures arranged in echelon, with a typical width of 0.1 mm (Sommer, 1969). Joints in rock about 0.01 to 1 m width exhibit echelon patterns that can generally be traced to a single parent joint (Hodgson, 1961; Lutton, 1971). Ryan and Sammis (1978) gave several examples of the echelon geometry of joints in basaltic flows and offered a particularly lucid account of their origin, using fracture-mechanics concepts. The width of echelon dike segments commonly are 10 to 100 m. Thus, this phenomenon of formation of segments or partial fractures that rotate into echelon patterns is observed over a range of eight orders of magnitude in size and in materials as diverse as metal, glass, and rock.

Two mechanisms have been proposed to explain these echelon patterns. In strongly anisotropic materials, such as crystals, an abrupt reorientation of the weak planes at crystal boundaries causes breakdown of a single cleavage fracture into partial fractures having this new orientation (Broek, 1974). In isotropic materials, a reorientation of the stress field causes breakdown of a single fracture and propagation of partial fractures along surfaces that remain normal to the local principal tensile stress. In glass, Sommer (1969) found that a reorientation of the field by only 3° caused breakdown. Preexisting regional joints in the host rock could supply the anisotropy necessary for the first mechanism, but regional joints of the proper orientation do not exist at the northeastern dike. We believe that the systematic change in strike of dike segments over a range of 14° (fig. 6) is related to a continuous change in orientation of the axes of horizontal principal stress. We imagine a single dike at a depth where the least principal stress axis maintained a constant orientation along the dike (fig. 29). As the dike propagated upward toward the level of the present exposure, it encountered a region in which the orientation of the axis varied in the horizontal plane. This variation precipitated a breakdown into discrete segments, each of which propagated upward while maintaining orientations normal to the local stress direction.

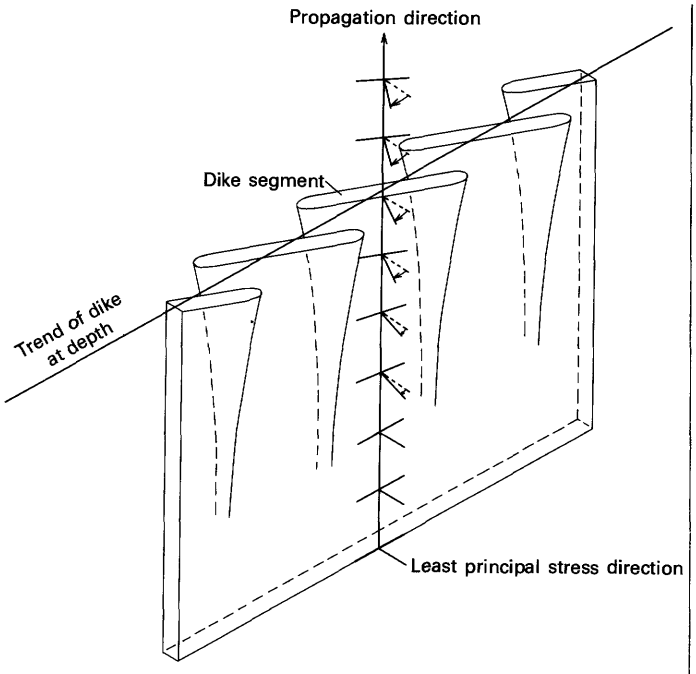

FIGURE 29.—Idealized three-dimensional form of a segmented dike. Segmentation is due to rotation of least principal stress axis during upward propagation.

MAGMA FLOW AND HEAT LOSS DURING DIKE EMPLACEMENT

In this section, our purpose is to evaluate the effects of conduit form on the rates of magma flow along dikes and of heat loss to wallrocks. Our analysis is prompted by the apparent temporal progression in shape from a dike, through a dike with buds or sites of brecciation along its width, to a well-developed plug with a dike extending from either end. Also, there is evidence for magma flow in the southern plug after complete solidification of the adjacent dike (fig. 17) which indicates that magma flow may persist longer in plugs than dikes. Apparently, certain dike segments, such as segment 9, and all buds and plugs have been enlarged by processes other than dilation. Erosion of wallrocks by flowing magma enlarges parts of dike segments, and these changes in form alter both the rate of flow of magma and the rate of heat loss to wallrocks. Although we ignore the problem of how breccias are formed, we present approximate expressions for magma-flow and heat-loss rates in conduits whose shape has been altered by erosion of wallrocks. Where conduits either are circular or locally widen from a tabular form, volumetric flow rate is substantially increased, rate of heat loss is relatively unaltered, and flow of magma can be expected to channel into those places while the remainder of the intrusion solidifies.

EQUATIONS FOR MAGMA AND HEAT FLOW

To calculate relations governing magma-flow and heat-transport rates, we idealize plugs and dikes as elliptical cylinders (fig. 30); later we consider more realistic conduit forms. Although the continuum properties of basaltic magmas are incompletely known, the viscosity, thermal conductivity, density, and heat capacity are functions of the chemistry, temperature, pressure, and strain rate. We use equations describing rates of mass, momentum, and energy transfer per unit volume as derived by Bird, Stewart, and Lightfoot (1960), which must be solved in conjunction with appropriate boundary conditions. The steady-state motion equation and an energy equation for the laminar flow of an incompressible Newtonian fluid with constant properties are

$$\frac{\partial^2 v}{\partial x^2}+\frac{\partial^2 v}{\partial y^2}=-\frac{\Delta P}{\eta L} \tag{23}$$

and

$$\frac{\partial^2 \theta}{\partial x^2}+\frac{\partial^2 \theta}{\partial y^2}=\frac{\rho \hat{C}_v}{k} v\left(\frac{\partial \theta}{\partial z}\right), \tag{24}$$

where x, y, and z are coordinate directions extending respectively along, across, and vertically away from a horizontal section of a cylindrical conduit; v is the velocity; θ is the temperature; ζ is the viscosity; ρ is the density; $\Delta P/L$ is the driving-pressure gradient, defined as the gradient in the difference between magma pressure p and hydrostatic head $P=p-\rho gz$; k is the thermal conductivity; and $\hat{C}_v$ is the heat capacity. Thus our model consists of fluid driven in the vertical z-direction by a uniform driving-pressure gradient and resisted by viscous drag and increased gravitational potential (fig. 30*A*), and of heat carried upward by fluid motion and conducted outward by the temperature difference between magma and wallrocks (fig. 30*B*). We assume that the importance of conduit geometry can be illustrated without inclusion of complex rheologies, temperature- and pressure-dependent fluid properties, viscous heat production, or unsteady flow behavior.

The energy equation (24) is further simplified by noting that gradients in temperature are great only near the walls of dikes. Thus, fluid in the central "core" of the conduit is approximately isothermal, and because temperature gradients in the downstream direction are vanishingly small, both sides of the energy equation (24) are sensibly zero in this region (fig. 31*A*). The velocity profile in the convective term on the right-hand side of equation 24 can be linearized in the near-wall thermal-boundary-layer region (fig. 31*A*), where both downstream and cross-stream temperature gradients are present. The approximation is

$$\frac{\partial^2\theta}{\partial n^2}=\frac{\rho\hat{C}_v}{k}\,n\left(\frac{dv}{dn}\right)_{wall}\left(\frac{\partial\theta}{\partial z}\right), \tag{25}$$

where the velocity distribution in the energy equation has been expanded to the first nonzero term in its Taylor series, $n(dv/dn)_{wall}$, and n is the coordinate normal to the conduit wall (fig. 30*B*). Because viscosity is known independently of temperature, we may easily integrate the momentum equation (23) for viscous flow in tabular, elliptical, and circular conduits (fig. 31*B*; table 5). The velocity gradient at the conduit wall is also known independently of the temperature distribution. We assume that temperature gradients along the walls in the s-direction (fig. 30*B*) are negligible.

A similarity solution (Bird and others, 1960, p. 349) to equation 25 is obtained by defining a new variable

$$\phi=\frac{n}{(9\beta z)^{1/3}}, \tag{26}$$

where $$\beta=\frac{k}{\rho\hat{C}_v}\left(\frac{dv}{dn}\right)_{wall}. \tag{27}$$

Existence of the similarity variable ϕ indicates that the magnitudes of downstream convection and cross-stream conduction are everywhere related by a cube-root relation and the group β, which measures the importance of convection relative to conduction. Solutions exist only if the boundary conditions can also be written in terms of this similarity variable. Consider the conditions

$$\begin{aligned}&\theta(n>0,\ z=0)=\theta_m,\\ &\theta(n=\infty,\ z<\infty)=\theta_m,\\ &\theta(n=0,\ z>0)=\theta_w,\end{aligned} \tag{28}$$

which specify constant temperatures at the wall (θ_w) and on the centerline and at the entrance of the conduit (θ_m). Because temperature varies only near

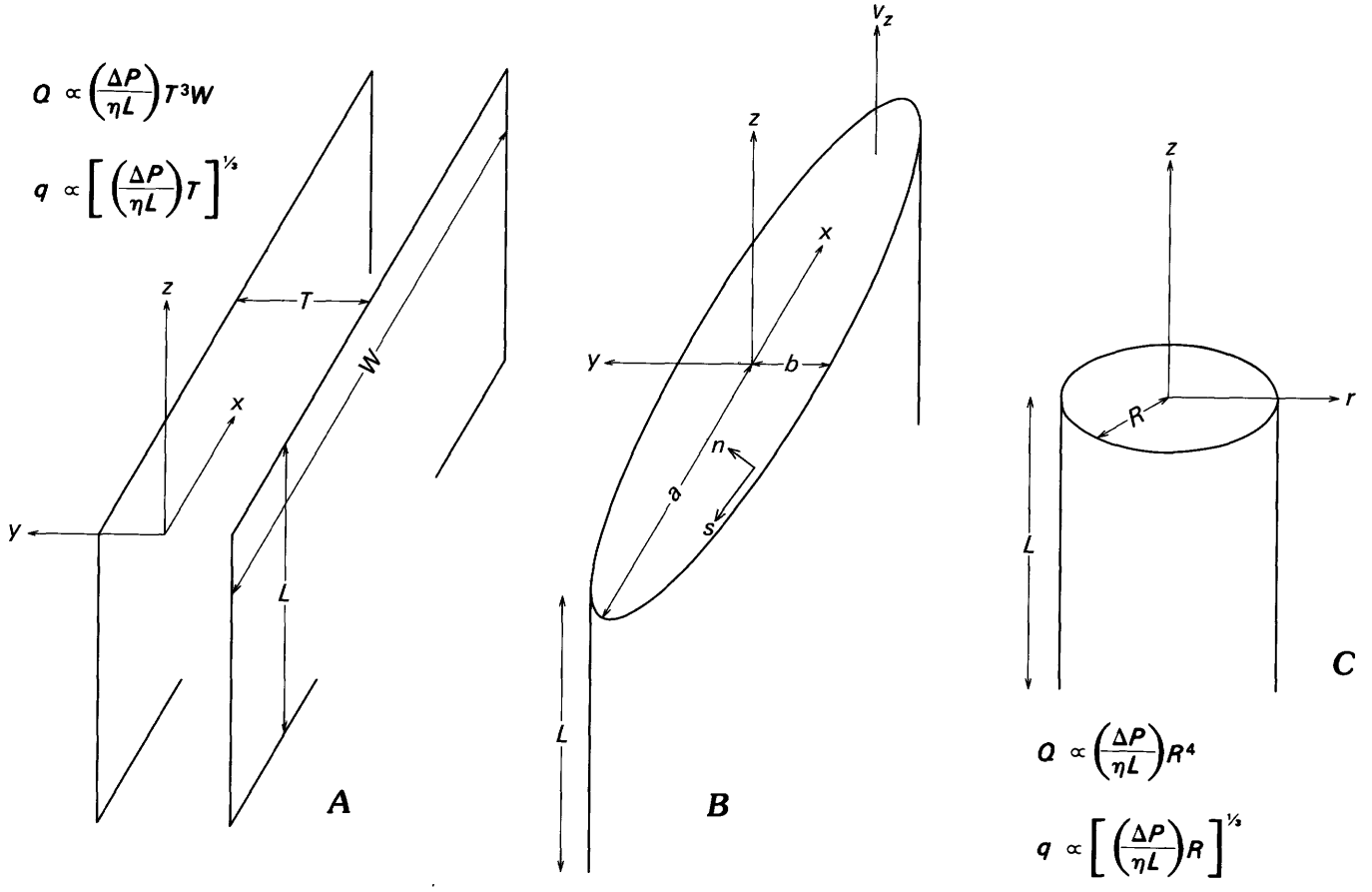

FIGURE 30.—Geometry and parameters of model for magma flow. *A*, Tabular conduit of thickness T, width W, and height L. *B*, Elliptical conduit with semimajor and semiminor axes a and b, respectively, and wall coordinate (s, n) defining distance along and normal to wall. *C*, Circular conduit of radius R. v, flow velocity; Q, volumetric flow rate; q_x, rate of heat loss at any position x along walls; η, viscosity; $\Delta P/L$, driving-pressure gradient. Flows in tabular and circular conduits are special cases of flow in an elliptical conduit (*B*); for an infinitely long dike (*A*), $a=\infty$ and $b=T/2$; and for a plug (*C*), $a=b=R$. Coordinate directions x, y, and z are used for tabular and elliptical conduits; r and z, for circular conduit.

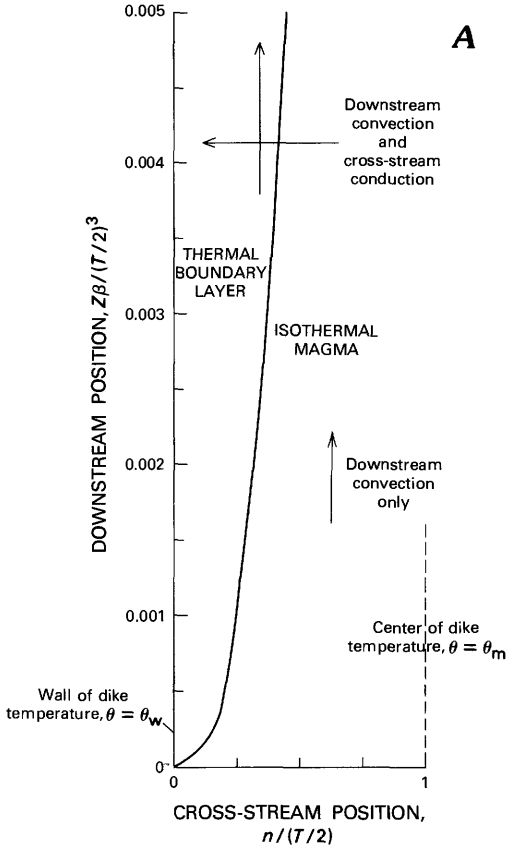
A
0.005
0.004
0.003
0.002
0.001
0
DOWNSTREAM POSITION, $Z\beta/(T/2)^3$
Downstream convection and cross-stream conduction
THERMAL BOUNDARY LAYER
ISOTHERMAL MAGMA
Downstream convection only
Center of dike temperature, $\theta = \theta_m$
Wall of dike temperature, $\theta = \theta_w$
0
1
CROSS-STREAM POSITION, $n/(T/2)$

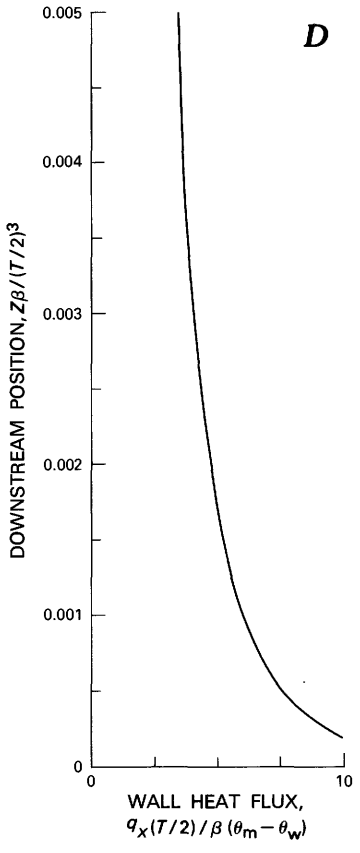
D
0.005
0.004
0.003
0.002
0.001
0
DOWNSTREAM POSITION, $Z\beta/(T/2)^3$
0
10
WALL HEAT FLUX, $q_x(T/2)/\beta(\theta_m - \theta_w)$

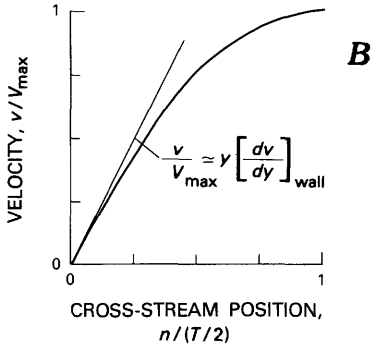
B
1
0
VELOCITY, v/V_{max}
$\frac{v}{V_{max}} \simeq y\left[\frac{dv}{dy}\right]_{wall}$
0
1
CROSS-STREAM POSITION, $n/(T/2)$

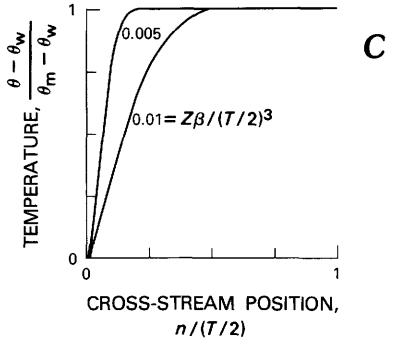
C
1
0
TEMPERATURE, $\frac{\theta - \theta_w}{\theta_m - \theta_w}$
0.005
0.01= $Z\beta/(T/2)^3$
0
1
CROSS-STREAM POSITION, $n/(T/2)$

TABLE 5.—*Solutions to equations for viscous flow in tabular, elliptical, and circular conduits*

Tabular	Elliptical	Circular
$V=\frac{1}{2}\frac{\triangle P}{\eta L}(T/2)^2\left(1-\frac{y^2}{(T/2)^2}\right)$	$V=\frac{1}{2}\frac{\triangle P}{\eta L}\frac{a^2b^2}{a^2+b^2}\left(1-\frac{x^2}{a^2}-\frac{y^2}{b^2}\right)$	$V=\frac{1}{4}\frac{\triangle P}{\eta L}R^2\left(1-\frac{r^2}{R^2}\right)$
$Q=\frac{2}{3}\frac{\triangle P}{\eta L}(T/2)^3W$	$Q=\frac{\pi}{4}\frac{\triangle P}{\eta L}\frac{a^3b^3}{a^2+b^2}$	$Q=\frac{\pi}{8}\frac{\triangle P}{\eta L}R^4$
$\frac{dv}{dx}=-\frac{\triangle P}{\eta L}y$	$\frac{dv}{du}=-\frac{\triangle P}{\eta L}\frac{a^2b^2}{a^2+b^2}\left(\frac{x^2}{a^2}+\frac{y^2}{b^2}\right)^{1/2}$	$\frac{dy}{dr}=-\frac{1}{2}\frac{\triangle P}{\eta L}r$

the wall, the isothermal boundary condition at the center of the conduit is effectively an infinite distance away. After using the similarity variable to eliminate n and z from both the energy equation (25) and the boundary conditions (26), we obtain the solution

$$\theta=\theta_w+\frac{\theta_m-\theta_w}{\Gamma}\int_{\phi}^{\infty}e^{-\phi^3}d\phi, \tag{29}$$

where

$$\Gamma=\int_0^{\infty}e^{-\phi^3}d\phi=0.983. \tag{30}$$

We now eliminate the similarity variable to obtain spatial variables. Unlike the velocity profile, the temperature varies in both the downstream and cross-stream directions (figs. 31*A*, 31*C*). Downstream position is normalized as $z\beta/(TR/2)^3$, where $T/2$ is the conduit half-thickness (fig. 30*A*). Details of the temperature field thus require a knowledge of distance from the source region, as well as of velocity of magma flow and conduit geometry.

The temperature distribution can be differentiated by the cross-stream variable n and evaluated at the conduit wall to obtain an expression for the rate of heat loss at any position s along a conduit:

$$q_s=-k\left(\frac{\partial\theta}{\partial n}\right)_{n=0}=-k\left(\frac{\partial\phi}{\partial n}\right)\left(\frac{d\theta}{d\phi}\right)_{\phi=0} \tag{31A}$$

$$=-k\left[\frac{\rho\hat{C}_v}{9zk}\left(\frac{dv}{dn}\right)_{wall}\right]^{1/3}\frac{\theta_m-\theta_w}{\Gamma}. \tag{31B}$$

Heat flux along the wall varies as the cube root of the velocity gradient and as the inverse cube root of the distance from the source region (fig. 31*D*). The velocity gradient at the wall is proportional to conduit thickness (table 5), and so heat loss at any position along the wall also varies as the cube root of conduit thickness (figs. 30*A*, 30*C*).

With constant physical properties and at constant wall temperatures, the similarity solution takes on a simple form, and the conduit thickness enters the solution (eqs. 29, 31*B*) only through the velocity-gradient term in the group β. The cube-root relation between thickness and wall heat flux is due solely to the similarity transformation (eq. 26) by the term $\partial\phi/\partial n$ in equation 31*A*, because $(d\theta/d\phi)_{\phi=0}$ is not a function of thickness. Such effects as spatial variation in fluid properties and boundary conditions can be included by using the similarity approach (Pigford, 1955; Sparrow and Yu, 1971), although simple analytic solutions are not available.

FLOW IN TABULAR AND CIRCULAR CONDUITS

In the motion equation (23), the rate at which magma flows toward its destination is inhibited by viscous drag imparted by the conduit walls. In the energy equation (24), the rate at which heat flows toward its destination is inhibited by conductive losses to the wallrocks. Conduits having small surface areas with respect to their volume minimize both viscous drag and heat losses. Of all possible conduit forms, the circular form of plugs minimizes the ratio of surface area to volume, whereas the tabular form of dike segments maximizes this ratio.

FIGURE 31.—Geometry, velocity, temperature, and wall heat flux for region of a conduit where thermal-boundary-layer approximation is valid. *A*, Geometry used for solution of energy equation (25). Cross-stream coordinate n is zero at wall and $T/2$ at centerline. Downstream coordinate z is zero at entrance and normalized by $(T/2)^3/\beta$, where β is given in equation 27. Temperature θ is that of uncooled magma θ_m along centerline and entrance, and θ_w along wall of conduit. Boundary between isothermal core and thermal boundary layer is arbitrarily given by isotherm corresponding to temperature $\theta=0.02(\theta_m-\theta_w)$. *B*, Velocity is known independently of temperature and is normalized by maximum velocity. Near-wall approximation to full velocity profile is also shown. *C*, Temperature profiles at two downstream positions. Temperature is normalized by overall difference $\theta_m-\theta_w$. *D*, Normalized heat flux at conduit wall as a function of normalized downstream position.

To compare the effects of viscous drag in plugs and in dikes, we first consider an elliptical conduit (fig. 30*B*; table 5) and note that the volumetric flow rate Q is proportional to the cube of the thickness T of an infinitely wide tabular conduit (that is, $Q \propto T^3$) (fig. 30*A*) and to the fourth power of the radius R of a circular conduit (that is, $Q \propto R^4$) (fig. 30*C*). Now, as a thought experiment, we consider circular and elliptical conduits containing fluids of the same viscosity and with equal pressure gradients along their lengths, so that the fluids in both conduits are expending energy, against viscous drag and gravitational potential energy, at equal rates. Here, the ratio of the volumetric flow rates in the two conduits is a function of geometry alone:

$$\frac{Q_e}{Q_c} = \frac{2(a/b)^3}{(R/b)^4[1+(a/b)^2]} \simeq \frac{2(a/b)}{(R/b)^4} \qquad (32)$$

where the subscripts c and e refer to circular and elliptical conduits, respectively. For most dikes, a/b ranges from 50 to 5,000, and so R/b must range from 3.2 to 10 to deliver magma at an equal rate. When the boundary conditions and the axial and wall temperatures are the same in both conduits, this relation holds for variable- as well as constant-viscosity fluids. Similarly, if the magma behaves as a Bingham substance (Shaw and others, 1968), then the above equation also is valid.

The general relation between volumetric flow rate, pressure gradient, and conduit geometry (fig. 32) indicates that for a given axial ratio a/b of an elliptical conduit, there exists a normalized radius R/b of a circular conduit for which the respective flow rates are equal. For relatively large increases in the axial ratio of an elliptical conduit, only small increases in the radius of a circular conduit are needed to accommodate the same volumetric flow at an equal driving-pressure gradient. For example, if $a/b=10^3$, then $R/b=6.7$ to accommodate the same volumetric flow rate. If a/b is increased tenfold to 10^4, then R/b is less than doubled to 11.9. In this case, the fluid in the circular conduit moves at an average velocity 22.3 times that of the fluid in the elliptical conduit. Thus, dikes must grow far wider to attain a rate of delivery of magma equal to what can be accomplished by a small increase in the radius of a plug.

To obtain a similar relation for rate of heat loss as a function of conduit geometry, we numerically integrate the local-heat-flux equation (31*B*) for q_s around the perimeters of elliptical and circular conduits (fig. 32) to obtain the overall heat flux q. For the conduits shown, if the flow rates and driving-pressure gradients are equal, the dike loses heat at a rate 7.45 times that of the plug. If the flow-rate ratio $Q_e/Q_c=2$, then $(\Delta P/L)_e/(\Delta P/L)_c=0.5$ and $q_e/q_c=9.4$. Here, a 100-percent increase in the flow rate ratio leads to only a 26-percent increase in the rate-of-heat-loss ratio.

Plugs should be preferred over dikes or dike segments for greater magma flow and less heat loss, as illustrated by the plot of measured values of plug radius and average dike width for the southern and northeastern plugs (fig. 32). Assuming that the pressure drop remained constant, the southern plug delivered magma at a rate 700 times that of its associated dike and lost heat at a rate about a third that of the dike. The ratios of flow rate and heat flux for the northeastern plug were about 1,500 and 0.2, respectively. In both examples, the flow rate relatively increased and the wall heat flux decreased as the intrusion evolved from a dike to a plug. Including dike segmentation in these estimates would increase the flow-rate ratios and leave the heat-flux ratios about the same.

Although we do not solve here the problem in which the momentum and energy equations are coupled, the above result indicates that increases in viscosity due to heat losses would have a greater effect in dikes than in plugs because, for a given volume of magma, dikes lose heat at a relatively greater rate. If magma is transported quickly from source region to destination and if the conduit has a comparatively small ratio of surface area to volume, magma will remain at a lower viscosity and be able to flow for longer periods. Thus a circular conduit has a distinct advantage over an elliptical conduit. If the pressure gradient between a magma chamber and the destination of an intrusion decreases over time, the delivery rate of magma may still increase when the conduit geometry changes appropriately.

SOLUTION FOR FLOW IN CONDUITS OF NONUNIFORM THICKNESS

Solving the problem of fluid flow and heat flux in elliptical and circular conduits provides insight into the relative efficiency of conduits with various idealized shapes with respect to the transport of magma. However, we have not considered the effects of changes in dike form due to erosion of wallrocks. Because of the sensitive relation between flow rate and conduit thickness (table 5), variations in flow rate and wall heat flux due to buds, offsets, cusps, and other deviations from idealized conduit forms may be large. We now derive an approximate solution to the flow in conduits of arbitrary shape, so that we may model flow in two types of idealized buds (figs. 33*A*, 33*B*) and in dike segments.

The geometry of the two walls of a conduit is defined by the functions $y=F(x)$ and $y=G(x)$, where $F(x)$ and $G(x)$ are constant in the vertical z-direction (fig. 33). The motion equation (23) is to be solved with the boundary conditions

$$\begin{aligned} v(x, F(x))&=0 \\ v(x, G(x))&=0, \end{aligned} \tag{33}$$

specifying that the velocity is zero along the walls. Lengths and velocities are nondimensionalized by defining $v^*=v/v_{max}=v/(\Delta P/2\eta L)(T/2)^2$, $x^*=x/(T/2)$, $y^*=y/(T/2)$, $z^*=z/(T/2)$, $F^*(x^*)=F(x)/(T/2)$, and $G^*(x^*)=G(x)/(T/2)$, where T is a characteristic conduit thickness. The motion equation and boundary conditions, respectively, then become

$$\frac{\partial^2 v^*}{\partial (x^*)^2} + \frac{\partial^2 v^*}{\partial (y^*)^2} = -2,$$

and

$$\begin{aligned} v^*(x^*, F^*(x^*))&=0, \\ v^*(x^*, G^*(x^*))&=0. \end{aligned}$$

We seek an acceptably accurate, though approxi-

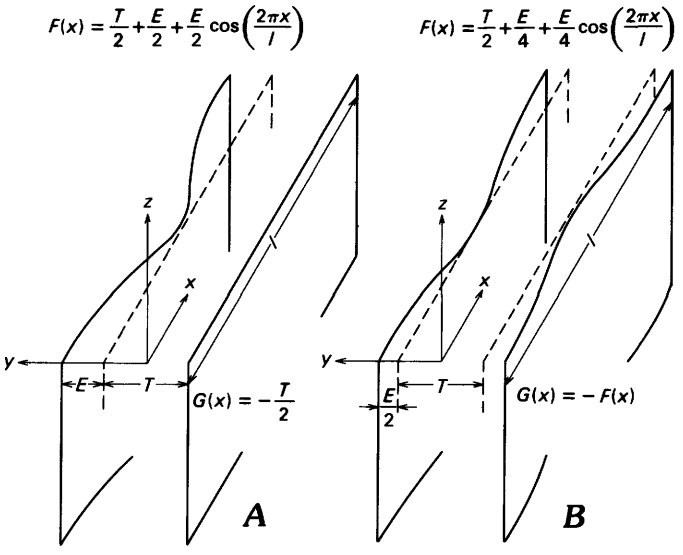

FIGURE 33.—Geometry and parameters of model used to calculate magma-flow and heat-loss rates in conduits of varying thickness. T, conduit thickness where not thickened; x, y, and z, coordinate directions. Limiting cases are that one wall (A) or both walls (B) vary sinusoidally according to functions $y=F(x)$ and $y=G(x)$. Wavelength and total amount of thickening of sinusoidal curves are given by l and E, respectively.

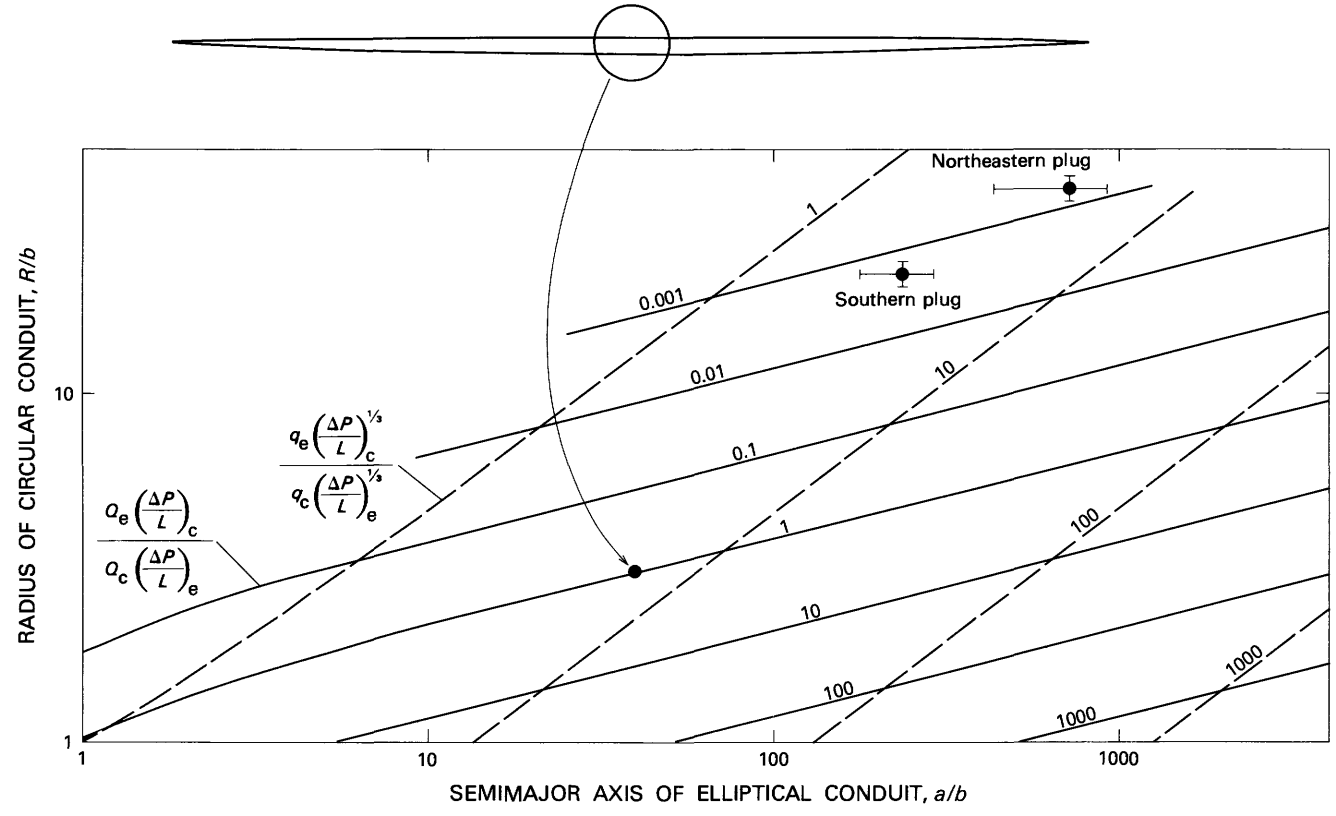

FIGURE 32.—Volumetric flow rate and wall heat-flux ratios for circular and elliptical conduits. Solid curves are for various ratios of volumetric flow rate and driving-pressure gradient. Radius R of circular conduit and semimajor axis a of elliptical conduit are normalized by semiminor axis b. For example sketched at top, R/b=10 and a/b=40, both conduits transport equal amounts of liquid for the same driving-pressure gradient, and elliptical conduit losses heat at a rate 7.45 times that in circular conduit. Subscripts c and e refer to circular and elliptical conduits, respectively. See figure 30 for explanation of other symbols.

mate, expression for $v^*(x^*, y^*)$ by noting that the velocity field varies much more rapidly across than along a long thin conduit. This statement is equivalent to writing $(v^*)_{xx} << (v^*)_{yy}$, where the parentheses denote differentiation with respect to each of the subscripts. If $F^*(x^*)=+1$ and $G^*(x^*)=-1$, then the velocity field is that of a tabular conduit and thus invariant to the x-direction, and $(v^*)_{xx}=0$.

If $F^*(x^*)$ and $G^*(x^*)$ define the form of an elliptical conduit, then $T=2b$ (fig. 30*B*), and we have an exact solution to the nondimensional equations:

$$v^* = \frac{1}{[1+(a/b)^2]}\left[1 - \frac{(x^*)^2}{(a/b)^2} - (y^*)^2\right]. \tag{36}$$

If $z/b=10$, then $(v^*)_{xx}=0.01(v^*)_{yy}$, and indeed the first term on the left in equation 34 is small compared to the second. We demonstrate this result more formally by noting that y^* ranges from +1 to −1, whereas x^* varies over a much wider range (from +10 to −10 for $a/b=10$) for long thin conduits. To make $(v^*)_{xx}$ of order unity, we can nondimensionalize it by specifying $x^{**}=x/2a$. The resulting nondimensional motion equation is

$$\frac{1}{(a/b)^2}\frac{\partial^2 v^*}{\partial (x^*)^2} + \frac{\partial^2 v^*}{\partial (y^*)^2} = -2. \tag{37}$$

In equation 37 each derivative is of order unity, and $1/(a/b)^2 << 1$. Thus the first term is indeed small in comparison with the second.

The weak x^*-dependence is used to solve equation 34 by the method of successive approximations (Van Dyke, 1975), assuming only that the forms of the walls (F^* and G^*) vary gradually in x^*. In the solution, the boundary conditions are satisfied exactly, even though we never completely satisfy the momentum balance. To a first approximation, we seek a solution $v^{*\mathrm{I}}$ by assuming that $(v^{*\mathrm{I}})_{xx} \simeq 0$. Thus equation 34 can be approximated as

$$\frac{\partial^2 v^{*\mathrm{I}}}{\partial (y^*)^2} = -2, \tag{38A}$$

which is directly integrable. Using the boundary conditions (35) to determine constants, the velocity field is given by

$$v^{*\mathrm{I}} = -F^*G^* + (F^*+G^*)y^* - (y^*)^2, \tag{39A}$$

a solution that is accurate to better than 3 percent in an elliptical conduit with an axial ratio $a/b=6.67$, and whose accuracy improves as a/b increases. The approximate motion equation (38*A*) neglects gradients in conduit thickness and is referred to as the *local-thickness approximation* because the velocity profile across the conduit is parabolic and only the local thickness is used to compute the velocity field. This approximation is locally equivalent to the solution for flow between two parallel walls (table 5). A better approximation $v^{*\mathrm{II}}$ is obtained by postulating that $(v^{*\mathrm{II}})_{xx} \simeq (v^{*\mathrm{I}})_{xx}$. Therefore, we must solve

$$\frac{\partial^2 v^{*\mathrm{II}}}{\partial (y^*)^2} = -2 - \frac{\partial^2 v^{*\mathrm{I}}}{\partial (x^*)^2}. \tag{38B}$$

Integrating and evaluating constants, the velocity field is given by

$$v^{*\mathrm{II}} = \left[1 - \tfrac{1}{2}(F^*G^*)_{xx}\right]\left[-F^*G^* + (F^*+G^*)y^* - (y^*)^2\right] - \left[\tfrac{1}{6}(F^*+G^*)_{xx}\right] \cdot \left[(F^*+G^*)F^*G^* - (F^*F^* + F^*G^* + G^*G^*)y^* + (y^*)^3\right]. \tag{39B}$$

By integrating over the entire area of the conduit, we can determine the overall volumetric flow rate. By differentiating, evaluating the velocity gradient normal to the conduit wall $(dv/dn)_{\mathrm{wall}}$ (fig. 30*B*), and inserting it into the heat-flux equation (25), we can determine the *local heat flux* q_x at any position along the conduit. Similarly, we define the *local volumetric flow rate* Q_x by considering the overall volumetric flow rate in a small element Δx^* as $\Delta x^* \to 0$:

$$\frac{Q_x^{\mathrm{I}}}{\bar{Q}} = \int_{G^*}^{F^*} v^{*\mathrm{I}} dy^*, \quad \frac{q_x^{\mathrm{I}}}{\bar{q}} = \frac{\left(\frac{dv^{*\mathrm{I}}}{dn^*}\right)^{1/3}_{F^*, G^*}}{\left(\frac{dv^*}{dn^*}\right)^{1/3}_{1,-1}}, \tag{40A}$$

$$\frac{Q_x^{\mathrm{II}}}{\bar{Q}} = \int_{G^*}^{F^*} v^{*\mathrm{II}} dy^*, \quad \frac{q_x^{\mathrm{II}}}{\bar{q}} = \frac{\left(\frac{dv^{*\mathrm{II}}}{dn^*}\right)^{1/3}_{F^*, G^*}}{\left(\frac{dv^*}{dn^*}\right)^{1/3}_{1,-1}}, \tag{40B}$$

Volumetric flow rate and wall heat flux are normalized by $\bar{Q}$ and $\bar{q}$, respectively, values for a conduit of arbitrary uniform thickness T, or $F(x^*)=1$ and $G(x^*)=-1$. In this manner, we can construct flow-rate and heat-flux profiles along any thin conduit. Such a nondimensional profile allows us to examine the effect of variations in conduit thickness on the rates of magma flow and heat loss without knowing the driving-pressure gradient or the viscosity of magma.

As changes in conduit thickness become more acute, the accuracy of our solution decreases. We can derive higher order approximations by using the same procedure, but we have no guarantee that each

successive approximation will be more accurate than the previous (Van Dyke, 1975). However, by inserting the velocity equations (39*A*, 39*B*) into the motion equation (34) we can evaluate the error at any point. The error introduced by our approximation technique causes a slight disequilibrium of the force balance at any point in the flow. For the applications that follow, this error is insubstantial; we have derived a third approximation v^{*III} as an additional check of accuracy. The flow-rate and heat-flux equations (40) are used to calculate magma flow in and heat flux from idealized buds and the northeastern dike in the next two sections.

FLOW IN BUDS

For a first estimate of the flow rate in a conduit of nonuniform thickness we use the local-thickness approximation, which shows that volumetric flow rate and wall heat flux should vary as the cube and cube root, respectively, of the local thickness. For the geologist in the field, this relation is an important rule of thumb. The approximation should break down, however, as lateral variations in conduit form, or gradients in thickness, become appreciable. The effect of variations in the thickness of a dike is examined by calculating volumetric flow rate and wall heat flux in tabular conduits (fig. 33) of which one wall or both walls are described by a sinusoidal curve. We examine two geometries of buds. The bud at 420 m reflects enlargement of one side of the dike (fig. 33*A*), and that at 1,000 m enlargement of both sides (fig. 33*B*). We define T as the initial uniform thickness of a conduit. We consider variations in the form of the conduit, such that the maximum thickness $T+E$ occurs at $x=0$ and E is the component of total thickness due to local enlargment of the conduit.

From equations 40*A* and 40*B* we calculate local volumetric flow rate and wall heat flux profiles (fig. 34) for flow in conduits with walls forming sinusoidal curves. We specify an arbitrary normalized wavelength $l/T=20$ and several normalized amplitudes E/T. For equal wavelength and amplitude, volumetric flow rates calculated for each of the two idealized geometries of buds (figs. 33*A*, 33*B*) agree to within a few percent. The bars on the vertical axes indicate flow rate and heat flux for the limiting case in which the normalized wavelength approaches an infinite value; that is, the thickness of the conduit is $E+T$ everywhere. If $E/T=3$, then the conduit has eroded by a thickness of wallrock equal to 3 times that of the initial conduit. For this amplitude and wavelength, the local flow rate Q_x increases 56 times as fast as the initial flow rate $\bar{Q}$ at $x/T=0$. As the wavelength increases from 20 toward ∞, the flow rate would increase to 64 times its initial value. Because wall heat flux is a function of the velocity gradient normal to the wall of the conduit, that from each of the two walls differs. In the plot of normalized heat flux (fig. 34*B*), the dashed curves show heat flux from the straight wall, and the solid curves that from the curved wall (fig. 34*B*). Heat fluxes from symmetrical conduits would plot between the solid and dashed curves. Where the conduit is thickest, $x/T=0$, and for

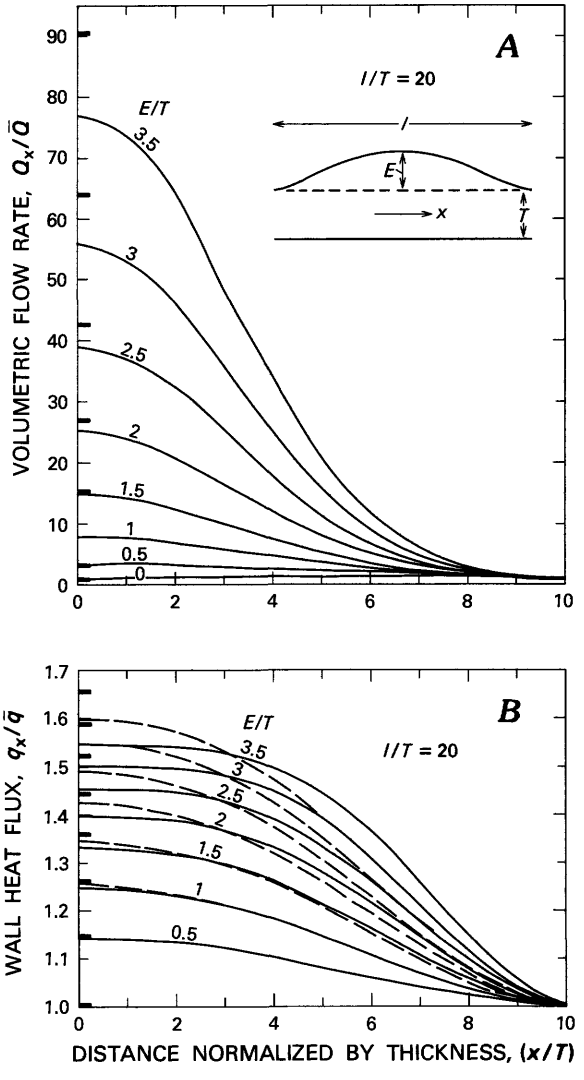

FIGURE 34.—Local volumetric flow rate (*A*) and wall heat flux (*B*) as functions of normalized distance along conduits illustrated in figure 33*A*. Here, wavelength of sinusoidal curve is 20 times initial conduit thickness ($l/t=20$), and total amount of thickening ranges as high as 3.5 times initial thickness $E/T \lesssim 3$. Local volumetric flow rate Q_x and wall heat flux q_x are normalized by those for a conduit of unit thickness T. Dashed curves show heat flow from straight wall of conduit, and solid curves that from curved wall. Solid bars on vertical axis show flow rate and heat flow for a conduit of uniform normalized thickness $(E/T)+1$.

E/T=3 the heat flux $q_x/\bar{q}$ is only 1.50 and 1.54 at each of the two walls. As the wavelength approaches ∞, $\bar{q}_x/\bar{q} \rightarrow 1.59$.

We plot local volumetric flow rate and wall heat flux at the widest part of the conduit, where x/T=0, for a variety of amplitudes E/T and wavelengths l/T (fig. 35). The local-thickness approximation is sufficiently accurate for small amplitudes ($E/T \lesssim 3$) to use the rule of thumb that the volumetric flow rate is proportional to the cube of conduit thickness and the wall heat flux to its cube root. Successive increments of amplitude cause ever-larger increases in flow rate and ever-smaller increments in heat flux. In other words, flow rate becomes ever more sensitive to increasing thickness, while heat flux becomes ever more insensitive to increasing thickness.

To relate these results to an actual example, we approximate the form of the bud on segment 12 of the northeastern dike (pl. 1) as a sinusoidal curve with E/T=3.2 and l/T=21.5. At this wavelength, the volumetric flow rate is about 60 times greater in the bud than in the nearby dike, and the heat flux from the wall of the bud is less than 1.6 times that at a point of average segment thickness.

FLOW IN THE NORTHEASTERN DIKE

The preceding analysis suggests that rates of magma flow should have varied considerably along a dike with such marked changes in thickness as the northeastern dike. Similarily, rates of heat loss to wallrocks should have been rather uniform. Our analysis allows construction of flow-rate and heat-flux profiles and an estimate of the relative rates of magma flow and heat loss among the 35 dike segments.

We begin by assuming that the monobreccia is essentially intact and can be regarded as wallrock, and that the heterobreccia flowed with the same viscosity as the magma. Conduit geometry is therefore defined by the contacts between minette and heterobreccia, and between Mancos Shale and monobreccia (fig. 36). The form of the dike is smoothed where one of the walls doubles back on itself, such as near 510 and 2,470 m. Because we have no knowledge of the three-dimensional form of the northeastern dike, we assume that its outcrop pattern extends downward unchanged. We also assume that the driving-pressure gradient for magma flow was constant along the entire width of the dike and that the temperature of the dike wall was the same everywhere.

Because the driving-pressure gradient and viscosity are unknown, we cannot calculate the actual flow-rate and heat-flux profiles. The thickness profile of the northeastern dike (fig. 12*B*) is normalized by its average thickness (2.0 m) in those parts unaltered by brecciation. Local flow rate Q_x and wall flux q_x are normalized by their respective mean values $\bar{Q}$ and $\bar{q}$ calculated for a tabular conduit of this thickness.

We can improve the solution for flow in a conduit of nonuniform thickness by noting that the motion equation (34) may be satisfied exactly at a single

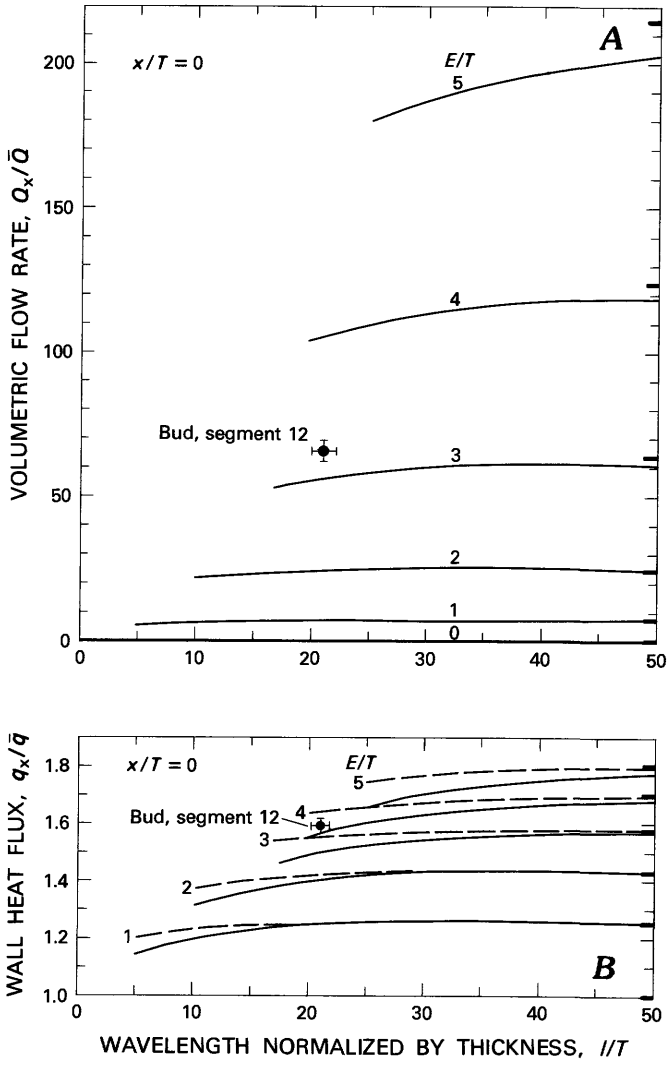

FIGURE 35.—Local volumetric flow rate (*A*) and wall heat flux (*B*) as functions of normalized wavelength at thickest parts of conduits (x/T=0) illustrated in figure 33*A*. Local volumetric flow rate Q_x and wall heat flux q_x are normalized by those for a conduit of unit thickness T. Dashed curves show heat flux from straight wall of conduit, and solid curves that from curved wall. Solid bars on vertical axes show local flow rate and heat flux for a conduit of uniform thickness (E/T)+1. Discharge of magma from thickest part of bud on segment 12 was probably about 60 times that in adjacent nonbrecciated parts of segment. Rate of heat loss, however, was probably less than 1.6 times greater than in narrower part of segment.

point by constructing a linear combination of the two approximate solutions (eqs. 39*A*, 39*B*):

$$v^*=(1-\omega)v^{*\mathrm{I}}+\omega v^{*\mathrm{II}}, \qquad (41)$$

where ω is some value that weights v^* and $v^{*\mathrm{II}}$. For example, if $v^{*\mathrm{II}}$ is an exact solution to the motion equation (34), then $\omega=1$. We commute $v^{*\mathrm{I}}$ and $v^{*\mathrm{II}}$ at each of the 2,726 pairs of positions that define the form of the northeastern dike, and we find the value of ω that minimizes the total error in momentum disequilibrium for each position along the dike. Thus we construct 2,726 velocity profiles, which we then integrate to obtain local volumetric flow rates (fig. 37*A*) and differentiate and evaluate at both walls to obtain the velocity gradients. Knowing the velocity gradient normal to the walls, we calculate the rate of heat loss at each point along the dike (fig. 37*B*) from

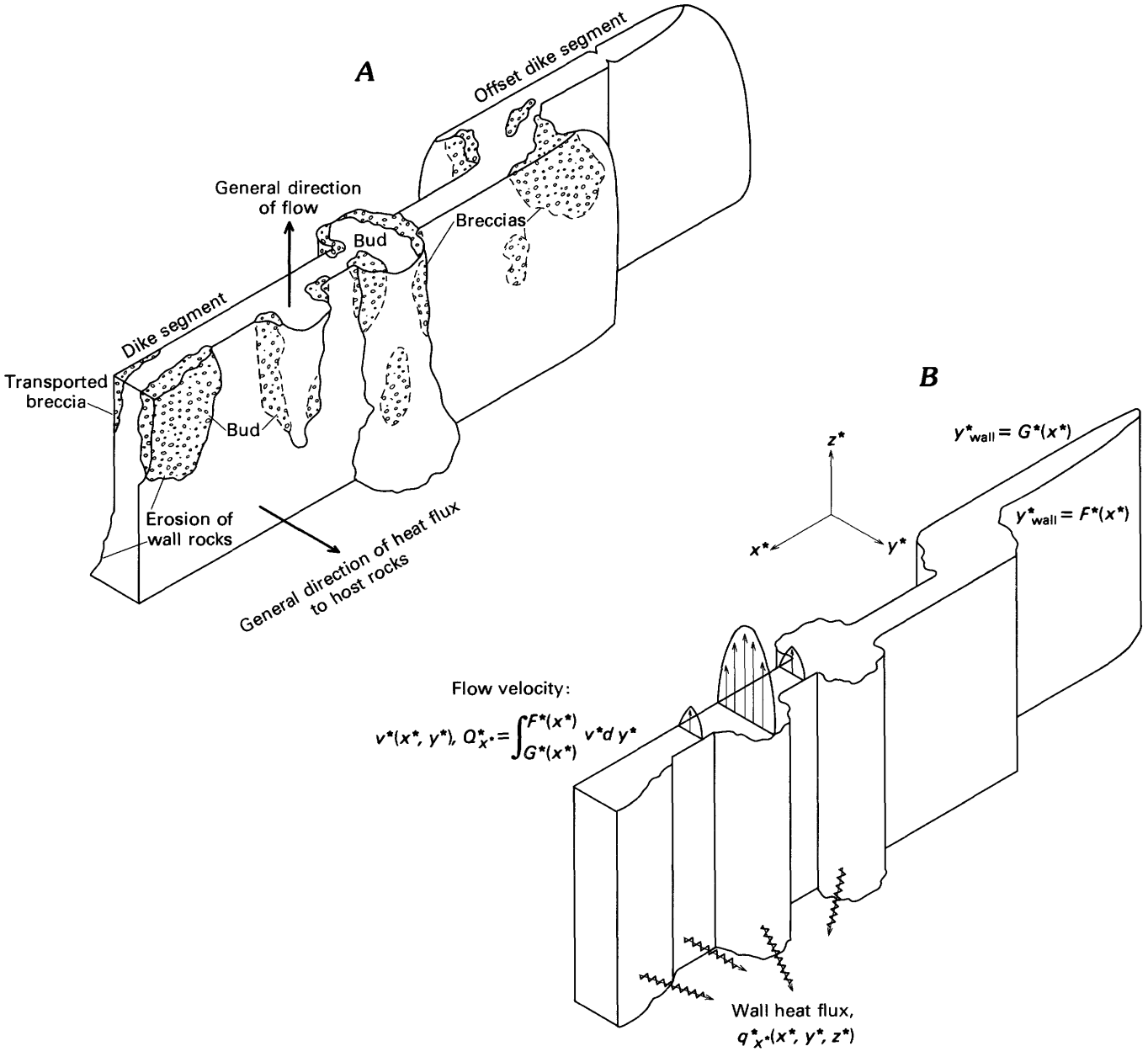

FIGURE 36.—*A*, Schematic and idealized dike segments, showing that form of segments is modified by brecciation and erosion of wallrocks, and that thickness is nonuniform in vertical as well as in horizontal dimension. *B*, Model used in calculation of flow rate and wall heat flux. Walls of conduit are given by $F^*(x^*)$ and $G^*(x^*)$, where x^* is direction along conduit width. Fluid flows with velocity v^* in vertical z^*-direction. Velocity profiles are integrated across conduit in horizontal y^*-direction to obtain local volumetric flow rate $Q^*|x^*|$. Rate of heat loss through walls is $q^*_{x^*}$.

the heat-flux equation (31). Because the heat-flux profiles for the northwest and southeast walls of the northeastern dike are similar, we present their average.

As expected, the most striking aspect of the volumetric flow rate profile is its large variation along the dike. The largest flow rates are in regions of nondilational enlargement, that is, in parts of the west half of the northeastern dike, where brecciation and erosion of wallrocks greatly influenced its final form. Where the dike attained its maximum thickness of 7.2 m, volumetric flow rate was 45 times that determined from the mean dilational thickness, and wall heat flux was less than twice that for the mean thickness. In that locality, magma flowing through the dike lost about 1/30 as much heat per unit volume as in places of mean flow. Similarly, where volumetric flow rate was less than that inferred from the mean thickness, wall heat flux was more nearly that determined from the mean thickness, and the heat lost per unit volume of magma was thus relatively larger than for the mean. Variations in heat-loss rate were greatest at the ends of dike segments, where velocity gradients were smallest.

We have numerically integrated volumetric-flow-rate and wall-heat-flux profiles along each of the 35 dike segments (table 6) and normalized them by the sum for all segments to yield a histogram showing the relative importance of each segment to the overall rates of flow (fig. 38). More than 20 percent of the discharge of magma was through a single dike segment (9), and approximately 40 percent of the discharge was through two segments (3 and 9). However, segments 3 and 9 account for only about 8 percent of the rate of heat loss from the entire dike. The average thicknesses of segments 3 and 9 are 3.8 and 4.9 m, respectively—greater than any of the others. Because dike form was altered significantly after the initial dilation, we infer that the flow-rate and heat-flux values near the east end of the dike (where no brecciation occurred) exemplify the early stages of intrusion. Variations in flow rate and heat flux were modest and due primarily to segmentation of the dike and secondarily to minor fluctuations in its thickness. As emplacement continued, changes in form due to brecciation and erosion of host rocks led to large increases in flow rate in the western part of the dike.

The volumetric flow rate and wall heat flux calculated for the entire northeastern dike are 2.63 and 1.07 times greater, respectively, than for a tabular conduit 2,900 m wide and 2 m thick. In general, segmentation increased the surface area of the conduit and reduced its flow rate. Thus, during the early stages of emplacement, we would overestimate discharge of magma by modeling the dike as a slit or a single elliptical conduit; progressive local widening of the dike at its west end counteracted this effect. In general, we cannot predict volumetric flow rate on the basis of total length and average thickness alone. These two parameters are probably sufficient, however, for the purpose of predicting heat flux to the wallrocks because of the weak dependence on details of conduit geometry.

DISCUSSION OF MAGMA-FLOW AND HEAT-TRANSPORT SOLUTIONS

Our model for magma flow in the northeastern dike assumes steady magma flow and heat transport of a fluid with constant mechanical and thermal properties, flowing in a conduit that does not change form in the vertical direction. Here, we evaluate these assumptions.

We postulated that the magma was incompressible. This postulate holds if the rate change of magma

TABLE 6.—*Volumetric flow rate and wall heat flux calculated for the northeastern dike*

Segment	Volumetric flow rate, $Q_x/\bar{Q}$	Wall heat flux, $q_x/\bar{q}$
1	0.18	0.81
2	2.93	1.05
3	9.75	1.23
4	.14	.76
5	2.86	1.06
6	2.23	1.07
7	1.08	.98
8	.70	.92
9	15.09	1.30
10	.80	.91
11	.03	.63
12	2.04	.82
13	.01	.56
14	.41	.86
15	3.83	1.08
16	2.36	1.07
17	2.34	1.05
18	.17	.77
19	4.07	1.14
20	1.52	1.00
21	1.98	1.04
22	1.47	.97
23	2.11	1.07
24	.80	.90
25	1.28	1.01
26	1.35	1.02
27	.97	.98
28	.79	.96
29	.20	.81
30	.05	.70
31	.03	.65
32	.54	.91
33	.85	.96
34	.73	.96
35	1.06	.98
Entire dike	2.63	1.07

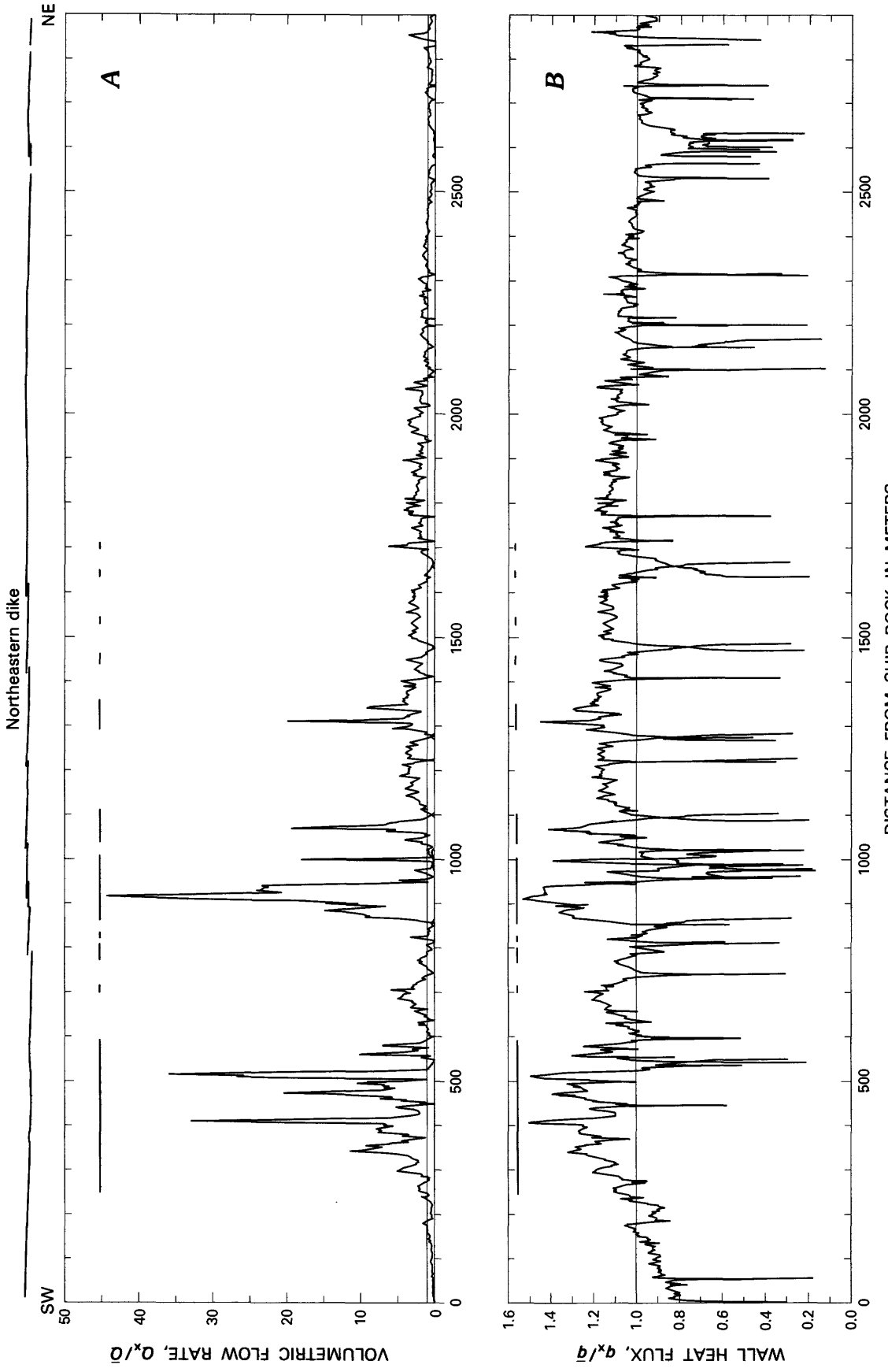

FIGURE 37.—Local volumetric flow rate (*A*) and average wall heat flux (*B*) in northeastern dike as functions of distance from Ship Rock. Outline of dike is shown for reference. Both flow rate Q_x and heat flux q_x are normalized by those calculated from mean nondilational thickness of dike (2.0 m); horizontal line across *A* and *B* represents flow rate and wall heat flux of unity. Broken line at top shows areas of nondilational thickening of dike by erosion of wallrocks.

density due to vesiculation and crystallization is negligible in comparison with the flow rate. No vesicles were observed in hand samples of minette from the east side of Ship Rock. In general, densities of basic crystalline rocks do not exceed 2.9 g/cm^3 (Daly and others, 1966), and those of basic magmas generally exceed 2.6 g/cm^3 where they are nonvesicular (Bottinga and Weill, 1970). This 10-percent variation in density does not allow for significant temporal or spatial gradients in density to develop.

The rheology of magmas is known to be complex, even under isothermal conditions. Some evidence exists that magmas may have a finite yield strength and exhibit time-dependent behavior (Shaw and others, 1968; Murase and McBirney, 1973). Presently, whether this complexity is due to the properties of the molten phase alone, or to interaction of the melt with crystalline and vapor phases, is unclear. Shaw, Wright, Peck, and Okamura (1968) suggested that the flow behavior of a Hawaiian tholeiitic lava at 1,130°C, containing 25 percent crystals and 2 to 5 percent gas bubbles, could be described by a Bingham plastic. A more general rheologic model is that of a pseudoplastic material. The constitutive relations between velocity gradient and shear stress τ_{yz} for these materials are (Bird and others, 1960, p. 11):

$$\frac{dv}{dy} = -\frac{1}{\eta_0}\tau_{yz} + \tau_0 \text{ for } |\tau_{yz}| > \tau_0,$$

$$= 0 \text{ for } |\tau_{yz}| \leq \tau_0; \qquad \text{(Bingham)}$$

and

$$\frac{dv}{dy} = -A\tau_{yz}^n \qquad \text{(pseudoplastic)}$$

where τ_0 is the yield strength, η_0 is similar to the Newtonian viscosity η, and A is a coefficient that reduces to $1/\eta_0$ when the power-law exponent n=1 (again, the case of Newtonian viscosity). For flow in tabular conduits (fig. 30*A*), the shear stress $\tau_{yz}=(\Delta P/L)y$. The two equations for a Bingham material emphasize that a central-plug flow exists where no velocity gradients are present. A yield strength of about 100 Pa is reported for the lava, containing about 25 percent crystals, studied by Shaw, Wright, Peck, and Okamura. The power-law exponent n is rarely less than unity. Although conduit thickness and velocity gradient at the wall are linearly related in a Bingham material, a pseudoplastic material may have a sensitive relation between thickness and velocity gradient and, thus,

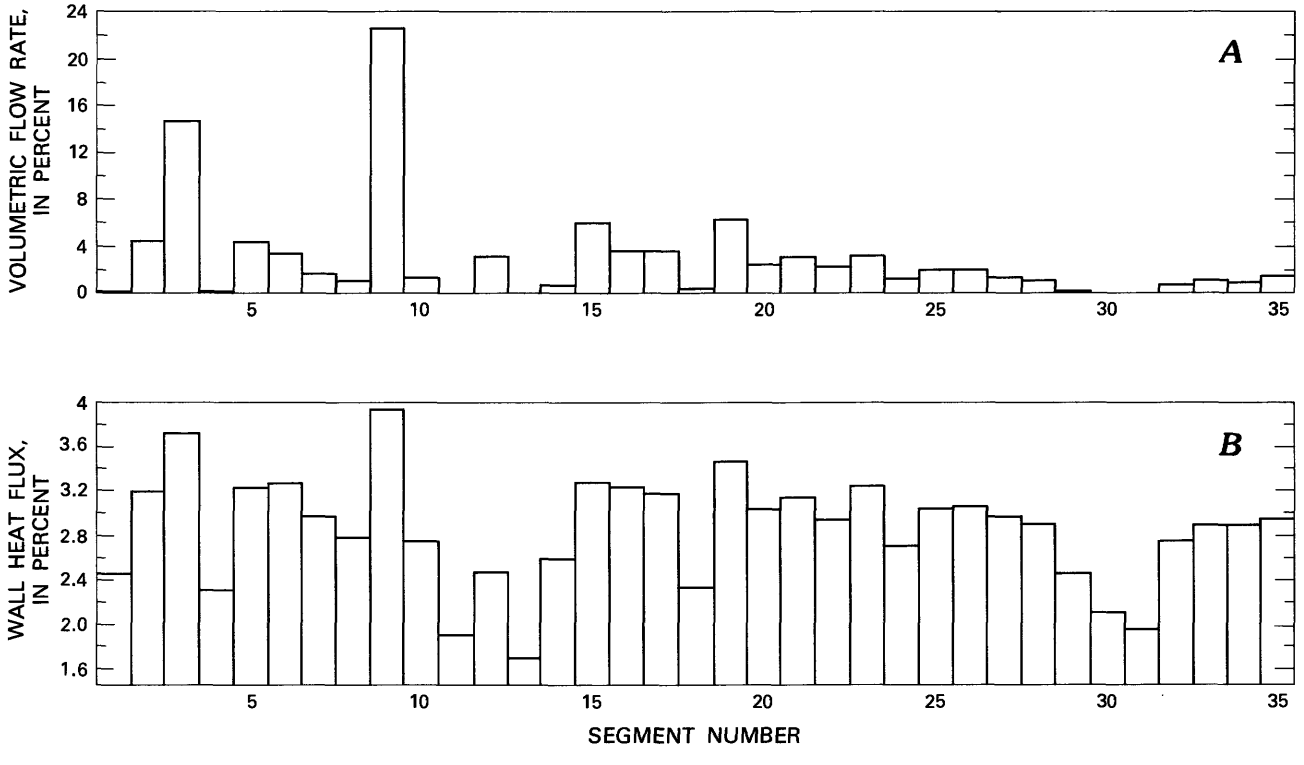

FIGURE 38.—Percentages of overall volumetric flow rate (*A*) and wall heat flux (*B*) for each of 35 segments of northeastern dike.

rate of heat loss. The volumetric flow rates are (Bird and others, 1960, p. 48; Johnson and Pollard, 1973):

$$Q=\frac{2}{3}\frac{\Delta P}{\eta_0 L}(T/2)^3 W\left\{1-\frac{3}{2}\frac{\tau_0}{(\Delta P/L)(T/2)}+\frac{1}{2}\left[\frac{\tau_0}{(\Delta P/L)(T/2)}\right]^3\right\}, \quad \text{(Bingham)}$$

$$Q=\frac{2A}{n+2}\left(\frac{\Delta P}{L}\right)^n (T/2)^{n+2} W. \quad \text{(pseudoplastic)}$$

Depending on the yield strength, a Bingham material may also exhibit a relation between volumetric flow rate and thickness that is somewhat less than the cubic relation for Newtonian fluids (table 5). Again, a pseudoplastic material can exhibit a much higher sensitivity between flow rate and conduit thickness than can a Newtonian fluid. Nevertheless, velocity gradient and volumetric flow rate differ dimensionally by the square of conduit thickness for flow in tabular conduits and by its cube for flow in circular conduits. Whereas the ratio of flow rate to heat loss scales as $T^3/T^{1/3}$ in a Newtonian fluid, it scales as $T^{n+2}/T^{n/3}$ in a pseudoplastic material. Thus, as thickness increases, even more magma is discharged, for a given amount of heat lost, than predicted earlier.

We obtained an estimate of the heat flux to wallrocks by linearizing the velocity field along the conduit wall (eq. 25). This linearization is fully applicable to the more complex fluids described above. However, the similarity solution thus derived (eq. 29) does not account for the temperature dependence of viscosity that is exhibited by all magmas. In addition, the solution does not account for the variations in temperature of the conduit walls at various downstream positions. As described earlier, these effects can be included by using the same similarity variable formulation and would, in general, alter the cube-root dependence between rate of heat loss and thickness. Because the constant-property model underpredicts viscosity near the wall, relative to the outside of the boundary layer, it also overpredicts the rates of downstream convection and cross-stream conduction.

We assumed that viscous dissipation is negligible—as indeed it is for flows with constant viscosity. Some theoretical evidence exists that dissipation is important during certain magmatic flows (Shaw, 1969; Fujii and Uyeda, 1974) in which viscosity drops as a result of viscous heating and the consequent increase in strain rate leads to runaway instabilities. Viscous runaway occurs most readily where there is no temperature difference between the walrocks and magma, and so viscous heat production is the only source of cross-stream conductive heat transport. Because temperature differences of hundreds of degrees Celsius probably existed between wallrocks and magma at Ship Rock, heat conduction due to these temperature differences would have been much larger than that due to viscous heat production.

We assumed that magma flow was laminar. Fluid mechanics recognizes that when a particular grouping of variables known as the Reynolds number **Re** exceeds a certain value, nonsteady, nonlaminar, or turbulent motion ensues. From experimental results, the critical Reynolds number is known to be about 2,000 (Bird and others, 1960, p. 187) by the relation $\mathbf{Re}=4R_h v\rho/\eta$, where R_h is the ratio of cross-sectional area to wetted perimeter, v is the average velocity, and η is the viscosity. A Reynolds number can be defined in terms of the volumetric flow rate Q, which has been measured during some volcanic eruptions:

$\mathbf{Re}=2Tv\rho/\eta=2Q\rho/\eta W$ for a tabular conduit,
$\mathbf{Re}=2Rv\rho/\eta=(2/\pi)Q\rho/\eta R$ for a circular conduit.

However, we have no way of knowing volumetric flow rate during emplacement of the northeastern dike and thus cannot directly calculate a Reynolds number. A magma with η=100 Pa·s and ρ=2.6 g/cm^3 (table 1) flowing through the northeastern dike would have had to deliver more than 0.12×10^6 m^3/s of magma to induce turbulent flow, with an average velocity greater than 1 km/min. If the dike vented at the Earth's surface, the resulting lava flow would have grown at a rate of 10 km^3/d. No evidence exists for such a flow at Ship Rock. If the magma did not vent, the driving pressure for dike propagation must have been relieved in less than the few minutes that it would have taken the dike to reach the surface. This result seems unlikely, also. The estimates of Reynolds number neglect segmentation of the dike, which would decrease the hydraulic radius R_h and increase the flow rate necessary to induce turbulent flow. Using the same values of the parameters given above, the volumetric flow rate through the southern plug must have been greater than 610 m^3/s for turbulent flow to occur. Average velocity for such a flow would have been greater than 0.9 m/s. This velocity seems physically reasonable. Indeed, in the next section we determine that when magmas are not vesiculating significantly, Reynolds numbers for eruptions at Kilauea Volcano in Hawaii are commonly well below the critical value, although velocities of magma ascent as great as 0.5 m/s have been recorded (Moore and Krivoy, 1964; Jackson and others, 1975). Flow in conduits with large ratios of cross-sectional area to

wall area, such as dikes, is likely to be laminar.

We assumed that changes in conduit form in the vertical z-direction could be neglected (fig. 36). We observed significant changes in form along the outcrop where the northeastern dike is segmented, offset, or enlarged owing to erosion of wallrocks; similar changes may exist below the present level of outcrop. The axial distance required for an initially flat velocity distribution, such as at the opening of a conduit, to develop its final parabolic form under a condition of steady-state flow is defined as the *momentum entry length*. For a constant-property fluid, the momentum entry length z^m, normalized for tabular and circular conduits, is given by (Kays, 1966)

$z^m/T=0.025\mathbf{Re}$ for a tabular conduit,
$z^m/R=0.1\mathbf{Re}$ for a circular conduit.

As the Reynolds number increases, the downstream distance required for the flow to readjust to changes in conduit form also increases. If $Q=10^3$ m^3/s (a large flow rate, by comparison with those observed on Hawaii) and using the same values of the parameters given above, we find that $\mathbf{Re}<20$ and that the flow would be fully developed over a distance equal to half the thickness of the conduit. Over such small distances, vertical changes in conduit form are probably negligible.

We assumed that, in the direction of flow, heat conduction is negligible in comparison with convection. The nondimensional grouping known as the Prandtl number $\mathbf{Pr}=(\eta/\rho)/(k/\rho\hat{C}_v)=\eta\hat{C}_v/k$—the ratio of the diffusivity of momentum to that of heat—can be used with the Reynolds number to verify this assumption. The thermal diffusivity $k/\rho\hat{C}_v$ of rock is relatively invariant and typically ranges between 10^{-7} and 10^{-6} m^2/s (table 1). Using the values in table 1, $\mathbf{Pr}=10^5$. The product $\mathbf{Re}\cdot\mathbf{Pr}$ provides a ratio of convective to conductive heat flow that, by experimental determination, must be less than 10^2 for downstream heat conduction to become significant in comparison with convection. Such a flow in the northeastern dike would have a Reynolds number of 10^{-3} and an average velocity of 10^{-5} m/s. This velocity is extremely slow relative to those measured on Hawaii.

The axial distance required for the cooling effects of the walls to be felt at the centerline of the conduit is defined as the *thermal entry length*. The thermal entry length z^θ, normalized for tabular and circular conduits, is given by (Kays, 1966):

$z^\theta/T=0.1\mathbf{Re}\cdot\mathbf{Pr}$ for a tabular conduit,
$z^\theta/R=0.05\mathbf{Re}\cdot\mathbf{Pr}$ for a circular conduit,

We are interested in estimating a minimum value for the thermal entry length. Using a low Reynolds number of 1 and a Prandtl number of 10^5, a minimum thermal entry length would be about $5{,}000T$, or 10 km, for the northeastern dike. In contrast to viscous effects, thermal effects are not readily transmitted in conduits. This result indicates that the cooling effects of wallrocks were probably not felt by magma flowing along the centerline of the dike and justifies the thermal-boundary-layer approximations used earlier.

We neglected time-dependent terms in the energy and momentum equations in our analysis; that is, the rates of accumulation of mass, momentum, and heat were assumed to be negligible in comparison to other terms. Although steady-state flow is never actually achieved, the temporal rate of change of magma flow is reckoned to be so small that a steady-state solution is accurate at an given moment. We have also ignored heat-transport mechanisms in the host rocks. The coupled heat flow that occurs between magma and host rocks is necessarily unsteady because the host rocks extend great distances from the dike. Because the proper thermal boundary conditions are quite complex and time dependent, and because of the exceedingly complex form of all dikes, we prefer to interpret our results as typical of the processes occurring during emplacement rather than as predictive of the flow rate and heat loss at that time.

OBSERVATIONS FROM MODERN FISSURE ERUPTIONS

Information concerning rates of dike propagation and magma discharge are unobtainable from our field data. In this section, we summarize several reports on modern basaltic volcanic eruptions to emphasize the similarities in eruptive geometries and observed sequences of events to those both observed and inferred at Ship Rock. We refer below to only a few of the numerous narratives of eruptions at Kilaeua Volcano published by members of the staff of the U.S. Geological Survey's Hawaiian Volcano Observatory. Eruptions are broadly divided into two types, summit and flank; the features described here are characteristic of both types.

Although the rate of magma supply to the surface at Kilaeua Volcano appears fairly constant when averaged over a period of decades (Swanson, 1972), the three longest historical eruptions have lasted more than 200 days, and the periods of quiescence more than 8 years (Macdonald and Abbott, 1970). Many eruptions were no longer than a day, and some were briefer than 6 hours. Eruptions have been

divided into phases of activity characterized by changes in extrusive behavior, such as periods of quiescence or variations in the locus of activity. For example, Kinoshita, Koyanagi, Wright, and Fiske (1969) recognized 31 phases, interrupted by periods of quiescence, for the 1967-68 summit eruption at Kilaeua, which lasted 250 days.

PROPAGATION OF ERUPTIVE FISSURES

Although the rate of magma ascent into the summit region of Kilauea is unknown, the rate of horizontal flow into the rift zones has been estimated. Deflation of the summit region commonly coincides with inflation of parts of either the southwest or east rift zones, presumably owing to dike intrusion. Dikes are observed in eroded rifts (Macdonald and Abbott, 1970), where thicknesses of 0.3 to 1.0 m are typical and maximum thicknesses of about 20 m have been reported. The presence of dikes in the rifts at Kilaeua was confirmed by observed gravity highs (Kinoshita and others, 1963; Kinoshita, 1965), seismic surveys (Hill, 1969), and patterns of surface deformation that correlate with dike inflation (Dietrich and Decker, 1975). Swanson, Jackson, Koyanagi, and Wright (1976) interpreted seismic activity and inflation in the rift zones as due to lateral migration of magma. Moore and Krivoy (1964), using seismic data, inferred that magma flowed almost horizontally along the northeast rift zone of Kilauea before the 1962 flank eruption, and calculated a maximum migration rate of about 0.4 m/s. Jackson, Swanson, Koyanagi, and Wright (1975) used geodetic data to calculate a rate of advance of about 0.45 m/s during the 1968 east-rift eruptions.

Virtually all historical eruptions on Hawaii have begun from fissures that propagated laterally to widths commonly in excess of 2 km. On May 31, 1954, an eruption broke out along a set of at least 14 parallel and echelon fissure segments on the floor of Kilauea caldera (Macdonald and Eaton, 1957). The line of narrow fissures grew to a total width of about 2.2 km in less than an hour, an average lateral propagation rate of 0.6 m/s. On February 28, 1955, an eruption began about 40 km from the caldera along a discontinuous chain of fissures that opened eastward to a width of 1.3 km at a rate of 5 cm/s (Macdonald and Eaton, 1964). The two principal fissures were about 100 m wide and sent out lava fountains 15 to 30 m high for 28 hours before activity ceased. Three days later, lava broke out nearby through fissures that grew to a width of 400 m in less than 5 minutes, a lateral propagation rate of 1.3 m/s. By May 27, all extrusive activity associated with the eruption that had begun 3 months earlier ceased, and more than 30 distinct fissures were mapped along a distance of almost 16 km.

During the eruption of Kilauea Iki beginning in November 1959 (Richter and others, 1970), a discontinuous system of fissures grew to a width of about 500 m in less than 30 minutes, an average rate of about 0.3 m/s. The fissures attained a maximum width of 800 m after about 90 minutes. This eruption was followed by another, 30 km away, on the flank of Kilaeua. There, the fissure system consisted of nine discrete vents that grew to a maximum width of 1.2 km in the first 90 minutes of the eruption, a lateral propagation rate of 0.2 m/s.

From these measurements of the lateral propagation rates of fissures, we infer characteristic dike-propagation rates at depth of 0.1 to 1 m/s; these rates are consistent with the estimated rates of magma advance in rift zones.

VOLUMETRIC FLOW RATE AND CHANNELIZATION OF MAGMA FLOW

During the eruptions at Kilauea, activity along most fissures began as a "curtain of fire" in which lava was extruded as a nearly continuous wall and reached heights commonly greater than 30 m. Rates of extrusion of lava, determined from volumes measured after degassing, may exceed 500 m^3/s (Kinoshita and others, 1969), although rates of less than 100 m^3/s are more typical. During all these eruptions, the curtain of fire gradually subsided, but extrusion continued from discrete sites along the initial fissure. This effect was well documented by Richter and others (1970) during the Kilaeua Iki eruption that began on November 14, 1959. During the first 90 minutes, lava fountains as high as 30 m issued from virtually the entire 800-m width of the fissure system along the slopes of a crater. Because all the lava flowed into the crater, detailed measurements of eruption rates could be recorded. After only 2 hours of activity, fountaining at the ends of the fissure system was retarded, but increased noticeably in the central part. After 8 hours, only two fissures remained active, and lava was ejected as high as 50 m from the central part of the initial fissure. After 24 hours and until the end of the eruption 36 days later, extrusion of lava was confined to a single vent. As the eruption continued over the next several days, both the rate of discharge of lava and the height of fountaining increased. By November 20, the height of fountains reached a maximum of 300 m, and the extrusion rate averaged about 100 m^3/s; but the eruption abruptly ceased the following day, bringing the first phase to

an end. During the next 4 weeks, 17 such phases were reported. Rates of extrusion were consistently greater during these later, shorter phases, and fountain heights commonly reached 600 m. A maximum extrusion rate of about 350 m^3/s was attained during the 16th phase. During the last 16 phases of eruption, the lava lake was repeatedly filling and emptying as the level of the lava lake reached that of the vent. The average rate of filling during that period was about 200 m^3/s, and the average rate of draining about 400 m^3/s. Examination of the vent after the eruption revealed an open conduit, roughly elliptical in cross section, about 15 by 30 m in axial dimensions near the surface, and about 10 by 15 m at a depth of about 25 m.

The simplifying assumption of laminar flow that we made in our analysis of the dike can be applied to the eruptions on Hawaii, as demonstrated by using the maximum estimate of volumetric flow rate during initial phases of the 1959 Kilauea Iki eruption. Choosing ρ=2.6 g/cm^3, η=50 Pa·s, and Q=100 m^3/s, the flow of lava in a dike would have to be confined to a width less than 6 m for turbulent flow to occur. If the flow were confined to a pluglike conduit, then its radius would have to be less than 2 m for turbulent flow to occur. Because both these dimensions are unrealistically small, the flow was probably laminar. Maximum flow rates recorded during drainback were as great as 500 m^3/s. The radius of a plug accepting lava at this rate would have to be less than 8 m for turbulent flow to occur; the observed conduit, however, was larger than this. These estimates assume that the magma was not vesiculating and thus are invalid for the final few hundred meters of its ascent. For typical rates of discharge, turbulent flow can be discounted in dikes but is somewhat more likely in plugs. For a discharge rate of 100 m^3/s, the rate of convective heat transport $\rho\hat{C}_v QT$ at the Earth's surface was about 0.3×10^{12} *W*. Later, we compare this rate of heat transport with an estimate of the heat flux during emplacement of the northeastern dike.

Field inspection of vents at Kilauea revealed that the final stages of virtually all eruptions are marked by a reversal in the direction of lava flow (Richter and others, 1964; Fiske and Koyanagi, 1968; Jackson and others, 1975). During some phases of an eruption, as much as 95 percent of the total volume of lava drains back into the vent. Drainback can occur along part of a fissure system as extrusion proceeds elsewhere, and it marks the final stages of many eruptions. This observation has implications for geologists studying subvolcanic dikes. For instance, magma may have descended from the Earth's surface after having ascended from a deep source region. The loss of volatile contents from such a magma before drainback may obscure its initial chemistry and alter its mineralogy. Drainback must be accompanied by a decrease in driving pressure that would cause dikes to deflate partially. Because most eruptions are marked by short periods of quiescence and drainback between extrusive events, magma may be reinjected into preexisting conduits with each phase of renewed activity. Thus, different magmas may be juxtaposed at the same outcrop of a dike.

DISCUSSION AND CONCLUSIONS

From our field data at Ship Rock, we have constructed mechanical models for dilation and propagation of dikes, flow of magma, and loss of heat. From the data and theory, we argue that the initial emplacement of magma was in a dike composed of discontinuous echelon segments with a variety of cross-sectional forms depending substantially on the proximity of adjacent segments. Strikes of segments range systematically along the outcrop width of the northeastern dike from N. 52° E. to N. 66° E. Local variations in strike may be appreciably greater within a single dike segment, owing to the presence of such minor structures as cusps, offsets, and buds. Wallrocks in certain places along the dike were fractured and comminuted to breccias that subsequently were eroded by flowing magma. Discharge from these buds, which served as channels to focus the flow, may have exceed that in adjacent parts of the dike by as much as an order of magnitude. Some buds grew into plugs or volcanic necks by further erosion of the wallrocks as magma in the dike cooled and stagnated. Flow rates in these plugs were higher than elsewhere; the rate of heat loss from plugs, however, was not appreciably greater.

Qualitatively, this hypothetical sequence of events correlates well with observations made at the ground surface during modern fissure eruptions on Hawaii. The initial eruption is from discontinuous, commonly echelon fissures approximately 100 m wide and 1 m thick; the line of fissures may extend for several kilometers and propagates to its final width in less than a few hours at rates generally less than 1 m/s. When the eruption continues for several hours or days, lava issues from discrete vents that grow to several tens of meters in diameter. Flow rates and heights of lava fountains increase as the eruption localizes, and then the greatest volume of lava is extruded from one or several vents that have taken over as the principal conduits. Volumetric flow rates are commonly less than 100 m^3/s.

DIKE DILATION AND PROPAGATION

It is remarkable that a geologic structure as discontinuous in form as the northeastern dike deviates less than 40 m from a straight line along its 2,900-m outcrop length. We feel that the overall alinement of dike segments reflects the presence of a rectilinear dike at depth; we infer that the dike broke down into many segments that propagated slightly out of plane owing to small vertical variations in the direction of horizontal principal stress. Each discrete segment propagated along a curved surface that was perpendicular to the axis of local least compressive stress.

The segmented form of dikes, as well as the presence of dike-parallel joints, has led some geologists to suggest that magma fills joints and other preexisting fractures in the host rocks (Johnson, 1961; Currie and Ferguson, 1970; Macdonald and Abbott, 1970). In general, systematic joints adjacent to the northeastern dike are oriented parallel to its walls. Because regional systematic joints of the same orientation are nearly absent, we conclude that the regional joint pattern played no role in dike emplacement. Ziony (1966) reported that minette dikes in Monument Valley, Utah, have dike-parallel joints, despite the absence of regional joints of similar orientation. Our analysis of dike dilation shows that both the form of segments and the stress intensities are incompatible with magma filling part of a preexisting joint. The form could be due to intrusion along preexisting joints only if the magma flowed to the tips of these joints and then propagated somewhat farther. Because the dike-parallel joint set is confined to a narrow region around the outcrop of the dike, the joints probably formed as a result of dike emplacement. We speculate that the joints formed from some combination of thermal stresses, stresses due to cooling and contraction of the dike, or tensile stresses above the periphery of the propagating dike.

The presence of numerous cusps and offsets along particular segments clearly indicates that as the northeastern dike grew, adjacent segments tended to coalesce. Experimental studies summarized in earlier sections of this report indicate that segmentation during fracture propagation is common, almost ubiquitous. Thus, many more segments are likely to be present around the periphery of a dike than elsewhere. With continued growth, segments with offsets less than a few meters would have coalesced into single segments at the present outcrop level. Although more cusps than offsets are exposed along the outcrop length of the northeastern dike, most discrete segments are offset relative to their neighbors. This observation implies that adjacent collinear segments tended to coalesce more easily than those that were offset. Our analysis of interacting pressurized cracks corroborates this interpretation because the mode I stress intensity at the ends of adjacent collinear cracks increases during propagation of the tips toward one another. Offset cracks tend to stop propagating as soon as overlap reaches a distance comparable to offset because the mode I stress intensity decreases as crack tips overlap.

The interaction of two offset cracks generates shear along the cracks and tends to induce propagation out of the crack planes at adjacent tips. Because the ratio of mode II to mode I stress intensity passes through a small positive maximum and then plunges to relatively large negative values, crack paths should diverge slightly and then converge as adjacent tips propagate past one another. The northeastern and southern dikes crop out in a configuration suggesting that this type of mechanical interaction did indeed occur. However, individual segments of the northeastern dike are nearly straight and do not follow the paths predicted by our analysis. Two factors not included in our analysis could have prevented the divergence and convergence of segment tips due to interaction: dike-parallel joints forming above the advancing segments would promote a straight path, and a relatively great compressive stress acting parallel to the segments would have a similar effect.

We are unable to account for the uniform thickness (excluding brecciated parts) of the northeastern dike if the host rock between each of the 35 segments behaved as a linear elastic material and the segments continued to great depth without coalescing. Indeed, the radii of curvature at the ends of segments are larger than can be accommodated by elastic deformation. A zone of inelastic deformation may have linked segment ends that are close to one another. Also, we suggest that all segment ends nearer than 10 m from one to another coalesce within several tens of meters below the outcrop. Thus, we calculate that the 35 dike segments behaved mechanically as if they were only 10.

Calculations of conduit form enable us to determine those ratios of driving pressure to elastic shear modulus for pressurized cracks that best mimic the geometry of the dike segments. We cannot distinguish between magmatic pressure and regional least principal stress unambiguously, but refer to the difference between these quantities as the driving pressure. To estimate driving pressure, we compare the average densities of static magma and of rock columns extending to the old surface, 1,000 m above the present outcrop. We do not know whether the northeastern dike propagated this distance, but accept this value as likely. Taking a difference in weight per unit

volume (table 1) of 2×10^3 Pa/m^3, the driving pressure would be 2 MPa. For a ratio of pressure to modulus of 1.7×10^{-3} (the result for the 10-crack model), we calculate as shear modulus of about 10^3 MPa. Using a ratio of 0.6×10^{-3} (the result for the single-crack model), we calculate a shear modulus of about 3×10^3 MPa. This value is an upper bound for the shear modulus, in that we neglect the resistance to dilation of all bridges of the Mancos Shale between segments. These results are consistent with laboratory and in-place determinations of friable sandstone and soft shale.

Accepting a shear modulus of 10^3 MPa, the driving-stress distribution for the single-crack model (table 3), as determined from equations 19*B* and 19*C*, is $(0.64+0.69\ |X|-0.28X)$ MPa. The driving stress decreases from 1.61 MPa on the southwest to 1.05 MPa on the northeast. Although the origin of the gradients identified by this analysis is obscure, we suggest several possibilities. A pressure in Ship Rock itself could create a circumferential tensile stress decreasing along lines radial to the throat. A crater above Ship Rock would form a topographic low and result in a lower lithostatic pressure at depth near Ship Rock relative to points at similar depths farther away. If the magma in the dike behaved like a fluid with strength, and if one component of flow was directed away from Ship Rock, then a pressure gradient would have been preserved along the dike after flow ceased. Although any of these possible origins may serve to explain the calculated decrease in driving stress from southwest to northeast, they do not explain the symmetrical part of the stress distribution that results in a low stress of 0.64 MPa near the middle of the northeastern dike and greater stresses toward either end. The only observed structure with this symmetry is the gentle syncline trending across the dike (see fig. 2). Greater compression near the core of the syncline relative to its limbs could explain the lower driving stress near the center of the dike.

We used the normalized mode I stress-intensity factors (table 4) calculated for the 10-crack model to estimate the fracture toughness of the Mancos Shale. If the driving pressure did not drop substantially after propagation ceased, then these normalized factors are a direct measure of fracture toughness. Choosing a driving pressure of 2 MPa and using the appropriate half-width for each segment, we calculate a range in fracture toughness of 30 to 110 MPa·m$^{1/2}$ and an average of about 75 MPa·m$^{1/2}$. These values are significantly greater than the range of 0.5-5.0 MPa·m$^{1/2}$ (table 1) reported from laboratory tests. We suggest two explanations for this great difference between laboratory and field determinations of fracture toughness. First, the laboratory results may not be relevant, either because the dike segments are orders of magnitude wider than laboratory cracks or because environmental conditions (for example, temperature or pressure) differ significantly. This possibility may be clarified by future laboratory work. Second, the two-dimensional analysis using uniform driving pressure and the mapped geometry of dike segments may not be adequate. We examine this possibility briefly below, although it fails to change the field determinations. Until the discrepancy is resolved, we cannot rely on laboratory values of fracture toughness in studies of large cracks in rock.

A nonuniform driving pressure could reduce the stress intensity at dike-segment tips and thereby reduce the estimates of fracture toughness. One mechanism for creating nonuniform pressure is an open crack extending ahead of the magma. Thus, a uniform driving pressure p is exerted only over a central width $2c$ of a segment of total width $2a$. The full strength of the regional compression s acts against dilation over a width $b=a-c$ at the segment ends. The mode I stress-intensity factor (Broek, 1974) for a crack subject to these loading conditions is $K_I=pa^{1/2}-(s+p)a^{1/2}[(2/\pi)\cos^{-1}(c/a)]$. To produce a stress intensity of 1 MPa·m$^{1/2}$ (representative of laboratory values) on a dike segment of total width $2a=100$ m and subjected to loads of $p=2$ MPa and $s=24$ MPa, we calculate $b=0.3$ m. Increasing the driving pressure to 5 MPa increases b to 1.7 m. The absence of compelling evidence for cracks extending ahead of the dike segments at Ship Rock casts doubt on, but does not rule out, this mechanism. Relatively poor exposure in the Mancos Shale, the possibility that such cracks would close without much trace, and the presence of joints parallel to the dike all tend to obscure definitive evidence.

A second mechanism for creating nonuniform pressure is an increased strength of magma upon cooling that preserved a pressure gradient $-(dp/dx)$ due to magma flow toward the ends of segments. From equation 18*D*, the mode I stress-intensity factor is $K_I=pa^{1/2}-(dp/dx)a^{1/2}(2a/\pi)$. A stress intensity of 1 MPa·m$^{1/2}$ on a dike segment of width $2a=100$ m and subjected to a driving pressure of 2 MPa requires a gradient dp/dx of 60 kPa/m. The normal stress acting on the dike wall changes from a compression of −2 MPa at the center to a tension of 1 MPa at the tips. We have no direct evidence either to support or to reject such a gradient. For such a nonuniform loading, centers of segments would bulge outward relative to more tapered forms near the tips (fig. 28). The close fit of the dilations due to uniform loading to the thickness data argues against this mechanism for reducing stress intensity.

Finally, we examine the possibility that the mapped widths of segments are inappropriate to our analysis. As echelon crack tips overlap, the mode I factor decreases markedly (fig. 24*B*), and so a greater width would lower the estimate of fracture toughness. Perhaps we overlooked thin sheets of minette beyond the mapped ends of segments, or perhaps the segment widths increase just below the outcrop. We compare the solution for cracks of mapped widths with a solution for extended cracks. Adding 1 m to each crack tip changes the mode I factors by an average of 5 percent, and adding 5 m changes these factors by an average of 30 percent—insufficient changes to account for the anomalously great fracture toughness. Therefore, we reject this explanation for the relatively great estimates of fracture toughness.

MAGMA FLOW AND HEAT TRANSPORT

In our analysis of magma flow and heat transport we chose not to derive equations that emphasize such factors as nonlinear or temperature-dependent flow properties, viscous heat production, or compressible-fluid flow, even though all these factors may be important under certain conditions. Instead, we focused on the fact that the geometry of igneous conduits plays a major role in determining the rate of discharge of magma and, thus, the rate of convective heat transport. However, variation in the conduit geometry from idealized forms does not significantly affect the rate of heat loss to wallrocks. To illustrate these conclusions, we use typical values of selected parameters (table 1) to convert our nondimensional flow rates and heat fluxes into dimensional estimates. As an example, we choose a driving-pressure gradient of 0.1 percent of the weight per unit volume of magma (26 Pa/m). Although this pressure gradient is small, larger gradients lead to volumetric flow rates that are orders of magnitude larger than those observed on Hawaii. Although such rates are possible, we find no reason to accept them as probable or characteristic. Exceedingly small variations in the pressure of the source region could have lowered the driving pressure below that necessary to support the magma column and resulted in drainback of lava and deflation of the dike.

In a previous section, we postulated that stresses acting on the walls of the northeastern dike were small in comparison to driving pressure for dilation. Using a maximum thickness of 7.2 m, a driving-pressure gradient as above, a viscosity of 100 Pa·s, and the solution for flow in a tabular conduit (table 5), we estimate a maximum shear stress of less than 1 Pa. This stress is indeed small relative to our estimate of driving pressure.

We used the values of parameters given in table 1 and above, and the dimensionless values in table 6, in conjunction with the measured widths of dike segments to estimate the flow rate and heat flux in each segment. If magma flowed through the entire dike at once, the volumetric flow rate would have been about 10^3 m^3/s. The flow rate predicated for a tabular conduit of the mean dilational thickness of the northeastern dike (2.0 m) would have been about 500 m^3/s, and the average velocity about 0.1 m/s. Using this velocity as a measure of the rate of magma ascent in the northeastern dike, the dike would have propagated 1,000 m upward in about 3 hours. If magma flowed only through the widest segment, 9, the volumetric flow rate would have been 270 m^3/s, and the average velocity about 0.6 m/s. These rates are of the same order of magnitude as those reported on Hawaii. Although our selection of the pressure gradient is arbitrary, exceedingly small pressures in excess of static pressure can clearly drive substantial magma flows.

The rate of heat loss is dependent on three additional unknowns: (1) distance from the source region, (2) three-dimensional conduit geometry, and (3) temperature difference between magma and host rocks. Conduit geometry is extremely important in determining the form of the thermal boundary layer. Offsets and irregularities in the dike wall may tend to mix convecting magma and thin the layer of nonuniform temperature. From continuity considerations, volumetric flow rates must have been about equal at all levels across the conduit. At the source region, for a dike similar in form to that presently exposed, the rate of energy convection ($\rho \hat{C}_v Q T$ was about 5×10^{12} W if magma flowed through the entire dike at once, or about 1×10^{12} W if it flowed only through a segment similar to 9. We assume that the source region was 2,000 m below the present outcrop and that the form of the conduit was similar to that either of the dike or of segment 9 throughout its vertical extent. Because continued convection of magma heats the adjacent wallrocks to a temperature well above the average for the initial magma and rock temperatures, we assume a temperature difference of 100°C. If magma flowed through the entire width of a conduit similar to the northeastern dike, then about 10×10^9 W of heat would have been lost through the walls, that is, about 0.2 percent of the energy convected up the conduit. If the magma flowed entirely through segment 9, the total rate of heat loss would have been about 0.5×10^9 W. If the source region was 5,000 m below the present outcrop, then the loss of heat would have been 20×10^9 W. At any moment during the emplacement process,

rates of heat loss are indeed negligible relative to the amount of heat transported in the flowing magma. Although these estimates are approximate for the reasons outlined above, the orders-of-magnitude difference between the amount of energy convected up the conduit and the heat conducted through the dike walls suggests that any uncertainty in the appropriate values of physical parameters and the temperature difference would not significantly alter our conclusions. These low rates of heat loss may be important when unsteady effects of magma solidification are considered (Delaney and Pollard, 1981).

GROWTH OF PLUGS AND BRECCIATION OF HOST ROCKS

A common feature of pluglike bodies throughout the Colorado Plateaus is the surprising absence of deformation of the adjacent host rocks (Johnson, 1906; Williams, 1936; McBirney, 1959). Commonly, host rocks are undisturbed or exhibit only minor baked zones, narrow regions of intense fracturing, or discrete faults that indicate slumping of host rocks into the intrusion (Williams, 1936; Hunt, 1938). Breccias are so common in plugs that virtually all the hypotheses advanced to account for plug growth (Geikie, 1902; Hunt, 1938; McBirney, 1959, 1963; Barrington and Kerr, 1961; Kerr and Barrington, 1963) regard brecciation as the primary process. Another common feature of plugs is their general occurrence in regions where dikes are also observed. This tendency is apparent within the Colorado Plateaus province of the Navaho and Hopi volcanic fields (Gregory, 1917), at Rio Puerco east of Mount Taylor volcano (Hunt, 1938), on the San Rafael Swell (Gilluly, 1929), and in the Chuska volcanic field (Appledorn and Wright, 1957). Furthermore, the plugs and necks in these areas commonly are arranged in linear arrays, and where the necks are elongate, their greatest dimension commonly parallels nearby dikes. It is of interest that the most deeply eroded neck in the Hopi field is laterally associated with a dike (Hack, 1942). Many workers, including Williams (1936), Hack (1942), Allen and Balk (1954), Shoemaker, Roach, and Byers (1962), and McGetchin (1968), suggested that the observed intrusions merge with dikes at depth.

The earliest mechanism proposed to account for the origin of plugs (Geikie, 1902; Williams, 1936) involves repeated "explosive boring" of roof rocks over an ascending magma body by the action of "subterranean gases." We note here that because no evidence exists for significant vesiculation of the minette near Ship Rock, the only gas available for such a mechanism of intrusion is steam converted from ground water.

McBirney (1959) extended a suggestion by Hunt (1938) that host rocks around an ascending plug may be eroded by surging and churning of the magma within. McBirney's (1959) model of plug growth accounts for brecciation of the host rocks by thermoelastic stressing of wallrocks and erosion of these rocks to breccia by free convection of magma within the intrusion. In addition, McBirney (1959) conjectured that fracturing induced by high pore-fluid pressures due to heating of wallrocks may also be important. This model does not account for the spatial association of plugs and dikes and, insofar as the emplacement process is driven by heat losses to wallrocks and the magma system is self-contained, does not adequately explain how the magma can remain mobile. In addition, thermally driven processes tend to produce bodies of equant geometry because heat transport is diffusional in nature. In experiments on blocks of wax heated from below, Hardee and Larson (1977) were unable to create pluglike bodies with axial lengths of more than a few times their diameter because the heat flux, which controls the rate of melting of the wax, became equally distributed over the entire area of the body and resulted in a semispherical intrusive form.

Pressurization of a cylindrical body applies a tension parallel to its walls. Excluding the region surrounding the tip of a dike, this tension is greater along the walls of a plug than of a dike. Heating of those walls allows the host rocks to expand and relieves the tensile stress. For failure to occur by cracking parallel to the walls, thermal expansion of the host rocks must first relieve the tensile stress and then build up a compressive stress greater than the magma pressure. Because tensile stresses along the walls of a dike are less than those along the walls of a plug, the dike wall should fail first if thermoelastic stresses are a governing mechanism of brecciation. However, breccias are everywhere observed to be associated with plugs and only locally with dikes. Therefore, the notion that thermoelastic stresses alone can account for brecciation is invalid. Our preliminary analyses reveal that pressurization of pore fluids due to heating can significantly increase effective stresses in rocks with permeabilities comparable to those of shale and siltstone (Delaney, 1980). We note that for water held at constant volume, pressure gradients of more than 1.5 MPa/°C are typical for conditions comparable to the upper few kilometers of the Earth's crust. Such a pore-pressure increase is a likely mechanism for brecciation and is an important avenue of future research.

Although the field relations at Ship Rock clearly indicate that at least some growth of the buds and plugs occurred after their associated dike was em-

placed, we cannot conclude that all plugs or breccia bodies generally grow along the walls of dikes. For instance, two plugs on the west side of Ship Rock (fig. 2) are alined along the projections of nearby dikes but do not visibly contact them. In those places, we infer that brecciation and invasion of magma occurred above or at the upper periphery of a dike. Future fieldwork on plugs and necks should include careful examination of the relations to nearby dikes and determinations of the three-dimensional form of breccia bodies.

REFERENCES CITED

Allen, J. E., and Balk, Robert, 1954, Mineral resources of Fort Defiance and Tohatchi quadrangles, Arizona and New Mexico: New Mexico Bureau of Mines and Mineral Resources Bulletin 36, 192 p.

Anderson, E. M., 1938, The dynamics of sheet intrusion: Royal Society of Edinburgh Proceedings, ser. B, v. 58, no. 3, p. 242-251.

Appledorn, C. R., and Wright, H. E., Jr., 1957, Volcanic structures in the Chuska Mountains, Navajo Reservation, Arizona-New Mexico: Geological Society of America Bulletin, v. 68, no. 4, p. 445-467.

Armstrong, R. L., 1969, K-Ar dating of laccolithic centers of the Colorado Plateau and vicinity: Geological Society of America Bulletin, v. 80, no. 10, p. 2081-2086.

Barrington, Jonathan, and Kerr, P. F., 1961, Breccia pipe near Cameron, Arizona: Geological Society of America Bulletin, v. 72, no. 11, p. 1661-1674.

Beaumont, E. C., 1955, Preliminary geologic map of the Ship Rock and Hogback quadrangles, San Juan County, New Mexico: U.S. Geological Survey Coal Investigations Map C-29, scale 1:48,000.

Birch, Francis, 1966, Compressibility; elastic constants, *in* Clark, S. P., Jr., ed., Handbook of physical constants (revised ed.): Geological Society of America Memoir 97, p. 97-173.

Bird, R. B., Stewart, W. E., and Lightfoot, E. N., 1960, Transport phenomena: New York, John Wiley & Sons, 780 p.

Blair, B. E., 1955, Physical properties of mine rock, part 3: U.S. Bureau of Mines Report of Investigations 5130, 69 p.

_____1956, Physical properties of mine rock, part 4: U.S. Bureau of Mines Report of Investigations 5244, 52 p.

Bottinga, Yan, and Weill, D. F., 1970, Densities of liquid silicate systems calculated from partial volumes of oxide components: American Journal of Science, v. 269, no. 2, p. 169-182.

Broek, David, 1974, Elementary engineering fracture mechanics: Leyden, Netherlands, Noordhoff, 408 p.

Carrier, G. F., Krook, Max, and Pearson, C. E., 1966, Functions of a complex variable: New York, McGraw-Hill, 438 p.

Clark, S. P., Jr., 1966, Thermal conductivity, *in* Clark, S. P., Jr., ed., Handbook of physical constants (revised ed.): Geological Society of America Memoir 97, p. 459-482.

Clifton, R. J., Simonson, E. R., Jones, A. H., and Green, S. J., 1976, Determination of the critical-stress-intensity factor K_{Ic} from internally pressurized thick-walled vessels: Experimental Mechanics, v. 16, no. 6, p. 233-238.

Crow, E. L., Davis, F. A., and Maxfield, M. W., 1960, Statistics manual: New York, Dover, 288 p.

Currie, K. L., and Ferguson, John, 1970, The mechanism of intrusion of lamprophyre dikes indicated by "offsetting" of dikes: Tectonophysics, v. 9, no. 6, p. 525-535.

Daly, R. A., Manger, G. E., and Clark, S. P., Jr., 1966, Density of rocks, *in* Clark, S. P., Jr., ed., Handbook of physical constants (revised ed.): Geological Society of America Memoir 97, p. 19-26.

Delaney, P. T., 1980, Expansion and pressurization of groundwater during heating from an igneous intrusion: A mechanism for brecciation of host rocks [abs.]: Eos (American Geophysical Union Transactions), v. 61, no. 46, p. 1146.

Delaney, P. T., and Pollard, D. D., 1981, Solidification of basaltic magma during flow in a dike: America Journal of Science [in press].

Dietrich, J. H., and Decker, R. W., 1975, Finite element modeling of surface deformation associated with volcanism: Journal of Geophysical Research, v. 80, no. 29, p. 4094-4102.

Dixon, S. J., 1970, Pressure meter testing of soft bedrock, *in* Determination of the *in situ* modulus of deformation of rock: American Society for Testing and Materials Special Technical Publication 477, p. 126-136.

Ehrenberg, S. N., 1978, Petrology of potassic volcanic rocks and ultramafic zenoliths from the Navajo volcanic field, New Mexico and Arizona: Los Angeles, University of California, Ph. D. thesis, 259 p.

Erdogan, Fazil, and Aksogan, O., 1974, Bonded half planes containing an arbitrarily oriented crack: International Journal of Solids and Structures, v. 10, no. 6, p. 569-585.

Fiske, R. S., and Koyanagi, R. Y., 1968, The December 1965 eruption of Kilauea Volcano, Hawaii: U.S. Geological Survey Professional Paper 607, 21 p.

Fujii, Naoyuki, and Uyeda, Seiya, 1974, Thermal instabilities during flow of magma in volcanic conduits: Journal of Geophysical Research, v. 79, no. 23, p. 3367-3369.

Geikie, Archibald, 1902, The geology of eastern Fife: Glasgow, J. Hedderwick & Sons, 421 p.

Gere, J. M., and Weaver, W. F., 1965, Matrix algebra for engineering: New York, Van Nostrand-Reinhold, 168 p.

Gilluly, James, 1929, Geology and oil and gas prospects of part of the San Rafael Swell, Utah *in* Contributions to economic geology. Part II.—Mineral fuels: U.S. Geological Survey Bulletin 806, p. 69-130.

Gregory, H. E., 1917, Geology of the Navajo country: U.S. Geological Survey Professional Paper 93, 161 p.

Hack, J. T., 1942, Sedimentation and volcanism in the Hopi Buttes, Arizona: Geological Society of America Bulletin, v. 53, no. 2, p. 335-372.

Hanley, E. J., DeWitt, D. P., and Roy, R. F., 1978, The thermal diffusivity of eight well-charcterized rocks for the temperature range 300-1000 K: Engineering Geology, v. 12, no. 1, p. 31-47.

Hardee, H. C., and Larson, D. W., 1977, The extraction of heat from magmas based on heat transfer mechanisms: Journal of Volcanology and Geothermal Research, v. 2, no. 2, p. 113-144.

Hendron, A. J., Mesri, Gholamreza, Gamble, J. C., and Way, Grover, 1970, Compressibility characteristics of shales measured by laboratory and *in situ* tests, *in* Determination of the *in situ* modulus of deformation of rock: American Society for Testing and Materials Special Technical Publication 477, p. 137-153.

Hill, D. P., 1969, Crustal structure of the Island of Hawaii from seismic-refraction measurements: Seismological Society of America Bulletin, v. 59, no. 1, p. 101-130.

Hodgson, R. A., 1961, Classification of structures on joint surfaces: American Journal of Science, v. 259, no. 7, p. 493-502.

Howard, G. C., and Fast, C. R., 1970, Hydraulic fracturing: Henry L. Doherty Series Monograph, v. 2: New York, Society of Petroleum Engineers of AIME, 203 p.

Hubbert, M. K., and Willis, D. G., 1957, Mechanics of hydraulic

fracturing: American Institute of Mining, Metallurgical, and Petroleum Engineers Transactions, v. 210, p. 153-168.

Hunt, C. B., 1938, Igneous geology and structure of the Mount Taylor volcanic field, New Mexico: U.S. Geological Survey Professional Paper 189-B, p. 51-80.

Jackson, D. B., Swanson, D. A., Koyanagi, R. Y., and Wright, T. L., 1975, The August and October 1968 east rift eruptions of Kilauea Volcano, Hawaii: U.S. Geological Survey Professional Paper 890, 33 p.

Johnson, A. M., 1970, Physical processes in geology: San Francisco, Freeman, Cooper, 577 p.

Johnson, A. M., and Pollard, D. D., 1973, Mechanics of growth of some laccolithic intrusions in the Henry Mountains, Utah, I: Field observations, Gilbert's model, physical properties and flow of magma: Tectonophysics, v. 18, no. 3, p. 261-309.

Johnson, D. W., 1906, Volcanic necks of the Mount Taylor region, New Mexico: Geological Society of America Bulletin, v. 18, p. 303-324.

Johnson, R. B., 1961, Patterns and origin of radial dike swarms associated with West Spanish Peak and Dike Mountain, south-central Colorado: Geological Society of America Bulletin, v. 72, no. 4, p. 579-589.

Kay, R. W., and Gast, P. W., 1973, Rare earth content and origin of alkali-rich basalts: Journal of Geology, v. 81, no. 6, p. 653-682.

Kays, W. M., 1966, Convective heat and mass transfer: New York, McGraw-Hill, 385 p.

Kelley, V. C., and Clinton, N. J., 1960, Fracture systems and tectonic elements of the Colorado Plateau: University of New Mexico Publications in Geology 6, 104 p.

Kerr, P. F., and Barrington, Jonathan, 1963, Breccia pipe near Cameron, Arizona: Reply: Geological Society of America Bulletin, v. 72, no. 2, p. 233-237.

Kinoshita, W. T., 1965, A gravity survey of the Island of Hawaii: Pacific Science, v. 19, no. 3, p. 339-340.

Kinoshita, W. T., Koyanagi, R. Y., Wright, T. L., and Fiske, R. S., 1969, Kilauea volcano: The 1967-68 summit eruption: Science, v. 166, no. 3904, p. 459-468.

Kinoshita, W. T., Krivoy, H. L., Mabey, D. R., and MacDonald, R. R., 1963, Gravity survey of the Island of Hawaii, *in* Short papers in geology and hydrology: U.S. Geological Survey Professional Paper 475-C, p. C114-C116.

Lachenbruch, A. H., 1961, Depth and spacing of tension cracks: Journal of Geophysical Research, v. 66, no. 12, p. 4273-4292.

Levinson, Norman, and Redheffer, R. M., 1970, Complex variables: San Francisco, Holden-Day, 429 p.

Luth, W. C., 1967, Studies in the system $KAlSiO_4$-Mg_2SiO_4-SiO_2-H_2O: I, Inferred phase relations and petrologic applications: Journal of Petrology, v. 8, no. 3, p. 372-416.

Lutton, R. J., 1971, Tensile fracture mechanics from fracture surface morphology, *in* Clark, G. B., ed., Dynamic rock mechanics: Symposium on Rock Mechanics, 12th, Rolla, Mo., 1970, Proceedings, p. 561-571.

Macdonald, G. A., and Abbott, A. T., 1970, Volcanoes in the sea: Honolulu, University of Hawaii Press, 441 p.

Macdonald, G. A., and Eaton, J. P., 1957, Hawaiian volcanoes during 1954: U.S. Geological Survey Bulletin 1061-B, p. 17-72.

———1964, Hawaiian volcanoes during 1955: U.S. Geological Survey Bulletin 1171, 170 p.

McBirney, A. R., 1959, Factors governing emplacement of volcanic necks: American Journal of Science, v. 257, no. 6, p. 431-448.

———1963, Breccia pipe near Cameron, Arizona: Discussion: Geological Society of American Bulletin, v. 74, no. 2, p. 227-232.

McGetchin, T. R., 1968, The Moses Rock dike: Geology, petrology and mode of emplacement of a kimberlite-bearing breccia dike, San Juan County, Utah: Pasadena, California Institute of Technology, Ph. D. thesis, 440 p.

Moore, J. G., and Krivoy, H. L., 1964, The 1962 flank eruption of Kilauea Volcano and structure of the east rift zone: Journal of Geophysical Research, v. 69, no. 10, p. 2033-2045.

Murase, Tsutomu, and McBirney, A. R., 1973, Properties of some common igneous rocks and their melts at high temperatures: Geological Society of America Bulletin, v. 84, no. 11, p. 3563-3592.

Muskhelishvili, N. I., 1919, Sur l'integration de l'equation biharmonique: Akademii Nauk SSSR Izvestiya, ser. 6, no. 12-15, p. 663-686.

———1975, Some basic problems of the mathematical theory of elasticity: Leyden, Netherlands, Noordhoff, 732 p.

Naeser, C. W., 1971, Geochronology of the Navajo-Hopi diatremes, Four Corners area [Colorado]: Journal of Geophysical Research, v. 76, no. 20, p. 4978-4985.

Nicholls, J. W., 1969, Studies of the volcanic petrology of the Navajo-Hopi area, Arizona: Berkeley, University of California, Ph. D. thesis, 107 p.

O'Sullivan, R. B., and Beikman, H. M., compilers, 1963, Geology, structure, and uranium deposits of the Shiprock quadrangle, New Mexico and Arizona: U.S. Geological Survey Miscellaneous Geologic Investigations Map I-345, scale 1:250,000.

Pigford, R. L., 1955, Nonisothermal flow and heat transfer inside vertical tubes: Chemical Engineering Progress Symposium Series, v. 51, no. 17, p. 79-92.

Pollard, D. D., 1973, Derivation and evaluation of a mechanical model for sheet intrusions: Tectonophysics, v. 19, no. 3, p. 233-269.

———1976, On the form and stability of open hydraulic fractures in the Earth's crust: Geophysical Research Letters, v. 3, no. 9, p. 513-516.

Pollard, D. D., and Holzhausen, Gary, 1979, On the mechanical interaction between a fluid-filled fracture and the Earth's surface: Tectonophysics, v. 53, no. 1, p. 27-57.

Pollard, D. D., and Muller, O. H., 1976, The effects of gradients in regional stress and magma pressure on the form of sheet intrusions in cross section: Journal of Geophysical Research, v. 81, no. 5, p. 975-984.

Pollard, D. D., Muller, O. H., and Dockstader, D. R., 1975, The form and growth of fingered sheet intrusions: Geological Society of America Bulletin, v. 86, no. 3, p. 351-363.

Pŭcik, T. A., 1972, Elastostatic interaction of cracks in the infinite plane: Pasadena, California Institute of Technology, Ph. D. thesis, 129 p.

Reeside, J. B., Jr., 1924, Upper Cretaceous and Tertiary formations of the western part of the San Juan Basin, Colorado and New Mexico: U.S. Geological Survey Professional Paper 134, 70 p.

Richter, D. H., Ault, W. U., Eaton, J. P., and Moore, J. G., 1964, The 1961 eruption of Kilauea Volcano, Hawaii: U.S. Geological Survey Professional Paper 474-D, p. D1-D34.

Richter, D. H., Eaton, J. P., Murata, K. J., Ault, W. U., and Krivoy, H. L., 1970, Chronological narrative of the 1959-60 eruption of Kilauea Volcano, Hawaii: U.S. Geological Survey Professional Paper 537-E, p. E1-E73.

Roberts, J. L., 1970, The intrusion of magma into brittle rocks, *in* Newall, Geoffrey, and Rast, Nicholas, eds., Mechanism of igneous intrusion: Liverpool, Gallery Press, p. 287-338.

Ryan, M. P., and Sammis, C. G., 1978, Cyclic fracture mechanisms in cooling basalt: Geological Society of America Bulletin, v. 89, no. 9, p. 1295-1308.

Schmidt, R. A., and Huddle, C. W., 1977, Effect of confining pressure on fracture toughness of Indiana limestone: International Journal of Rock Mechanics and Mining Sciences & Geomechanics Abstracts, v. 14, no. 5-6, p. 289-293.

Secor, D. T., Jr., and Pollard, D. D., 1975, On the stability of open hydraulic fractures in the Earth's crust: Geophysical Research Letters, v. 2, no. 11, p. 510-513.

Shaw, H. R., 1969, Rheology of basalt in the melting range: Journal of Petrology, v. 10, no. 3, p. 510-535.

———1972, Viscosities of magmatic silicate liquids: An empirical method of prediction: American Journal of Science, v. 272, no. 9, p. 870-893.

Shaw, H. R., Wright, T. L., Peck, D. L., and Okamura, R. T., 1968, The viscosity of basaltic magma: An analysis of field measurements in Makaopuhi lava lake, Hawaii: American Journal of Science, v. 266, no. 4, p. 225-264.

Shoemaker, E. M., Roach, C. H., and Byers, F. M., Jr., 1962, Diatremes and uranium deposits in the Hopi Buttes, Arizona, *in* Engel, A. E. J., James, H. L., and Leonard, B. F., eds., Petrologic studies: A volume in honor of A. F. Buddington: New York, Geological Society of America, p. 327-355.

Sih, G. C., 1974, Strain-energy-density factor applied to mixed mode crack problems: International Journal of Fracture, v. 10, no. 3, p. 305-321.

Sih, G. C., Paris, P. C., and Erdogan, Fazil, 1962, Crack-tip stress-intensity factors for plane extension and plate bending problems: American Society of Mechanical Engineers Transactions, ser. E (Journal of Applied Mechanics) v. 84, no. 2, p. 306-312.

Sneddon, I. N., and Lowengrub, Morton, 1969, Crack problems in the classical theory of elasticity: New York, John Wiley & Sons, 221 p.

Sokolnikoff, I. S., 1956, Mathematical theory of elasticity: New York, McGraw-Hill, 476 p.

Sommer, Erwin, 1969, Formation of fracture "lances" in glass: Engineering Fracture Mechanics, v. 1, no. 3, p. 539-546.

Sparrow, E. M., and Yu, H. S., 1971, Local non-similarity thermal boundary-layer solutions: American Society of Mechanical Engineers Transactions, ser. C (Journal of Heat Transfer), v. 93, no. 4, p. 3328-3340.

Strobell, J. D., 1956, Geology of the Carrizo Mountains area in northeastern Arizona and northwestern New Mexico: U.S. Geological Survey Oil and Gas Investigations Map OM-160, scale 1:48,000.

Swain, M. V., and Hagan, J. T., 1978, Some observations of overlapping interacting cracks: Engineering Fracture Mechanics, v. 10, p. 299-304.

Swanson, D. A., 1972, Magma supply rate at Kilauea Volcano, 1952-1971: Science, v. 175, no. 4018, p. 169-170.

Swanson, D. A., Jackson, D. B., Koyanagi, R. Y., and Wright, T. L., 1976, The February 1969 east rift eruption of Kilauea Volcano, Hawaii: U.S. Geological Survey Professional Paper 891, 30 p.

Tetelman, A. S., and McEvilly, A. J., 1967, Fracture of structural materials: New York, John Wiley & Sons, 697 p.

Timoshenko, Stephen, and Goodier, J. N., 1951, Theory of elasticity: New York, McGraw-Hill, 506 p.

Van Dyke, Milton, 1975, Perturbation methods in fluid dynamics: Stanford, Calif., Parabolic Press, 271 p.

Wentworth, C. K., and Jones, A. E., 1940, Intrusive rocks of the leeward slope of the Koolau Range, Oahu [Hawaii]: Journal of Geology, v. 48, no. 8, p. 975-1006.

Williams, Howel, 1936, Pliocene volcanoes of the Navajo-Hopi country: Geological Society of America Bulletin, v. 47, no. 1, p. 111-171.

Woodward, L. A., 1973, Structural framework and tectonic evolution of the Four Corners region of the Colorado Plateau, *in* James, H. L., ed., New Mexico Geological Society Society Field Conference, 24th, Guidebook: p. 94-98.

Woodward, L. A., and Callender, J. F., 1977, Tectonic framework of the Sand Juan Basin, *in* Fasset, J. E., ed., New Mexico Geological Society Field Conference, 28th, Guidebook: p. 209-212.

Ziony, J. I., 1966, Analysis of systematic jointing in part of the Monument Upwarp. southeastern Utah: Los Angeles, University of California, Ph. D. thesis, 152 p.

GPO 587-041/22